UNIVERSITÀ
DI PARMA

PhD Programme in Industrial Engineering (Cycle XXXVIII)
Department of Engineering for Industrial Systems and Technologies
University of Parma

Dynamic Stiffness Modelling and Finite Element Analysis of Fluid-Filled Structures with Periodic Liquid Dampers under Axial Vibration

Coordinatore:
Prof. Alessandro Tasora

Tutore:
Prof. Elisabetta Manconi

Dottorando:
Alireza Ghazizadeh Ahsaei

November 2025
Anni Accademic 2022/2023-2024/2025

Declaration

I hereby declare that this thesis, entitled

"Dynamic Stiffness Modelling and Finite Element Analysis of Fluid-Filled Structures with Periodic Liquid Dampers under Axial Vibration",

is the result of my own original research and has not been submitted elsewhere for any degree or qualification, and all sources of information used have been duly acknowledged.

Alireza Ghazizadeh Ahsaei
Parma, Italy
November 2025

Acknowledgments

I would like to express my deepest gratitude to my supervisors, Prof. Elisabetta Manconi, for her exceptional guidance, inspiration, and patience throughout the course of this research. Her expertise in vibration control, coupled with her constant encouragement, has shaped both my technical understanding and academic growth. Working under her supervision has been a truly rewarding experience.

I am sincerely thankful to the Department of Engineering for Industrial Systems and Technologies of the University of Parma for providing a stimulating research environment, access to computational resources, and continuous academic support. Special thanks are extended to my colleagues and friends in the research group for their collaboration, insightful discussions, and for creating a friendly and motivating atmosphere during this journey. I also acknowledge the broader scientific community whose work in the areas of periodic media, metamaterials, and computational mechanics has provided a strong foundation for this thesis. Participation in academic seminars and conferences has greatly enriched my research perspective.

On a personal note, my heartfelt appreciation goes to my beloved family for their unwavering love, encouragement, and patience. Their belief in me has been a constant source of strength, especially during the most demanding phases of this study.

Sommario

Questa tesi presenta uno studio analitico e numerico sul comportamento dinamico di strutture con fluido che integrano smorzatori a liquido periodici (PLDs), con l'obiettivo di ridurre le vibrazioni in componenti e sistemi strutturali ingegneristici. Lo studio è motivato dalla crescente necessità di migliorare le strategie di mitigazione delle vibrazioni in ambito strutturale, aerospaziale e marino, dove i dispositivi passivi convenzionali spesso offrono un'efficacia limitata su ampi intervalli di frequenza, in presenza di fluidi e di condizioni di carico dinamico complesse.

La prima parte del lavoro presenta una panoramica sugli approcci numerici e teorici d'interesse per il presente lavoro e sull'isolamento dalle vibrazioni, con particolare attenzione ai principi fisici che governano i sistemi fluido–struttura accoppiati e le strutture riempite di liquido. Lo studio dello stato dell'arte evidenzia i recenti sviluppi nel campo degli smorzatori a liquido, tuned liquid dampers (TLD), dei metamateriali periodici con risuonatori locali e delle formulazioni agli elementi finiti per l'analisi vibroacustica. Su queste basi viene sviluppato un modello analitico semplificato mediante l'approccio della Matrice di Rigidezza Dinamica (Dynamic Stiffness Matrix, DSM), che consente l'analisi delle caratteristiche di propagazione dei disturbi elastici nella struttura e della pressione nel fluido, dei fenomeni di risonanza locali e della formazione di band gaps quando la struttura analizzata è periodica. Queste band gaps rappresentano intervalli di frequenza in cui le onde elastiche e di pressione non possono propagarsi, determinando un'attenuazione naturale delle vibrazioni strutturali. Quando la struttura è periodica, la formulazione DSM modella in modo efficiente una singola cella unitaria periodica, accoppiando la rigidezza dinamica della struttura ospite con quella degli smorzatori a liquido, fornendo così uno strumento computazionalmente efficace per l'analisi e l'ottimizzazione della formazione delle stop band e del comportamento dinamico del sistema periodico. Le condizioni al contorno periodiche di Bloch–Floquet vengono applicate per prevedere le relazioni di dispersione e la trasmissibilità, consentendo di identificare facilmente le zone di frequenza in cui la propagazione delle onde è inibita e le vibrazioni risultano dunque attenuate.

Contestualmente allo studio analitico, sono stati sviluppati modelli agli elementi finiti (FE) per simulare sia la cella unitaria periodica sia la corrispondente struttura finita, confrontando i risultati ottenuti con quelli derivati dalla formulazione DSM. Sebbene l'approccio DSM fornisca una previsione rapida e intuitiva della propagazione dei disturbi nella struttura e della formazione delle band gap, i modelli FEM consentono una rappresentazione più completa dei fenomeni fisici che avvengono nei sistemi in cui è presente accoppiamento fluido–struttura. In particolare, la formulazione FEM consente di includere nel modello effetti dinamici complessi, difficilmente riproducibili con modelli analitici semplificati, come la distribuzione della pressione all'interno del fluido, i modi di sloshing superiori degli smorzatori

liquidi e i fenomeni localizzati derivanti dall'interazione fluido–struttura. I modelli FE sviluppati tengono infatti conto sia del dominio strutturale (solido) sia di quello fluido: il dominio solido è descritto mediante la formulazione elastodinamica standard, mentre il dominio fluido è rappresentato dall'equazione delle onde acustiche, permettendo una simulazione accurata della propagazione delle onde di pressione e della loro interazione con le vibrazioni strutturali; l'accoppiamento tra i due domini è ottenuto tramite vincoli di interazione fluido–struttura (FSI) che impongono la continuità dell'accelerazione normale e della pressione sulle interfacce comuni. Questo quadro numerico multifisico fornisce lo strumento per validare le previsioni analitiche, esplorare gli effetti dinamici di ordine superiore e valutare l'influenza dei parametri geometrici e dei materiali sulla formazione delle band gap vibroacustiche nei sistemi periodici con fluido.

Sono quindi sviluppati esempi numerici di strutture periodiche rappresentative di sistemi tubo-serbatoio, con analisi parametriche volte a valutare l'influenza del livello del fluido, della geometria del serbatoio e del tipo di eccitazione sulla risposta dinamica. I risultati mostrano la comparsa di band gaps a bassa frequenza, associate a fenomeni di Bragg scattering e di risonanza locale, dimostrando la possibilità dei risuonatori a liquido periodici di ridurre passivamente le vibrazioni. Ulteriori analisi confrontano diverse strategie di modellazione — tra cui simulazioni puramente acustiche, puramente strutturali e FSI complete — per validare le previsioni semplificate del modello DSM e valutare il compromesso tra costo computazionale e accuratezza. Sono inoltre analizzati gli effetti del raffinamento della mesh, della definizione della superficie libera e dell'implementazione delle condizioni al contorno, portando a un setup FEM ottimizzato per l'analisi di sistemi oggetto di studio.

I modelli sviluppati forniscono indicazioni generali applicabili a futuri studi su strutture in cui gli smorzatori liquidi periodici (PLD) potrebbero fungere da assorbitori passivi di vibrazioni, ad esempio in strutture civili, in applicazioni aerospaziali o marine. Sebbene questo lavoro non intenda fornire linee guida progettuali specifiche, i risultati contribuiscono a individuare e verificare i meccanismi fondamentali di attenuazione ondosa e formazione di band gap in sistemi accoppiati fluido–struttura con smorzatori liquidi periodici. Nel complesso, lo studio approfondisce la comprensione teorica delle configurazioni periodiche riempite di liquido con dispositivi di sloshing, che possono costituire la base per futuri sviluppi nel controllo passivo delle vibrazioni ispirato ai metamateriali con fluido.

Abstract

This thesis presents an analytical and numerical investigation of the dynamic behaviour of fluid-filled structures incorporating periodic liquid dampers (PLDs), aimed at reducing vibrations in engineering components and structural systems. The study is motivated by the growing need to improve vibration mitigation strategies in modern structural, aerospace, and marine applications, where conventional passive devices often provide limited broadband effectiveness under complex dynamic loading conditions.

The research begins with a theoretical and numerical overview of vibration isolation, emphasizing the underlying physics of liquid-filled and fluid–structure coupled systems. The literature review highlights recent advancements in tuned liquid dampers (TLDs), periodic and locally resonant metamaterials, and vibroacoustic finite element formulations. Building on these foundations, a simplified analytical model is developed using the Dynamic Stiffness Matrix (DSM) approach, which enables the prediction of wave propagation characteristics, resonance phenomena, and the formation of band gaps. These band gaps correspond to frequency ranges where elastic and pressure waves cannot propagate, leading to natural attenuation of vibrations and noise transmission. The DSM formulation efficiently models a single periodic unit cell by coupling the dynamic stiffness of the host structure with that of the liquid dampers, providing a computationally effective framework for analyzing stop-band formation and dynamic behavior in periodic fluid–solid systems. Bloch–Floquet periodic boundary conditions are applied to predict the dispersion relations and transmissibility, allowing for an easy identification of frequency zones where wave propagation is inhibited, and vibrations are attenuated.

Finite element (FE) models are subsequently developed to simulate both the periodic unit cell and the corresponding finite structure, and their results are compared with those obtained from the analytical DSM formulation. While the DSM approach provides a fast and insightful prediction of wave propagation and band gap formation, FE models enable a more comprehensive representation of the physical phenomena occurring in fluid–structure coupled systems. Specifically, the FE formulation captures complex dynamic effects that are difficult or impossible to reproduce with simplified analytical models, such as detailed pressure distribution within the fluid, higher sloshing behavior of the liquid dampers (LDs), and localized phenomena arising from fluid–structure coupling. The FE model accounts for both structural (solid) and fluid domains. The solid domain is described using the standard elastodynamic formulation, while the fluid domain is represented through the acoustic wave equation, enabling accurate simulation of pressure wave propagation and its interaction with structural vibrations. The coupling between these two domains is established through surface-based fluid–structure interaction (FSI) constraints, which enforce the continuity of normal acceleration and pressure across the

shared interfaces. This detailed multiphysics framework provides a tool for validating analytical predictions, exploring higher-order dynamic effects, and assessing the influence of geometrical and material parameters on the formation of vibroacoustic band gaps in periodic liquid-filled systems.

Numerical case studies of representative periodic pipe-tank unit cells are developed, and various parametric analyses are conducted to evaluate the influence of fluid level, tank geometry, and excitation type on the dynamic response. The findings reveal the emergence of distinct low-frequency band gaps associated with Bragg scattering and local resonance effects, demonstrating PLDs' passive ability to reduce vibration. Additional investigations compare different modelling strategies, including acoustic-only, structural-only, and full FSI simulations, to validate the simplified DSM predictions and to assess the trade-off between computational cost and accuracy. The roles of mesh density, free surface definition, and boundary condition implementation are also examined in detail, leading to an optimized FE setup suitable for large-scale periodic systems.

The developed models provide general insights that may apply to future studies of systems in which periodic liquid dampers (PLDs) could serve as passive vibration absorbers, such as in buildings, aerospace, or marine applications. Although this work does not intend to offer specific design guidelines or engineering solutions, the results help clarify the fundamental mechanisms of wave attenuation and band-gap formation in coupled fluid-structure systems with LDs. Overall, the study enhances the theoretical understanding of periodic liquid-filled configurations with sloshing devices, which could serve for future developments in passive vibration control using fluidic metamaterial-inspired concepts.

Contents

List of Figures

List of Tables

Chapter 1

Introduction

The problem of unwanted vibrations in engineering structures remains a major concern across a wide range of fields, including civil, mechanical, aerospace, and marine engineering. When oscillations persist without adequate control, they may accelerate fatigue, reduce operational reliability, or even compromise the safety of the entire system. As modern designs push towards higher performance and stricter safety requirements, the need for effective vibration–mitigation strategies has become increasingly evident. Among the available solutions, damping mechanisms that rely on fluid motion have gained significant attention. In particular, fluid-filled components incorporating periodic liquid dampers have been used as an option for improving vibration control due to their adaptability [98]. Fluid-based damping devices offer several appealing features, including the ability to tune their dynamic response, adapt to different operating conditions, and dissipate energy through internal fluid motion. These characteristics make them suitable for mitigating vibrations at low frequency. The mitigation of axial vibrations, in particular, is and interesting applications as they act along the main load-carrying direction of many engineering members.

Fluid-filled components are already common in numerous applications—such as propellant tanks in spacecraft, liquid containers in industrial facilities, and underwater structural elements—where their dynamic response plays an essential role [209]. The interaction between the enclosing structure and the internal fluid introduces fluid–structure interaction (FSI) effects that can either increase or reduce vibration levels, depending on the geometry, the excitation input, and the boundary constraints [22]. When properly configured, these coupled effects can be used to achieve passive or semi-active damping.

In this context, periodic liquid dampers (PLDs) integrated within fluid-filled structures can offer an additional degree of control. By arranging these dampers in a repeating configuration along the length or surface of the structure, it becomes possible to exploit band gap behavior as in phononic crystals (PCs) and acoustic/elastic metamaterials [232]. This periodic arrangement can prevent certain vibration frequencies from propagating, thereby enhancing the overall attenuation performance of the system. A periodic arrangement — whether created through geometry, material gradation, or repeated boundary constraints — can give rise to frequency ranges in which vibration waves fail to propagate. These so-called bandgaps make periodic liquid dampers (PLDs) an intersting approach to be studied for suppressing unwanted vibrations, including those linked to axial deformation.

To study and refine systems of this nature, finite element (FE) modelling can be a useful tool. Through FE simulations, the coupled response of the fluid and structural domains can be represented with considerable detail, allowing the influence of the periodic dampers to be assessed and their configuration optimized. Nevertheless, accurately capturing the behaviour of fluid-filled structures equipped with PLDs introduces several challenges, e.g., when both the internal fluid motion and the periodic arrangement of the dampers must be fully resolved, the resulting numerical model can become increasingly complex and computationally demanding.

Axial vibrations can arise in slender or elongated structural components under various operating or environmental conditions. These longitudinal oscillations may be induced by external actions, such as wind or seismic excitation—as well as by internal or operational sources, including propulsion systems, machinery, or fluid motion within the structure [209]. When these oscillations occur near the natural frequencies of the structure, resonance effects may arise, leading to increased vibration amplitudes, accelerated fatigue, reduced structural reliability, and unwanted noise or discomfort. Traditional damping strategies, including viscoelastic treatments, tuned mass dampers (TMDs), or other passive devices, often struggle to meet the requirements of adaptability, efficiency, or compatibility with fluid–structure interaction. This motivates the interest in fluid-based damping devices [111]. Fluid-filled structures are systems where the internal cavities are partially or fully filled with liquid. These structures inherently possess damping capabilities because of the inertia and viscosity of the fluid. When subjected to axial motion, the fluid resists displacement, dissipating energy through shear and pressure gradients. PLDs improve this concept by introducing a repeating array of fluid chambers along the structure [175]. Each chamber acts as a localized damper and the periodic arrangement creates a distributed damping effect. In this thesis, the behavior of fluid-filled periodic structures equipped with liquid dampers is examined using both analytical and numerical tools. A simplified analytical model based on the Dynamic Stiffness Matrix (DSM) formulation is first developed to describe wave propagation, local resonances, and the formation of stop bands within a periodic unit cell. This method enables an efficient evaluation of how elastic and hydrodynamic disturbances travel through the structure and how periodicity influences vibration attenuation.

To complement and validate the analytical predictions, detailed finite element (FE) models are then constructed. These include the structural domain, the acoustic fluid domain, and the fluid–structure interaction (FSI) coupling at their interface. Unlike the simplified DSM formulation, the FE models account for higher-order sloshing modes, pressure distribution within the fluid, and localized interaction effects that may significantly influence the dynamic response. This dual-modelling approach allows a direct comparison between analytical and numerical results, clarifies the range of validity of the simplified model, and highlights the additional phenomena that emerge only when the full FSI physics is resolved.

The thesis therefore establishes the motivation, context, and scope for using a simplified model and an FE models to analyze axial vibration attenuation in fluid-filled periodic systems. It first introduces the essentials of vibration control and the characteristics of axial vibration in slender structures, followed by a discussion of the mechanics of fluid–structure interaction and the role of the fluid as both a dynamic load and a potential source of damping. The theoretical background of periodic structures—Bloch–Floquet theory, dispersion relations, and band gap formation is

then reviewed to frame the analytical and numerical developments that follow. The combined analytical–numerical approach ultimately provides a comprehensive understanding of wave attenuation mechanisms in periodic fluid–structure systems and forms a basis for future research on liquid-based vibroacoustic metamaterials.

1.1 Background on Vibration Control in Engineering

The study of vibration control in structural systems is an evolving field in modern engineering, encompassing a wide range of applications in civil, mechanical, aerospace, and marine structures. Vibrations, when persistent and unmitigated, can cause serious challenges such as structural fatigue, loss of stiffness, noise generation, reduced operational efficiency, and, in extreme cases, catastrophic structural failure. As engineering design trends shift toward lighter, more flexible and higher-performance structures, these systems have become increasingly sensitive to dynamic excitations arising from environmental sources such as wind, waves, and seismic activity, as well as operational inputs such as machinery vibration and fluid flow. Consequently, ensuring vibration stability and control is essential to maintain both functionality and safety throughout the service life of engineering systems. The growing demand for high-performance, reliable, and durable structures has intensified the need for innovative vibration mitigation strategies capable of addressing complex dynamic behaviors across a broad range of frequencies. Conventional vibration control solutions are often limited in their adaptability or efficiency, especially when applied to slender or fluid-interacting systems where traditional damping materials and configurations may prove inadequate. In this context, the design and implementation of efficient, robust, and adaptable vibration attenuation mechanisms have emerged as one of the fundamental pillars of modern structural engineering.

The field now increasingly integrates concepts from advanced materials science, computational mechanics, and system optimization to develop next generation damping technologies. These technologies aim not only to suppress harmful vibrations but also to enhance overall performance, extend service life, and reduce maintenance demands. As such, vibration control has become an interdisciplinary research area that bridges analytical modeling, experimental validation, and numerical simulation, providing engineers with comprehensive tools for predicting and mitigating dynamic responses in increasingly sophisticated structural systems.

1.2 Passive Control Approaches and Tuned Dampers

Vibration mitigation techniques are generally categorized as active, semi-active, or passive, depending on the level of external energy input and control involved. Among these, passive devices are the most widely adopted due to their simplicity, robustness, cost-effectiveness, and independence from external power sources. A classical example is the Tuned Mass Damper (TMD), which consists of an auxiliary mass attached to the primary structure through a combination of spring and damper elements. The TMD is tuned to a specific frequency of the host structure to counteract excessive vibrations through resonance cancellation. Such systems have been successfully implemented in tall buildings, long-span bridges, towers, and rotating

machinery to enhance comfort and structural safety. However, their effectiveness is often constrained by narrow frequency bandwidths, sensitivity to detuning, and the need for significant added mass. These limitations have motivated the development of alternative passive concepts that exploit fluid motion instead of solid masses—namely, fluid-based damping mechanisms.

1.3 Tuned Liquid Dampers (TLDs) and Fluid-Based Systems

A Tuned Liquid Damper (TLD) utilizes the sloshing motion of a contained fluid to counteract the vibration of the host structure through the dynamic exchange of momentum between the fluid and the structure. By carefully adjusting parameters such as tank geometry, liquid height, and aspect ratio, the natural sloshing frequency can be tuned to coincide with the dominant vibration mode of the structure [98]. This tuning allows the fluid motion to generate out-of-phase forces that effectively reduce structural oscillations. TLDs are inherently adaptive and self-dissipative systems that rely on viscous, gravitational, and pressure effects to absorb and dissipate vibrational energy without the need for external power or complex control systems. Owing to these advantages, TLDs have been widely adopted in civil, mechanical, and marine structures for mitigating vibrations induced by wind, waves, and seismic excitations [204].

Fluid-filled structures, where cavities are partially or fully filled with liquid, exhibit intrinsic damping characteristics due to the inertia and viscosity of the fluid. When subjected to dynamic loading, the internal fluid resists displacement and motion, thereby dissipating energy through shear and pressure gradients within the cavity. Consequently, liquid dampers offer a robust, reliable, and energy-efficient method of passive vibration control, particularly suited for environments that inherently involve fluid–structure interaction (FSI).

1.4 Fluid-Filled Structures and Fluid–Structure Interaction (FSI)

Fluid-filled structures are ubiquitous in engineering and can be found across a wide range of applications, including aerospace fuel tanks, liquid storage containers, underwater vehicles, nuclear reactor components, and pressurized pipelines that transport fluids such as water, oil, or cryogenic propellants [24]. In these systems, the interaction between the structural components and the internal fluid gives rise to complex coupled dynamics, commonly referred to as fluid–structure interaction (FSI). The presence of the internal fluid alters the effective stiffness, mass, and damping characteristics of the host structure, thereby shifting its natural frequencies and modifying its overall dynamic response. Depending on the excitation frequency, fill ratio, and boundary conditions, this coupling can either amplify structural vibrations—leading to instability—or, conversely, enhance damping and energy dissipation.

Finite Element (FE) modelling offers a rigorous and versatile framework for capturing such interactions with high fidelity [246]. It allows simultaneous represen-

tation of the structural and acoustic or pressure fields, enabling a detailed analysis of modal coupling, wave propagation, and energy exchange mechanisms [18]. In complex geometries or under transient loading conditions, FE techniques provide engineers with powerful computational tools to predict dynamic responses, evaluate the performance of damping systems, and design optimized configurations that effectively harness FSI effects for improved vibration control and structural resilience in real-world applications.

1.5 Periodic Configurations and Band-Gap Mechanisms

The integration of Periodic Liquid Dampers (PLDs) into fluid-filled structures extends the traditional concept of Tuned Liquid Dampers (TLDs) by introducing a periodic arrangement of multiple liquid chambers along the length of the host structure. Each chamber behaves as a local resonator that interacts dynamically with the structure, while the periodic distribution of these resonators gives rise to collective wave phenomena. This configuration allows the system to exploit both Bragg scattering and local resonance effects, leading to the emergence of frequency band gaps in which vibrational energy propagation is strongly suppressed [226]. These mechanisms are rooted in the broader framework of phononic crystals and acoustic metamaterials, whose unique dynamic behavior arises not from material composition but from geometric periodicity and structural arrangement [57, 94].

Bragg-type band gaps occur when the wavelength of the propagating vibration is comparable to the periodic spacing between adjacent cells, resulting in destructive interference of forward and backward travelling waves. In contrast, local-resonance-type band gaps are generated when each unit cell contains a resonant substructure—such as a fluid chamber or internal resonator—capable of storing and dissipating vibrational energy within a narrow frequency range. The coupling of these two mechanisms produces a hybrid attenuation effect that extends over a wider frequency spectrum. As a result, PLDs can effectively suppress both high- and low-frequency oscillations, including challenging low-frequency axial modes that are often difficult to mitigate using conventional dampers [131, 81]. This combination of periodicity and fluid dynamics enables engineers to design lightweight, passive vibration control systems with tunable and broadband performance, offering significant potential for advanced applications in civil, mechanical, marine, and aerospace engineering structures.

1.6 Finite Element Modelling for Fluid–Structure Periodic Systems

To analyze such complex coupled systems (FSI), FE modelling is indispensable. The FE method provides a versatile and powerful numerical framework capable of simulating the coupled dynamic behavior of both fluid and structural domains within periodic configurations. By discretizing the governing equations of motion for the solid and the fluid, FE models can capture the interactions between pressure waves, elastic displacements, and interface forces. These simulations allow the evaluation of

vibration characteristics, the investigation of wave propagation phenomena, and the identification of frequency ranges where attenuation occurs due to either periodicity or resonance mechanisms. Moreover, FE analysis facilitates the study of design parameters such as cell geometry, fluid depth, and material properties, which directly influence the system's dynamic response and the formation of stop bands.

In periodic systems, the application of Bloch–Floquet boundary conditions enables the computation of dispersion relations that describe how wave frequency varies with wavenumber [172]. These relations are essential for predicting wave propagation characteristics, mapping band gap regions, and distinguishing between propagating and evanescent modes. Through dispersion analysis, engineers can assess how modifications in geometry or fluid properties alter the position and width of band gaps, allowing systematic optimization of PLD configurations. Advanced computational schemes, such as coupled acoustic–structural solvers, have further expanded the ability of FE models to represent physical behavior [214]. These solvers incorporate the continuity of pressure and normal displacement at the fluid–structure interface, thereby ensuring a consistent exchange of energy between the two media. The result is a detailed and physically accurate description of resonance and attenuation mechanisms in PLD-equipped structures. Despite these advancements, several challenges remain. The combined influence of Bragg scattering and local resonance in fluid–structure periodic models has not yet been fully understood, particularly regarding how fluid compressibility, viscosity, and free-surface effects modify dispersion and damping characteristics [223]. Continued development of FE formulations and computational strategies is therefore essential for predicting these phenomena and for guiding the design of next generation periodic liquid damper systems capable of broadband vibration mitigation in complex engineering applications.

1.7 Motivation and Research Gaps

Axial vibrations, though often less visually evident than lateral motions, can produce significant detrimental effects, including material fatigue, reduced service life, instability, and acoustic noise transmission along the structure [235]. Traditional liquid-based damping systems—such as Tuned Liquid Column Dampers (TLCDs) and Tuned Liquid Mass Dampers (TLMDs)—have demonstrated effectiveness in attenuating structural vibrations at specific target frequencies. However, these devices are primarily optimized for narrow-band response and tend to lose efficiency when the excitation spectrum is broadband or shifts due to operational variability [109, 6]. Periodic Liquid Dampers (PLDs) offer an alternative by combining local resonance with periodicity-induced Bragg scattering to achieve broader and more controllable attenuation bands. The interaction between these two mechanisms enables energy suppression across both high and low frequencies, making PLDs interesting for complex fluid-filled systems where multiple vibration modes coexist [42].

This thesis contributes to addressing these knowledge gaps by developing, implementing, and validating finite element models capable of predicting vibration attenuation in fluid-filled structures equipped with periodic liquid dampers. The models are used to complement the analytical formulation and to provide deeper insight into wave propagation, fluid–structure interaction effects, and the mechanisms leading to stop-band formation. The work enhances the understanding of vibration control in coupled fluid–structure systems and establishes a basis for future

developments in liquid-based damping concepts for engineering applications.

1.8 Objectives of the Research

Objectives of the Thesis

The main objectives of this thesis are outlined as follows:

1. **Develop a simplified analytical model based on the DSM formulation:** construct a dynamic-stiffness-based analytical model capable of describing wave propagation, local resonances, and band-gap formation in fluid-filled periodic structures equipped with periodic liquid dampers (PLDs).

2. **Construct finite element models incorporating fluid–structure interaction:** develop detailed FE–FSI models that capture the coupled dynamics of the structural and fluid domains, including hydrodynamic pressure, sloshing effects, and localized interaction phenomena.

3. **Compare analytical and numerical predictions:** evaluate the accuracy, robustness, and limitations of the DSM analytical formulation through comparison with FE simulations for both the periodic unit cell and the corresponding finite structure.

4. **Characterize wave attenuation and band-gap mechanisms:** identify the frequency regions where vibration transmission is inhibited and analyse the underlying physical mechanisms, such as periodic scattering and local resonances induced by the liquid cavities.

5. **Perform parametric studies:** investigate the influence of geometric properties, fluid level, cavity configuration, and excitation type on the vibroacoustic response and stop-band characteristics of the periodic system.

6. **Assess modelling strategies and computational trade-offs:** examine different modeling approaches—purely structural, purely acoustic, and full FSI—to establish guidelines on the balance between computational cost and physical accuracy for periodic fluid–structure systems.

1.9 Scope and Contributions

The scope of this thesis encompasses the analytical and numerical investigation of fluid-filled structural systems equipped with periodic liquid dampers (PLDs), with the objective of understanding their dynamic behavior under axial vibration. The work focuses on modelling the coupled fluid–structure response and analysing how periodicity and liquid-induced resonances influence wave propagation and vibration attenuation.

The study comprises two complementary components. First, a simplified analytical model based on the Dynamic Stiffness Matrix (DSM) formulation is developed to describe dispersion characteristics, local resonances, and stop-band formation in a

representative periodic unit cell. Second, detailed finite element (FE) models incorporating fluid–structure interaction (FSI) are constructed to resolve the structural, acoustic, and coupled dynamics with higher fidelity. These FE models serve both to validate the analytical formulation and to capture additional physical phenomena—such as pressure distribution, higher-order sloshing modes, and localized interaction effects—that lie beyond the reach of simplified analytical approaches.

The main original contributions of this thesis can be summarized as follows:

1. **Development of a periodic fluid–structure modelling framework:** A unified analytical–numerical framework is established for the investigation of axially vibrating fluid-filled structures equipped with periodic liquid dampers. The framework explicitly captures the interaction between structural elasticity, fluid inertia, and free-surface dynamics within a periodic setting.

2. **Extension of DSM formulation to fluid-filled periodic systems:** The Dynamic Stiffness Matrix (DSM) approach is extended to account for liquid-induced local resonances and dispersion effects in a representative pipe–tank unit cell. This formulation enables the systematic identification of stop bands and the interpretation of wave attenuation mechanisms.

3. **Coupled FE modelling with FSI for periodic PLD systems:** High-fidelity finite element models incorporating structural, acoustic, and fully coupled FSI formulations are implemented and compared. This provides a rigorous assessment of modelling strategies and quantifies the influence of coupling assumptions on predicted band gaps and transmissibility.

4. **Quantitative analysis of resonance–periodicity interaction:** The interplay between Bragg scattering and liquid-induced local resonance is analysed to clarify the physical origin of low-frequency attenuation regions, demonstrating how periodic liquid dampers modify wave propagation characteristics.

5. **Parametric investigation for design-oriented insights:** The influence of key design parameters—including fluid height, cavity geometry, and boundary conditions—is systematically evaluated to establish guidelines for enhancing vibration attenuation in fluid-filled periodic structures.

6. **Validation and comparative assessment of modelling fidelity:** The analytical predictions are validated against detailed FE simulations, highlighting the accuracy limits of simplified models and identifying scenarios where full FSI coupling becomes essential.

1.10 Thesis Organization

The present thesis is organized into eight main chapters, followed by appendices and a list of published works. Each chapter is designed to build progressively toward an understanding of the modeling, analysis, and application of fluid-filled structures equipped with periodic liquid dampers for axial vibration attenuation.

Chapter 1 – Introduction

The chapter outlines the motivation, background and scope of the study, discussing the importance of vibration control in engineering systems and introduces the study

of fluid-filled structures with periodic liquid dampers (PLDs). The objectives and research methodology adopted in this work are also introduced.

Chapter 2 – Literature Review The chapter provides a literature review on vibration isolation, fluid–structure interaction, and periodic damping systems. An emphasis is placed on the development of finite element (FE) approaches for coupled fluid–solid systems and the role of periodicity in achieving vibration attenuation through band gap phenomena.

Chapter 3 – Simplified Model Chapter 3 introduces an exact dynamic model based on the Dynamic Stiffness Matrix (DSM) approach. The model provides an analytical formulation that is used to study the fundamental characteristics of wave propagation and investigate the mechanisms of vibration suppression in a host structure equipped with PLDs.

Chapter 4 – Finite Element Formulation This chapter is dedicated to the presentation of the FE modelling for coupled fluid–structure domains. The structural and acoustic formulations are presented, and the coupling interface is introduced, showing the appropriate boundary conditions for fluid-structure interaction. The chapter also outlines the assumptions, discretization techniques, and numerical implementation used.

The FE modelling of periodic liquid dampers and their integration into the host structure is also presented. This includes the definition of geometric parameters, mesh generation, and coupling techniques within commercial FE platforms such as ANSYS.

Chapter 5 – Numerical Results and Analysis This chapter presents the numerical simulations, including modal, harmonic, and transient analyses. The results are used to evaluate the performance of PLDs in reducing axial vibrations, and the influence of design parameters such as the fill ratio, tank geometry, and excitation frequency is discussed.

Chapter 7 – Conclusions and Future Work This final chapter summarizes the key findings and contributions of the thesis. Ideas are proposed for future research, including the extension of FE models to non-linear regimes, adaptive damping strategies, and experimental validation.

Chapter 2

Literature Review

The study of structures, whether empty or fluid-filled, equipped with liquid dampers (LDs) aims to understand and reduce their dynamic response under external excitations. Such structures (including storage tanks, pipelines, and aerospace fuel containers) are typically vulnerable to vibration-induced failures. In this context, periodic Liquid Dampers (PLDs), consisting of spatially repeated fluid chambers filled with fluid, can offer a passive, scalable, and frequency-tunable damping solution by exploiting fluid-structure interaction (FSI), local resonance phenomena and periodicity effects. The foundational framework for modeling of fluid-structure interaction (FSI) in finite element (FE) analysis is attributed to Zienkiewicz [246], with further contributions by Belytschko et al. [21], allowing simulation of coupled acoustic-structural behavior. These models were expanded by Faltinsen and Timokha [68] to include dynamic sloshing effects, which play a key role in axial load fluctuations. The application of arbitrarily Lagrangian-Eulerian (ALE) formulas [92] allows effective tracking of fluid domain deformations, enhancing model fidelity. The introduction of PLDs into FE models is inspired by concepts from phononic crystals and acoustic metamaterials, where periodicity and local resonances creates frequency band gaps that inhibit wave propagation [94, 188]. When embedded in fluid-filled structures, LDs interact with vibratory energy, leading to attenuation through localized resonances. Numerical investigations by Chen and Wang [41] and Liu et al. [128] confirmed this effect using detailed FE simulations, highlighting the role of damper configuration, fluid depth, and material properties in tuning band gap characteristics.

Modern research emphasizes optimization and scalability. Xu et al. [222] explored how geometric parameters, including spacing and liquid fill level, influence the formation and bandwidth of stop bands. Hybrid methods that use reduced-order modeling (ROM) have been implemented to accelerate simulation while maintaining accuracy in capturing critical dynamics [147]. Meanwhile, data-driven techniques such as those employed by Zhou et al. [243] offer real-time monitoring and predictive control within FE frameworks. However, challenges persist in modeling three-dimensional interactions, material heterogeneity, and long-term damper behavior under cyclic loading. Nguyen et al. [156] argue for advanced multiphysics platforms that incorporate thermal, fluid, and structural coupling to fully capture PLD performance in complex environments.

2.1 Vibration Isolation in Engineering Structures

Vibration isolation is a fundamental aspect of engineering design and is crucial to improving the performance, longevity, and safety of various structures and systems. Vibrations, originating from sources such as machinery, traffic, or environmental factors, can lead to structural fatigue, noise, and reduced operational efficiency. Effective vibration isolation techniques are essential to mitigate these adverse effects and ensure the integrity of engineering structures [74].
In engineering applications, vibration isolation can be achieved through passive and active methods. Passive isolation systems, such as rubber pads, springs, and dampers, absorb and dissipate vibrational energy, providing a straightforward and cost-effective solution. These systems are designed to reduce the transmission of vibrations by altering the natural frequency of the structure, thus minimizing resonance effects. Tuned mass dampers, for example, are widely used in tall buildings [3].

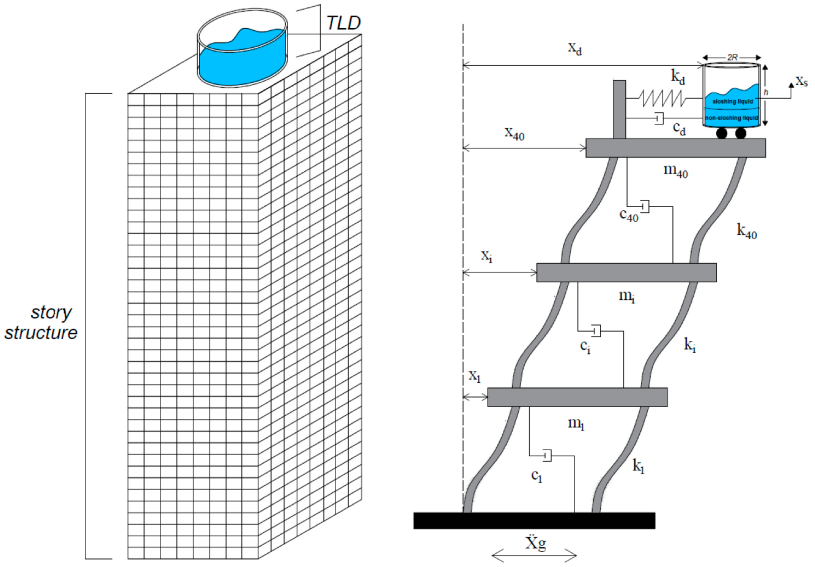

Figure 2.1: Tuned liquid damper of a tall story structure models

Active isolation systems, on the other hand, employ sensors and actuators to detect and counteract vibrations in real-time. These systems are more complex and expensive, but offer superior performance in dynamic environments. Active isolation is particularly beneficial in precision engineering applications, such as aerospace and automotive industries, where maintaining stability and accuracy is paramount [155].

FE modeling is a powerful tool in the design and optimization of vibration isolation solutions. By simulating the dynamic behavior of structures under various vibrational loads, FEM enable engineers to predict the effectiveness of different isolation strategies and identify optimal configurations. This computational approach allows for a detailed analysis of fluid-structure interactions, material properties, and geometric factors, leading to more efficient and targeted isolation designs [154]. Innovative approaches, such as periodic liquid dampers, have shown promise in improving vibration isolation in fluid-filled structures. These dampers can be strategically placed to attenuate axial vibrations, improving the dynamic response and stability

of the system. Integrating periodic liquid dampers into FE models provides control over vibration attenuation, offering advantages over traditional methods [125].
Den Hartog [55] authored the classic text on vibration problems in engineering, introducing tuned mass dampers as practical solutions. His formulations for optimal tuning remain a cornerstone in passive vibration control. Many modern isolation strategies still trace their roots to theoretical models. Frahm [75] patented the first version of a tuned mass damper (TMD). His invention used a secondary mass-spring system to cancel vibrations in ship engines. This early contribution inspired later applications of TMDs in civil and mechanical systems. Soong and Dargush [192] provided a comprehensive overview of passive energy dissipation systems. They classified dampers into metallic, friction, viscoelastic, and liquid types, offering principles and design applications. Their book remains one of the most cited references in structural vibration control. Kareem and Kline [109] investigated vibration mitigation in tall buildings using tuned dampers. Their studies showed how passive devices can significantly reduce wind-induced accelerations. This work influenced design practices in skyscraper engineering. Warburton [214] developed generalized design formulas for TMDs. He demonstrated how optimal tuning depends on the damping ratio, frequency ratio, and excitation type. His simplified formulas are widely used in preliminary damper design. Kwok and Samali [117] analyzed the performance of TMDs under wind and earthquake loads. They demonstrated both numerical and experimental results on tall structures. Their work validated TMDs as effective devices for serviceability and safety enhancement. Rana and Soong [174] published a review of tuned mass dampers. They summarized theoretical, experimental, and practical developments over several decades. This paper became a standard reference for research on TMDs. Symans [200] explored semi-active and hybrid vibration isolation strategies. They discussed how devices such as controllable fluid dampers outperform purely passive systems. Their review bridged passive and active isolation technologies. Chopra [45] covered both analytical modeling and real-world case studies of isolation devices. His text remains essential for students and engineers alike.

Xu and Kwok [224] investigated the application of multiple TMDs in tall buildings. They found that distributed dampers can outperform a single device. Their findings influenced the design of multi-modal isolation strategies. Villaverde [211] studied seismic isolation systems in buildings. He highlighted how base isolation reduces structural demand during earthquakes. His work provided experimental and theoretical evidence for its efficiency. Skinner [189] reviewed the development of base isolation in New Zealand. They documented the first large-scale implementation of lead-rubber bearings. Their work helped to spread isolation internationally. Kelly [111] advanced the theory of seismic isolation bearings. He presented mathematical models and design recommendations for elastomeric and sliding bearings. His contributions shaped seismic isolation codes around the world. Buckel [29] analyzed active vibration isolation in aerospace systems. They demonstrated the effectiveness of actuators in counteracting high-frequency vibrations. Their results motivated active isolation in sensitive equipment. Housner [88] summarized the U.S. National Science Foundation report on structural control. They emphasized the integration of passive, active, and hybrid systems. This report set the research agenda for modern structural control. Tsai [208] developed analytical models for liquid column dampers

used in vibration isolation. They showed how orifice losses and liquid mass tuning govern performance. Their work established TLCDs as viable vibration isolation devices. Samali [183] investigated smart dampers for tall buildings. They compared passive and semi-active devices through simulations and experiments. Their results highlighted the benefits of magnetorheological (MR) dampers in vibration isolation. Spencer [193] introduced structural control strategies with MR dampers. They demonstrated the feasibility of semi-active isolation in earthquake engineering. Their paper accelerated the development of adaptive isolation systems. Lamarque [121] explored nonlinear isolation using vibro-impact dampers. They showed that controlled impacts can significantly reduce resonance amplitudes. Their findings expanded the toolbox of unconventional vibration isolation methods. Preumont [171] presented a textbook on vibration control of active structures. He explained collocated control, piezoelectric actuators, and feedback algorithms. His book remains a reference for active isolation systems.
Sun [197] studied TLDs as isolation devices under excitation. They derived analytical expressions for the reduction of the structural response. Their work connected random vibration theory with liquid damper applications. Erkus [64] analyzed base isolation with nonlinear viscoelastic bearings. They found that nonlinear damping improves performance under near-fault ground motions. Their results informed the design of modern isolation bearings. Lu [133] implemented semi-active control in base-isolated bridges. They used MR dampers with feedback algorithms to adapt isolation properties. Their experiments confirmed improved performance over passive bearings. Higashino [85] published practical guidelines on base-isolated buildings in Japan. They reviewed numerous applications in hospitals, schools, and residential towers. Their book served as a technical manual for practitioners. Nagarajaiah [151] reviewed structural control strategies, with an emphasis on semi-active isolation. They highlighted challenges in real-time control under seismic loading. Their review shaped future developments in smart isolation systems. Nashif [153] published the classic book on viscoelastic damping in vibration isolation. They provided models for frequency-dependent material behavior and practical design methods. This text remains a key reference for engineers using viscoelastic materials in passive isolation. Snowdon [191] wrote one of the earliest engineering texts dedicated to vibration isolation. He systematically discussed transmissibility, damping ratios, and mounting strategies. His book laid the foundation for practical isolation design in mechanical systems. Panossian [163] studied damping treatments for aerospace structures. He showed how constrained-layer damping improves vibration isolation in aircraft panels. His findings directly influenced aerospace noise and vibration control practices. Hunt [93] developed a nonlinear damping model for vibration isolation. They demonstrated how hysteretic and velocity-dependent damping mechanisms alter transmissibility curves. This model has been widely adopted in nonlinear vibration analysis. Jung [105] investigated active vibration isolation in precision engineering. Using piezoelectric actuators and real-time feedback, they achieved submicrometer stability in sensitive equipment. Their work illustrated the practical superiority of active isolation in high-tech applications.

2.2 Fluid-Filled Structures and Their Dynamic Behavior

Fluid-filled structures, such as pipelines, storage tanks, and hydraulic systems, exhibit complex dynamic behavior as a result of the interactions between the fluid and the structure. Understanding these interactions is crucial for the design and optimization of engineering systems to ensure their stability, safety, and efficiency [206]. The dynamic behavior of fluid-filled structures is influenced by various factors, including fluid properties, structural characteristics, and external forces. Fluid structural interaction (FSI) plays an important role in determining the response of these systems to dynamic loads. Studies have shown that FSI can cause phenomena such as waterhammer, cavitation, and vibration, which can adversely affect the performance and integrity of the structure [70].
Research on the dynamic behavior of fluid-filled structures has employed both experimental and numerical methods. Experimental studies provide valuable insight into the real-world behavior of these systems, while numerical simulations, particularly FEM, offer detailed and predictions of their dynamic response [168]. FE models allow the analysis of fluid-structure interactions, material properties, and geometric factors, enabling engineers to optimize designs and mitigate vibration-related issues. An area of focus in recent research is the use of periodic liquid dampers to attenuate axial vibrations in fluid-filled structures. These dampers can be strategically placed to improve the dynamic response and stability of the system. Studies have shown that the integration of periodic liquid dampers into FE models provides precise control over vibration attenuation, offering advantages over traditional damping methods [207].
Housner [89] was one of the first to systematically investigate sloshing in tanks during earthquakes. He showed that liquid motion could be modeled with impulsive and convective components, laying the foundation for modern seismic design of liquid-filled structures. Veletsos [210] extended Housner's work by analyzing earthquake-induced vibrations in liquid storage tanks. They derived frequency and pressure distribution expressions for tanks with flexible walls, showing how fluid–structure interaction alters seismic response. Haroun [84] developed dynamic models of liquid storage tanks that account for wall flexibility and fluid sloshing. Their formulations improved the prediction of hydrodynamic pressures in seismic events, influencing design codes. Chakrabarti [33] reviewed the hydrodynamic aspects of offshore and marine structures, highlighting the importance of sloshing and hydrodynamic loading. His work emphasized the dynamic coupling between fluids and flexible container structures in ocean engineering. Abramson [1] compiled the dynamic behavior of liquids in moving containers (NASA SP-106), which became a seminal reference for aerospace applications. He described sloshing in rockets and spacecraft fuel tanks, including resonance and control strategies. Faltinsen [68] published a modern monograph on sloshing, combining theoretical models with experimental validation. They emphasized non-linear effects, energy transfer, and violent sloshing relevant to marine and aerospace tanks. Veletsos [210] investigated the dynamic pressures in liquid storage tanks and clarified the role of impulsive and convective components. He provided simplified expressions for seismic design that were later integrated into building codes. Malhotra [136] studied simplified procedures for seismic analysis of liquid storage tanks. They proposed practical guidelines validated against experi-

ments that influenced the Eurocode and ACI standards. Kareem [110] examined the effects of fluid-structure interaction in tuned liquid column dampers (TLCD). They showed how fluid oscillations could be used to mitigate vibrations in tall buildings. Shih [185] analyzed the free vibration of circular cylindrical tanks partially filled with liquid. They showed that the height of the fluid and the flexibility of the wall significantly affect the natural frequencies. Park [164] investigated nonlinear sloshing in rectangular tanks under horizontal excitation. Their experiments highlighted the onset of chaotic fluid motion and its impact on tank-wall stresses.

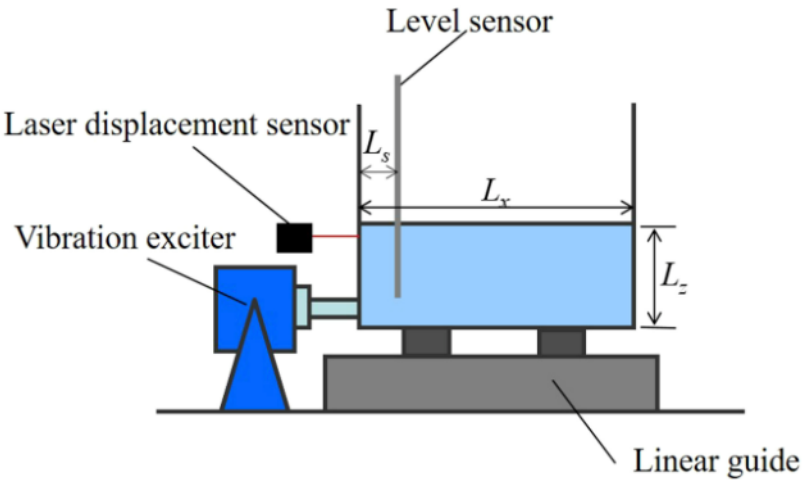

Figure 2.2: Experimental apparatus for sloshing test [164]

Yao [235] studied the longitudinal vibration of liquid-filled pipelines under dynamic loading. They analyzed the coupling between the motion of internal fluids and the walls of pipes, which is important for the safety of pressure vessels and nuclear plants. Bauer [17] explored fluid–structure interaction in elastic containers subjected to impulsive loading. His work clarified how wave propagation in fluids interacts with flexible walls, particularly in defense and aerospace contexts. Chen [42] demonstrated low-frequency band gaps in periodic fluid–solid systems. They showed that the presence of fluid significantly alters the dispersion relations, suggesting applications in vibration attenuation. Panigrahy [162] performed experimental studies on sloshing in baffled tanks. They demonstrated how internal baffles suppress violent sloshing, making this relevant to ship and offshore engineering. Younes and Lee [237] investigated the dynamic behavior of elevated water tanks under seismic loading. They highlighted vulnerability due to fluid–structure resonance, recommending design modifications for improved safety. Khare [113] studied dynamic pressures on offshore structures induced by wave–tank interactions. Their results emphasized the importance of coupled dynamics between structural motions and fluid sloshing. Ramaswamy [173] examined the coupled vibration of liquid-filled shells of revolution. They showed that including fluid inertia in FE models significantly changes predicted natural frequencies. Chen [39] analyzed the sloshing and dynamic pressures in flexible tanks using FE models. Their results showed nonlinear effects and highlighted limitations of simplified impulsive–convective models. Chakrabarti [34] studied liquid-filled offshore caissons, emphasizing dynamic behavior under combined wave and seismic loads. They provided insights into structural resonance and fluid-induced forces in marine applications. Chandrasekaran [35] investigated the

seismic performance of elevated water tanks with flexible staging. They highlighted how fluid–structure interaction combined with structural flexibility increases vulnerability during earthquakes.
Ni [157] examined dynamic responses of liquid-filled pressure vessels. Their finite element simulations revealed how internal fluid resonance amplifies stress in thin-walled vessels, with implications for nuclear engineering. Yamada [232] studied seismic responses of oil storage tanks subjected to base excitation. They introduced simplified formulas for the design, focusing on convective and impulsive pressure components. Darbre [53] analyzed the dynamic safety of large dams with reservoirs, focusing on hydrodynamic pressures. Their work connected sloshing behavior with structural integrity in civil infrastructure. Belytschko and Lin [20] applied explicit finite element methods to model fluid–structure interaction in tanks under impulsive loading. Their results showed advantages of time-domain FE analysis for transient sloshing. Cho [44] studied nonlinear sloshing effects in LNG tanks. Their work highlighted the importance of the motion of large-amplitude fluids in structural stresses and fatigue, particularly in offshore and ship engineering. Aquelet [8] developed ALE (Arbitrary Lagrangian–Eulerian) formulations for liquid-filled tanks under impact. They showed that ALE-FE simulations could capture violent sloshing and fluid breakup more accurately than traditional methods. Kumaraswamy [115] investigated sloshing in elevated tanks through experiments and FE simulations. They provided information on damping mechanisms and fluid–structure resonance under earthquake loads. Reid [179] explored the hydroelastic vibration of large water-filled pipes. He showed how internal pressure waves are coupled with shell vibrations, leading to significant amplification at resonance frequencies. Gupta [82] examined nonlinear fluid–structure interaction in partially filled cylindrical tanks. They demonstrated that nonlinear fluid motion can cause unexpected dynamic pressures not predicted by linear models, stressing the need for advanced FE simulations.

2.3 Finite Element Methods in Vibroacoustics

FEM has become a cornerstone in the field of vibroacoustics, providing a robust framework to analyze the interaction between structural vibrations and acoustic fields. This review of the literature explores the evolution, applications, and advances of FEM in vibroacoustic analysis. The usage of FEM in vibroacoustics involves discretizing the governing equations over the geometry of interest, allowing for detailed analysis of complex structures under various boundary conditions and loads. FEM is particularly effective for interior vibroacoustic problems, where it helps predict sound radiation and transmission characteristics of structures [150]. A significant area of research is the vibroacoustic analysis of advanced material structures, such as laminated composites and functionally graded materials (FGMs). These materials are favored in high-performance applications due to their superior strength-to-weight ratios and enhanced dynamic properties. Studies have shown that FEM can model the vibroacoustic behavior of these materials, accounting for their unique properties and environmental effects [54]. Another critical development is the integration of FEM with other computational methods, such as Boundary Element Methods (BEM). This hybrid approach leverages the strengths of both methods, providing more accurate and efficient solutions for complex vibroacoustic problems. For example, FEM is used to model the structural domain, while

BEM handles the acoustic domain, resulting in a comprehensive analysis of fluid-structure interactions [10]. Recent advances in FEM have also focused on improving computational efficiency and accuracy. High-resolution FE meshes are essential for capturing the dominant wavelengths in structures, especially at higher frequencies, where modal densities are high. Techniques such as Dynamical Energy Analysis (DEA) have been developed to complement FEM, providing a more detailed understanding of the distribution of energy in vibroacoustic systems [238].
Everstine [65] introduced a symmetric potential formulation for fluid–structure interaction. His method allowed structural displacement and acoustic pressure to be coupled efficiently in a single variational framework. This was one of the first clear demonstrations that FEM could treat vibroacoustic coupling rigorously. Everstine [66] later provided a comprehensive survey of finite element formulations for structural acoustics. He compared primal, mixed, and reduced formulations, highlighting the trade-offs in numerical stability, computational cost, and accuracy. This work served as a reference point for engineers in deciding which FE approach to adopt. Morand and Ohayon [148] offered one of the first systematic treatments of fluid–structure interaction using numerical methods. They described practical FE discretization techniques for coupled systems and showed how to maintain stability in fluid–structure computations. Their book remains a foundational reference for applied vibroacoustics. Ohayon and Soize [160] built on this work by formalizing structural–acoustic coupling within rigorous variational principles. They presented mechanical models and discretization strategies that preserved matrix symmetry and avoided numerical instabilities. This text became a cornerstone for theoretical developments in vibroacoustics. Fahy and Gardonio [67] emphasized the physical interpretation of vibroacoustic FE models. They explained how structure-borne vibrations translate into sound radiation and how FE results can be used to predict transmission, radiation efficiency, and damping. Their book made the subject more accessible to practicing engineers. Marburg and Nolte [138] edited a volume on computational acoustics, bringing together leading research on FEM for noise propagation. The book includes applications to exterior and interior acoustics, ranging from vehicle noise to building acoustics. It became a practical reference for engineers tackling real-world noise problems with FE.
Atalla and Sgard [10] presented a modern account of finite and boundary methods in structural acoustics and vibration. They focused on practical industrial applications, particularly automotive and aerospace, and showed how FE can be combined with BEM. Their work also addressed poroelastic materials and their numerical treatment. Allard and Atalla [5] contributed a dedicated text on porous media explaining how Biot's theory could be implemented in FEM to model porous absorbers. They validated the models with experimental data for foams and fibrous materials. This work has been widely used to predict noise control in cars, aircrafts, and buildings. Ihlenburg [99] investigated FEM for acoustic scattering and identified the so-called pollution error that arises at high wave numbers. His analysis highlighted the limitations of standard FEM in high-frequency acoustics. This book is still cited for discussing numerical dispersion in Helmholtz problems. Ihlenburg and Babuška [100] studied the hp-version of FEM for the Helmholtz equation. They showed that using higher-order basis functions combined with mesh refinement significantly reduces dispersion errors. Their work provided the mathematical foundation for adaptive FEM in acoustics. Harari and Hughes [83] developed cost-effective absorbing

boundary conditions for the Helmholtz equation. Their approach made it possible to model unbounded domains without spurious reflections in FE simulations. This contribution has been adopted in many commercial FE codes. Astley [9] reviewed the concept of infinite elements and explained their application to wave propagation problems. He showed how infinite elements could mimic radiation into unbounded domains within FEM. His paper remains a standard reference for engineers modeling open acoustic domains. Bermúdez [22] proposed perfectly matched layers (PML) for time-harmonic acoustics. They proved mathematically that PMLs could absorb outgoing waves without reflection and tested them in FE implementations. Today, PML is considered one of the most robust domain truncation methods. Givoli [78] authored a monograph on non-reflecting boundary conditions. He compared different approaches, including absorbing boundary conditions, infinite elements, and exact operators, and gave guidelines for their use. This book provided a comprehensive resource for anyone working on open-domain vibroacoustics.
Shorter and Langley [186] introduced a hybrid finite element–statistical energy analysis (FE–SEA) method. They combined the deterministic accuracy of FEM at low frequencies with the statistical efficiency of SEA at high frequencies. This hybrid method solved the long-standing mid-frequency "gap" problem in vibroacoustic analysis. Bathe [16] published Finite Element Procedures, a widely used general FEM textbook. Although not specific to acoustics, it introduced time integration schemes and eigenvalue extraction methods crucial for vibroacoustic analysis. Many engineers still use Bathe's formulations as a foundation for structural acoustic calculations. Hughes [91] reissued his classic text on finite element methods, covering linear static and dynamic problems. His treatment of variational principles and dynamics remains fundamental to vibroacoustic FE analysis. The book is often cited as the theoretical backbone of structural and acoustic FEM.
Zienkiewicz [246] offered the seventh edition of The Finite Element Method: Its Basis and Fundamentals. Their book synthesized decades of FE theory, including convergence, stability, and variational consistency. These principles directly underpin vibroacoustic FEM implementations. Rienstra [181] published lecture notes on acoustics, focusing on linear applications. They illustrated how FEM can be applied to model aeroacoustic waveguides. Their notes are widely used in aeroacoustic and duct acoustics research. Marburg and Ihlenburg [137] edited several special issues on advances in acoustic finite elements. These collections presented the latest developments in stabilization, reduced-order modeling, and enriched basis functions. Their editorial work has helped define research directions in FEM vibroacoustics over the last two decades.
Thompson [205] demonstrated how structures FE models could be combined with BEM for the surrounding fluid, significantly reducing computational cost compared to full FE modeling of large domains. This coupling approach became a prototype for modern vibroacoustic solvers. Craggs [48] was one of the first to apply finite elements to acoustic problems, presenting numerical solutions for interior acoustic fields. His pioneering work laid the groundwork for applying FEM to the Helmholtz equation long before commercial codes existed. It is often cited as the historical beginning of acoustic FEM. Petyt [166] developed one of the first systematic applications of FEM in acoustic cavities. They explored modal solutions of the Helmholtz equation in enclosures and validated the approach experimentally. Their contributions helped demonstrate that FEM could rival analytical methods for cavity

acoustics. Zhu and Ciskowski [244] published a book on Boundary Element Methods in Acoustics, complementing FEM by focusing on efficient exterior acoustics. Although the work emphasized BEM, it played an important role in encouraging hybrid vibroacoustic modeling of FE-BE. This reference is still widely cited in coupled approaches. Johnson and Ezquerra [103] applied FEM to study fluid–structure interaction in cylindrical shells containing fluid. Their results highlighted the importance of properly coupling shell vibrations with internal fluid modes. This paper remains a classic in the study of vibroacoustic coupling in aerospace and marine structures. Williams [216] investigated structural vibration and sound transmission through double panels using FEM. They showed how panel spacing, damping, and material parameters influenced acoustic insulation. Their study had a lasting impact on building acoustics and vehicle noise control. Bécot and Atalla [19] introduced finite element formulations for poroelastic materials using Biot's theory, focusing on automotive noise control. They validated their FE approach with experimental data and demonstrated improved accuracy over simplified models. This work strengthened the role of FEM in poroacoustics. Langley [123] examined wave finite element methods (WFEM) for periodic structures. They demonstrated that FE could be adapted to capture dispersion relations in vibroacoustic waveguides. This laid the foundation for today's wave-based FEM in periodic and metamaterial structures. Desmet [56] developed the "Wave Based Method" (WBM) as an alternative to FEM for mid-frequency vibroacoustics. His work illustrated how enriched wave functions could reduce numerical dispersion compared to conventional FEM. Although not strictly FEM, WBM is frequently compared and hybridized with FEM in vibroacoustics. Kessissoglou [112] edited the works on optimization and design in vibroacoustics using FEM. They explored parameter sensitivity, optimization strategies, and inverse methods for reducing noise radiation. This direction pushed FEM beyond analysis into active design and optimization.

2.4 Liquid Dampers: Types and Mechanisms

Liquid dampers are essential components in structural engineering, designed to mitigate vibrations and enhance the stability of structures subjected to dynamic loads such as wind, earthquakes, and machinery operations. This section delves into the various types of liquid dampers and their underlying mechanisms. Types of liquid dampers are:

1. Tuned Liquid Dampers (TLDs): TLDs utilize the sloshing motion of a liquid within a container to dissipate energy and reduce structural vibrations. They are particularly effective in absorbing low-frequency vibrations. The movement of the liquid counteracts external forces, thus stabilizing the structure [231].
2. Tuned Liquid Column Dampers (TLCDs): A specialized form of TLD, TLCDs consist of a U-shaped tube filled with liquid. The damping effect is achieved through the motion of the liquid column, which counteracts the external excitations [231].
3. Viscous Liquid Dampers: These dampers use a viscous fluid to absorb energy. The fluid passes through an orifice or between piston-cylinder arrangements, converting kinetic energy into heat. Viscous dampers are widely used in buildings and bridges due to their effectiveness in reducing seismic and wind-induced vibrations [247].

The primary mechanism of liquid dampers is the utilization of the dynamic proper-

ties of the liquid to absorb and dissipate energy. The sloshing motion of the liquid within the container or column generates a counteracting force that mitigates vibrations. This mechanism can be broken down into several key components:
1. Sloshing Motion: The movement of the liquid within the container or column is driven by external forces acting on the structure. This sloshing motion generates a damping force that counteracts vibrations. The effectiveness of the damper depends on the characteristics of the liquid, such as density and viscosity [159].
2. Hydraulic Head Loss: In TLCDs, the damping effect is achieved through the loss of the hydraulic head of the liquid as it passes through an orifice. This loss of consciousness creates resistance to the motion of the liquid, thereby dissipating energy and reducing vibrations [120].
3. Viscous Action: The viscous action in the boundary layers of the liquid also contributes to the damping effect. The interaction between the liquid and the walls of the containers generates friction, which dissipates energy and reduces the dynamic response of the structure [120].
4. Optimization: Recent studies have focused on optimizing the performance of liquid dampers by analyzing the effects of different liquid characteristics. For example, the adaptive harmony search algorithm has been used to optimize TLDs considering the density and viscosity of the liquid [159].
Housner [89] was one of the first to propose that sloshing of liquids could be used for structural control. He conceptualized the tuned liquid damper (TLD) as a passive vibration suppression device. His foundational work remains the theoretical basis for modern liquid damping research. Fujino [76] carried out pioneering experiments on tuned liquid dampers for tall buildings. They showed that the sloshing frequency of a tank could be tuned to match the structural frequency, achieving a substantial reduction in vibration. Their study provided the first large-scale experimental validation of TLDs. Sun [196] analyzed the damping mechanisms in TLCDs. They demonstrated that energy dissipation arises primarily from head loss in the orifice and the effects of the viscous boundary layer. Their work guided the design formulas for TLCDs in practice. Kareem [107] examined the application of liquid dampers to tall buildings exposed to the wind. He illustrated through simulations and wind tunnel experiments that TLDs significantly reduce crosswind responses. This study encouraged the adoption of TLDs in civil structures. Yamaguchi [233] developed mathematical models for tuned liquid column dampers. They identified the key role of orifice loss in controlling energy dissipation. Their research influenced the early installation of TLCD in Japan. Tamura [201] studied the effectiveness of TLDs under both harmonic and random excitations. He showed that liquid depth, tank geometry, and excitation frequency govern damper performance. His results provided guidelines for TLD tuning in tall buildings. Shum [187] analyzed TLCDs through theoretical and experimental studies. They confirmed that TLCDs are especially efficient against low-frequency excitations. Their work provided validation for simplified TLCD design formulas. Banerji [13] investigated liquid dampers for the earthquake-resistant design of buildings. Their studies revealed that TLCDs can significantly mitigate seismic responses when properly tuned. They emphasized the role of orifice opening ratios in damping efficiency. Kareem [110] studied tuned liquid column dampers under random wind loading. They found that TLCDs provided robust damping across a wide range of stochastic excitations. Their work highlighted the stochastic reliability of liquid dampers.

Yalla [227] proposed hybrid liquid column dampers that combine the TLD and TLCD mechanisms. Their experimental work showed improved damping efficiency and robustness compared to conventional designs. This innovation expanded the scope of liquid damper applications. Nagarajaiah [152] developed semi-active liquid column dampers with controllable orifices. They demonstrated that adaptive control strategies improve damper performance under variable excitations. This was among the first attempts at smart liquid dampers. Rega [178] investigated nonlinear effects in liquid damper systems. They showed that strongly nonlinear sloshing phenomena can influence effectiveness. Their findings suggested caution when designing dampers for large-amplitude excitations. Chang [37] applied tuned liquid dampers to high-rise buildings in Taiwan. They reported case studies in which sloshing dampers reduced wind-induced accelerations to acceptable comfort levels. Their field implementations demonstrated practical feasibility. Yalla [229] studied multiple TLCD systems. They found that arrays of smaller dampers could outperform a single large damper. Their research paved the way for modular damper systems. Ikeda [101] investigated liquid dampers under bidirectional excitations. They emphasized that performance decreases when structural excitation is multidirectional, prompting new design strategies. Their findings were crucial for bridge and offshore applications. Sun [197] studied coupled TLD-structure systems under random vibrations. They derived closed-form solutions that show significant reductions in response variance. Their study improved the stochastic modeling of liquid dampers. Wakahara [212] analyzed nonlinear sloshing in rectangular TLDs. They showed that shallow-water conditions enhance damping but also risk resonance shifts. Their study helped refine TLD tuning strategies. Li [127] tested liquid dampers in offshore platforms. They showed that TLDs effectively reduced wave-induced vibrations in marine structures. This broadened the use of liquid dampers beyond civil engineering. Fujino [77] evaluated tuned liquid dampers in large-scale structures in Japan. They demonstrated consistent performance in reducing wind responses. Their practical implementations boosted confidence in the adoption of TLDs.

Yalla [228] explored multimodal tuning of TLCDs. They proposed designs that target multiple vibration modes simultaneously. Their findings expanded damper applications for complex structures. Bachmann [11] studied human comfort improvements in buildings using liquid dampers. They showed that TLDs significantly reduced floor accelerations caused by human-induced vibrations. This extended damper applications into serviceability design. Banerji [14] implemented TLCDs in Indian buildings. They reported significant reductions in seismic response. Their research marked one of the first real-world TLCD deployments in India. Chang [36] proposed analytical design procedures for TLDs. His methods simplified the computation of sloshing frequencies and damping ratios. This work helped to integrate liquid dampers into design codes. Yalla [230] investigated hybrid passive-active liquid dampers. They showed that incorporating control elements with liquid dampers significantly improves performance under non-stationary loads. This work marked an early step toward adaptive liquid damping systems. Kwon [118] studied the seismic performance of tunable liquid column dampers in bridge structures. They showed that TLCDs could be tuned effectively for long-span bridges, reducing responses under harmonic and seismic loads. Their work extended liquid damper applications from buildings to large civil infrastructure.

Colwell [47] proposed an innovative tuned liquid column–gas damper (TLCGD).

They introduced a compressible gas chamber into the TLCD system, which improved energy dissipation and adaptability. This hybrid concept broadened the range of controllable damping strategies. Kareem and Gurley [108] reviewed the state of vibration control in tall buildings, paying significant attention to liquid dampers. They highlighted successful case studies and compared TLDs and TLCDs with other passive devices. Their review provided one of the first comprehensive perspectives on damper design in civil structures. Ibrahim [98] published a review on the dynamics of liquid sloshing and its application in vibration mitigation. He discussed nonlinear sloshing models and their practical integration into TLD design. This work bridged fluid mechanics and structural vibration control. Banerji and Samanta [15] examined multi-degree-of-freedom structures equipped with multiple tuned liquid dampers. They showed that distributing smaller dampers across different locations improves robustness against mode coupling. Their findings influenced the practical design in seismic zones.

2.5 Periodic Structures and Meta-materials

Periodic structures and meta-materials have received significant attention in recent years due to their unique properties and potential applications in various fields, including electromagnetic, acoustics, and mechanics. This section explores the foundational concepts, types, mechanisms, and emerging applications of these advanced materials.

- Periodic Structures: Periodic structures are materials or systems with repeating units or patterns at regular intervals. These structures can manipulate wave propagation, leading to phenomena such as band gaps, where certain frequency ranges are prohibited from propagating through the material [104]. Photonic crystals are prime examples of periodic structures, used to control light and sound waves, respectively [87].

- Metamaterials: Metamaterials are artificially engineered materials designed to achieve properties that are not found in naturally occurring materials. They are structured on a scale smaller than the wavelength of the phenomena they influence, allowing for unprecedented control over electromagnetic waves, elastic waves, and other physical phenomena. Metamaterials can exhibit negative refraction and cloaking, among other extraordinary properties [87].

- Electromagnetic Metamaterials: These metamaterials are designed to control electromagnetic waves. They can be classified into several types on the basis of their properties, such as negative-index metamaterials, which have a negative refractive index, and chiral metamaterials, which exhibit optical activity and circular dichroism [4]. The mechanism behind these materials involves the interaction of electromagnetic waves with sub-wavelength structures, leading to unique responses. Metamaterials are being explored for use in advanced lenses, antennas, and cloaking devices. Superlenses made from negative index metamaterials can achieve resolutions beyond the diffraction limit, while cloaking devices can render objects invisible by guiding light around them.

- Acoustic Metamaterials: Acoustic metamaterials manipulate sound waves and vibrations. They can achieve a negative effective mass density or bulk modulus, enabling applications such as sound insulation and vibration control [87]. The mechanism involves the resonance of the sub-wavelength structures, which can trap and

manipulate sound waves. In acoustics, metamaterials are used for noise reduction, soundproofing, and acoustic imaging. They can create acoustic band gaps to block specific frequencies, making them ideal for sound insulation in buildings and vehicles.
- Mechanical Metamaterials: These metamaterials are designed to control mechanical properties such as stiffness, strength, and deformation. Examples include auxetic materials, which have a negative Poisson's ratio and expand laterally when stretched. The mechanism involves the geometric arrangement of the microstructure of the material, leading to unconventional mechanical behavior. Mechanical metamaterials are applied in areas that require lightweight and strong materials, such as aerospace and civil engineering. Auxetic materials, for example, are used in protective gear and medical implants due to their unique deformation properties [87].
Pendry [165] introduced the concept that conductors arranged in periodic forms could mimic magnetic responses at microwave frequencies. They showed how such arrangements could yield negative permeability, something that is not found in natural materials. This breakthrough laid the foundation for negative index metamaterials and inspired a new generation of engineered media. Smith [190] provided the first experimental demonstration of a composite medium with both negative permittivity and permeability. By carefully designing split-ring resonators and metallic wires, they confirmed theoretical predictions of negative-index behavior. This work marked the transition of metamaterials from theory to laboratory reality. Shelby [184] experimentally verified negative refraction in a metamaterial at microwave frequencies. They demonstrated that waves could be bent in the opposite direction to what naturally occurs in conventional media. This validation opened the door for applications in superlensing, cloaking, and waveguiding. Liu [131] studied locally resonant sonic materials, demonstrating that acoustic band gaps can be engineered at frequencies far below the Bragg scattering limit. They achieved this using resonators embedded in a host medium, which showed a negative effective mass density. This pioneering work created the foundation for acoustic metamaterials. Joannopoulos [102] published a comprehensive book on photonic crystals explaining both theoretical underpinnings and experimental realizations. The text covered band gap theory, defect states, and waveguiding in periodic dielectric structures. Their book remains a primary reference for researchers working on photonic and phononic band gap materials. Engheta [63] edited a collection that unified theoretical and practical perspectives on electromagnetic metamaterials. The book covered both fundamental physics and engineering explorations, bridging disciplines from optics to RF applications. It established a reference framework for understanding metamaterials in different physical domains.

Caloz [32] introduced the concept of transmission line metamaterials, showing how artificial lines can mimic left-handed media. They explained how compact microwave circuits can be realized using these principles. Their approach greatly influenced telecommunications and antenna design. Yang [234] presented the first realization of a membrane-type acoustic metamaterial that exhibited a negative effective mass density. Their experimental design showed how subwavelength membranes could block sound waves at specific frequencies. This paper demonstrated how lightweight structures can achieve unprecedented control over acoustics. Fang

[69] reported on ultrasonic metamaterials that exhibited negative modulus. They proved the ability to bend and focus sound beyond the diffraction limit. This work expanded the scope of metamaterials into medical imaging and the design of ultrasound devices. Ma [135] provided a review of acoustic metamaterials, summarizing the developments from local resonance mechanisms to more advanced architectures. They highlighted how metamaterials could control noise, vibrations, and acoustic waveguides. Their review illustrated the maturity of the field and pointed toward emerging applications such as cloaking and sound absorption. Cummer [50] delivered a high-impact review of acoustic metamaterials and metasurfaces. They explained the design principles of negative density and negative module structures and their integration into acoustic devices. Their article helped establish metasurfaces as a key direction for practical acoustic wave manipulation. Zhu [245] proposed elastic metamaterials that exhibited negative refraction of waves at deep-subwavelength scales. They demonstrated that single-phase materials could be structured to achieve wave control previously thought impossible. This opened new perspectives for vibration mitigation and structural waveguiding. Hussein [94] produced a comprehensive review of phononic materials and periodic structures. They discussed historical origins, mathematical modeling approaches, and applications in band gap engineering. Their paper bridged classical periodic media with modern metamaterials, providing a unified framework.

Mei [144] introduced the concept of dark acoustic metamaterials, designed as super absorbers of low-frequency sound. Their design achieved nearly perfect absorption of sound in subwavelength structures. This breakthrough suggested applications in architectural acoustics and stealth technologies. Li [126] demonstrated a double negative acoustic metamaterial. They combined resonant structures that created negative effective bulk modulus and negative effective mass density simultaneously. This study was critical in establishing the experimental validation of theoretical acoustic metamaterial models. Kadic [106] analyzed the feasibility of pentamode mechanical metamaterials, which behave like fluids in terms of elasticity. They showed how such structures could be fabricated and discussed their applications in transformation mechanics. Their study provided the theoretical basis for elastic cloaking. Bertoldi [23] reviewed recent advances in flexible mechanical metamaterials. They explained how geometric instabilities, buckling, and programmable designs can be exploited for tunable material properties. This work inspired the creation of adaptive and reconfigurable mechanical devices. Grima [80] studied geometric auxetic materials formed by rotating squares. They showed analytically and experimentally that such arrangements could yield negative Poisson ratios. Their work provided an intuitive pathway for engineering auxetic metamaterials. Lakes [119] was the first to experimentally realize an auxetic foam. He measured negative Poisson's ratio values in reentrant foams, confirming theoretical predictions. This finding sparked decades of research into auxetic materials and their unique properties.

Milton [146] proposed the concept of pentamode materials, theoretical elastic media with fluid-like properties. They argued that such materials could be engineered with almost zero shear modulus while retaining bulk stiffness. This opened a new branch of mechanical metamaterials research. Norris [158] developed a theoretical framework for acoustic cloaking. He showed how coordinate transformations could be applied to sound propagation to make objects effectively invisible to acoustic

waves. This introduced the concept of transformation acoustics into the metamaterials field. Brun [28] applied transformation elastodynamics to design elastic cloaks. They experimentally demonstrated control over in-plane elastic waves using specially engineered materials. Their results extended the concept of cloaking from acoustics and electromagnetics to solid mechanics. Christensen [46] reviewed anisotropic and plasmonic metamaterials. They explained how structured metals could manipulate both optical and acoustic waves at the nanoscale. Their work connected periodic metallic systems with broader metamaterial concepts. Cai [30] published a comprehensive book on optical metamaterials. They covered negative-index materials, transformation optics, and plasmonic systems. The book provided detailed design principles and examples for applications in superlensing and cloaking. Christensen [46] demonstrated anisotropic acoustic metamaterials that allow full control of sound waves. Their experiments confirmed how carefully engineered anisotropy could bend, focus, and cloak acoustic fields. This provided practical proof that anisotropic designs expand the range of functionalities of acoustic metamaterials.

2.6 Research Gaps and Motivation

Despite the extensive body of research on sloshing dynamics, tuned liquid dampers, fluid–structure interaction, and periodic structures, several important limitations remain that hinder a comprehensive understanding of axially vibrating fluid-filled systems equipped with distributed liquid attachments.

First, most studies on liquid dampers concentrate on single or isolated configurations, primarily in the context of seismic mitigation in buildings or vibration suppression in discrete structural components. While these contributions have significantly advanced the understanding of liquid-induced damping mechanisms, the dynamic behaviour of spatially periodic liquid-based systems remains comparatively underexplored. In particular, the propagation characteristics of axial waves in structures equipped with periodically distributed liquid reservoirs have not been systematically investigated from a dispersion-based perspective.

Second, fluid–structure interaction effects are frequently simplified through reduced-order mechanical analogies, such as equivalent mass–spring models. Although these approaches provide valuable physical intuition and computational efficiency, they do not fully capture the coupled dispersion characteristics, wave interactions, and spatial phase relationships that arise in continuous fluid-filled periodic systems. As a result, important phenomena such as mode hybridization, avoided crossings, and coupling-induced band formation may not be accurately represented within simplified formulations.

Third, the combined influence of Bragg scattering and liquid-induced local resonance on axial wave propagation has not been systematically quantified within a unified analytical–numerical framework. Existing literature often treats periodicity-driven band gaps and resonance-driven attenuation as separate mechanisms. However, in fluid-filled periodic assemblies, these mechanisms can coexist and interact, leading to complex attenuation patterns that require integrated modelling strategies for proper interpretation.

Furthermore, limited attention has been devoted to the comparative assessment of modelling strategies—structural-only, acoustic, and fully coupled FSI approaches—in predicting band gaps and vibration attenuation in periodic fluid–structure

systems. A rigorous comparison of these modelling levels is essential to clarify the role of fluid compressibility, free-surface dynamics, and coupling strength in shaping the dispersion response.

These gaps collectively highlight the need for a comprehensive framework capable of capturing structural elasticity, fluid inertia, free-surface behaviour, and spatial periodicity within a unified setting. The present thesis addresses these challenges by developing an integrated analytical–numerical methodology that combines dispersion analysis with high-fidelity finite element simulations. By systematically investigating the interaction between periodicity and liquid-induced resonances, the proposed framework provides deeper physical insight into wave attenuation mechanisms and establishes a rational basis for the design of periodic liquid damper configurations. This structured approach directly motivates the modelling strategies and numerical investigations presented in the following chapters.

This chapter has reviewed the fundamental principles governing fluid–structure interaction in liquid-filled systems and examined the state of the art on liquid dampers, periodic structures, and wave attenuation mechanisms. Particular emphasis has been placed on the role of local resonance, Bragg scattering, and modelling strategies ranging from simplified mechanical analogies to fully coupled FSI formulations. The identified research gaps underline the necessity of a structured modelling approach capable of isolating and interpreting the physical mechanisms responsible for band gap formation and vibration mitigation in periodic liquid-based systems.

To address these challenges progressively, the following chapter introduces a simplified analytical representation of the problem. By modelling the fluid-filled tube with periodically attached tanks as an axially vibrating beam coupled with discrete resonators, the essential features of wave propagation and band gap generation are first established in a reduced-order setting. This analytical foundation provides the conceptual basis for the more detailed numerical and coupled formulations developed in the subsequent chapters.

Chapter 3

Simplified Model

The scope of this chapter is to present a simplified analytical model capable of capturing the main characteristics of a tube with periodically attached simple tanks. The system is modelled as a simplified mechanical configuration consisting of a beam in axial vibration coupled with periodic resonators. This model allows to identify the key features of band gap formation, vibration attenuation, and can serve as a useful tool for optimization purposes. In the chapter, the theoretical background for wave propagation in a simplified beam structure under axial vibration is provided, as well as a simplifed model of the sloshing due to the periodic tank containing fluid. The coupling between the resonators and the host structure is discussed, the Dynamic Stiffness Matrix (DSM) formulation is derived, and the effects of periodicity are analyzed.

3.1 Wave Propagation in Periodic Beam Structure in Axial Vibration

Wave propagation in uniform and periodic beams has been extensively studied over the past decades due to its fundamental importance in a wide range of engineering applications, including vibration control, noise reduction, and the design of phononic and elastic metamaterials. Early studies focused on the propagation of longitudinal and flexural waves in continuous and discrete beam systems, establishing the theoretical basis for dispersion analysis and stop band prediction [26, 140]. Subsequent research extended these analyses to periodic beam-like structures, where the introduction of periodically distributed masses, springs, or resonators leads to the formation of band gaps and localized vibration modes [143, 94]. In particular, the propagation of axial and flexural waves in beams with periodic attachments has been the subject of detailed investigation, providing essential insights into the mechanisms of vibration attenuation.

When a wave travels through a periodic medium, it experiences repeated scattering and interference, leading to frequency ranges in which wave propagation is inhibited called stop band, or band gap [220]. This is particularly valuable in vibration attenuation and noise reduction applications. The study of axial vibration in such systems reveals how longitudinal elastic waves interact with the structure's periodicity. The basic governing equation for axial vibration in a homogeneous one-dimensional beam is [176]:

$$\frac{\partial^2 u(x,t)}{\partial t^2} = c^2 \frac{\partial^2 u(x,t)}{\partial x^2} \tag{3.1}$$

where $u(x,t)$ is the displacement, $c = \sqrt{E/\rho}$ is the wave speed, E is Young's modulus, and ρ is the density. This is also the equation representing non dispersive wave propagation and its solutions describe how axial waves propagate through the beam.

A periodic beam structure can be considered as an arbitrary periodic structure, consisting of repeating units (unit cells) along its length, whose period is of arbitrary length. These units may vary in material properties (e.g., changing layers of different materials), geometry (e.g., varying cross-sectional area), or both. The periodicity introduces unique wave propagation characteristics that are not present in uniform beams. The periodic nature of the structure leads to the formation of band gaps: frequency ranges where wave propagation is prohibited. In fluid-filled structures, the interaction between the structure and the internal fluid leads to coupled dynamics.

To study the periodic behvior of structures, periodicity conditions are applied. In this section, the concept of periodicity is introduced to describe the repetitive nature of the structural configuration. The periodic beam is modeled as an infinite repetition of an elementary unit cell composed of a structural segment with or without an attached resonator or liquid-filled substructure. The dynamic behavior of the entire system can therefore be represented by analyzing a single unit cell subjected to appropriate boundary conditions. Periodicity is enforced through the Bloch–Floquet theorem, which relates the state variables at the two ends of the unit cell by a complex phase shift that depends on the wavenumber. In the finite element model, this condition is implemented by coupling the degrees of freedom of the left and right boundaries of the unit cell using the propagation constant. As a result, only one representative segment needs to be analyzed, significantly reducing computational effort while retaining the essential information about wave propagation. The introduction of periodicity modifies the system's dispersion characteristics, leading to the formation of frequency band gaps where wave propagation is inhibited and pass bands where it is allowed. These features are illustrated through the dispersion curves, which reveal the relation between the excitation frequency and the wavenumber. The slope of each branch in the dispersion diagram represents the phase velocity of the propagating mode, whereas the presence of flat or discontinuous regions indicates stop bands due to Bragg scattering or local resonance effects. Physically, the periodicity introduces a constructive and destructive interference mechanism along the beam, resulting in attenuation zones within specific frequency ranges. This phenomenon is analogous to the propagation of elastic waves in phononic crystals or acoustic metamaterials, where the repetition of structural and material parameters induces dispersion. In the present work, these effects are captured numerically by computing the eigenfrequencies of the unit cell under Bloch–Floquet boundary conditions. The resulting dispersion curves allow identifying the stop bands and quantifying the efficiency of the periodic arrangement in mitigating axial vibrations along the host structure using a simplified system.

3.2 Exact Dynamic Stiffness Matrix Formulation

The Dynamic Stiffness Matrix (DSM) is a frequency domain technique used in structural dynamics to study dynamic response of a system from exact formulation. For any linear undamped structure, the time-domain equation of motion is the following:

$$\mathbf{M}\,\ddot{\mathbf{u}}(t) + \mathbf{K}\,\mathbf{u}(t) = \mathbf{f}(t) \tag{3.2}$$

Assuming harmonic excitation and response, the displacement and force vectors are written as

$$\mathbf{u}(t) = \hat{\mathbf{u}}\, e^{i\omega t}, \qquad \mathbf{f}(t) = \hat{\mathbf{f}}\, e^{i\omega t} \tag{3.3}$$

Substituting into Equation (3.2) yields

$$\left(-\omega^2\mathbf{M} + \mathbf{K}\right)\hat{\mathbf{u}} = \hat{\mathbf{f}} \tag{3.4}$$

This leads to the dynamic stiffness formulation:

$$\mathbf{D}(\omega)\,\hat{\mathbf{u}} = \hat{\mathbf{f}}, \qquad \mathbf{D}(\omega) = \mathbf{K} - \omega^2\mathbf{M} \tag{3.5}$$

If viscous damping is included, with damping matrix $\mathbf{C}$, the dynamic stiffness becomes

$$\mathbf{D}(\omega) = \mathbf{K} + i\omega\,\mathbf{C} - \omega^2\mathbf{M} \tag{3.6}$$

This frequency-dependent matrix, $\mathbf{D}(\omega)$, is the dynamic stiffness matrix, and express the exact dynamic behavior at any excitation frequency [12].

Unlike conventional stiffness matrices in the FEM, which rely on assumed shape functions and are frequency independent, the dynamic stiffness matrix is here derived directly from the exact solution of the governing differential equations of motion at each frequency [122, 12]. This makes the DSM particularly suitable for wave propagation, high-frequency vibration, and periodic structures [141].

Consider Figure (3.1), which represents a bar segment of length L, where $u(x)$ represents the displacement of the arbitrary point, u_1 and u_2 are the displacements of left and right, respectively. F_1 and F_2 are external forces applied at the two ends of the structure.

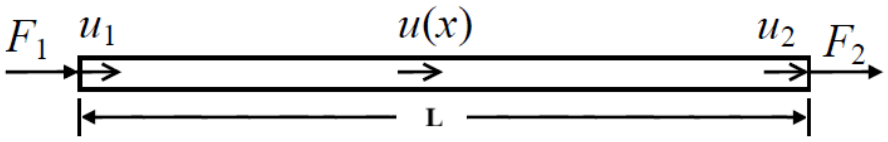

Figure 3.1: Axial deformation of a bar.

Now, we calculate the exact dynamic stiffness matrix for the rods. Consider a uniform axial rod of length L, area A, Young's modulus E, and density ρ (Figure 3.1). The partially differential equation for the axial displacement u(x,t) is:

$$\frac{\partial^2 u}{\partial x^2} = \frac{\rho}{E}\frac{\partial^2 u}{\partial t^2} \tag{3.7}$$

Assuming a harmonic solution $u(x,t) = U(x)e^{i\omega t}$, we get:

$$\frac{d^2U}{dx^2} + k^2U = 0, \quad \text{where} \quad k = \frac{\omega}{c}, \quad c = \sqrt{\frac{E}{\rho}} \tag{3.8}$$

The general solution:

$$U(x) = B_1\cos(kx) + B_2\sin(kx) \tag{3.9}$$

With reference to Fig. 3.1, boundary displacements at $x = 0$ and $x = L$ are

$$u_1 = U(0) = B_1, \quad u_2 = U(L) = B_1\cos(kL) + B_2\sin(kL) \tag{3.10}$$

Axial forces are related to the derivative:

$$F(x) = EA\frac{dU}{dx} = EAk(-B_1\sin(kx) + B_2\cos(kx)) \tag{3.11}$$

Evaluated at boundaries:

$$F_1 = -EAkB_2, \quad F_2 = EAk\left[-B_1\sin(kL) + B_2\cos(kL)\right] \tag{3.12}$$

Substituting Equation (3.10) into Eq. (3.12) give:

$$\begin{bmatrix} F_1 \\ F_2 \end{bmatrix} = \mathbf{D}(\omega)\begin{bmatrix} u_1 \\ u_2 \end{bmatrix} \tag{3.13}$$

where $\mathbf{D}(\omega)$ is the exact dynamic stiffness matrix becomes:

$$\mathbf{D}(\omega) = \frac{EAk}{\sin(kL)}\begin{bmatrix} \cos(kL) & -1 \\ -1 & \cos(kL) \end{bmatrix} \tag{3.14}$$

This matrix is frequency-dependent and represent an exact dynamic of a bar segment of the length L. This dynamic stiffness matrix can be efficiently used for evaluating the wave behavior of periodic structures as shown in Section (3.5).

The dynamic stiffness formulation can be compared with the formulation obtained using a finite element approximation. Note that this formation of DSM will also be discussed in more detail in Section (3.3).

3.2.1 Finite Element Approach to Obtain DSM

Using the finite element method, the displacement within a beam element in axial vibration of length L is approximated by a linear interpolation of the nodal displacements u_1 and u_2 as:

$$u(x) = N_1(x)u_1 + N_2(x)u_2, \tag{3.15}$$

where $N_1 = 1 - x/L$ and $N_2 = x/L$ are the linear shape functions associated with nodes 1 and 2.

The strain is obtained from the spatial derivative of the displacement field:

$$\varepsilon(x) = \frac{du}{dx} = \frac{dN_1}{dx}u_1 + \frac{dN_2}{dx}u_2 = \frac{1}{L}[-1 \quad 1]\begin{bmatrix} u_1 \\ u_2 \end{bmatrix}. \tag{3.16}$$

The stiffness matrix of the element is derived from the expression of strain energy as

$$U_e = \frac{1}{2}\int_0^L EA\,\varepsilon^2\,dx = \frac{1}{2}\mathbf{u}_e^T\left(\int_0^L B^T EAB\,dx\right)\mathbf{u}_e,$$

where $B = [-1/L \quad 1/L]$ and $\mathbf{u}_e = [u_1 \;\; u_2]^T$. Thus, the element stiffness matrix becomes:

$$\mathbf{K}_e = \frac{EA}{L}\begin{bmatrix} 1 & -1 \\ -1 & 1 \end{bmatrix}. \tag{3.17}$$

Similarly, the consistent mass matrix is obtained from the kinetic energy of the element,

$$T_e = \frac{1}{2}\int_0^L \rho A\dot{u}^2\,dx = \frac{1}{2}\dot{\mathbf{u}}_e^T\left(\int_0^L \rho AN^TN\,dx\right)\dot{\mathbf{u}}_e,$$

where $N = [N_1 \quad N_2]$. After performing the integration, one obtains:

$$\mathbf{M}_e = \frac{\rho AL}{6}\begin{bmatrix} 2 & 1 \\ 1 & 2 \end{bmatrix}. \tag{3.18}$$

Combining the stiffness and mass matrices, the finite element equilibrium equation for axial vibration becomes:

$$\left(\mathbf{K}_e - \omega^2\mathbf{M}_e\right)\mathbf{u}_e = \mathbf{0}, \tag{3.19}$$

which corresponds to the classical FE formulation for a 1D bar element in axial vibration [167].

Therefore, the DSM formulation using the FE approach is as follows

$$\mathbf{D}_{FE} = \mathbf{K}_e - \omega^2\mathbf{M}_e = \frac{EA}{L}\begin{bmatrix} 1 & -1 \\ -1 & 1 \end{bmatrix} - \frac{\omega^2\rho AL}{6}\begin{bmatrix} 2 & 1 \\ 1 & 2 \end{bmatrix} \tag{3.20}$$

Now, by considering a very small L ($(kL) \to 0$), we can obtain the DSM for this segment and compare with analytical solution:

$$\begin{aligned}
\mathbf{D}(\omega) &= \frac{EAk}{\sin(kL)}\begin{bmatrix} \cos(kL) & -1 \\ -1 & \cos(kL) \end{bmatrix} \\
&\approx \frac{EAk}{kL - \frac{1}{6}(kL)^3}\begin{bmatrix} 1 - \frac{1}{2}(kL)^2 & -1 \\ -1 & 1 - \frac{1}{2}(kL)^2 \end{bmatrix} \\
&\approx \frac{EA}{L}\left(1 + \frac{1}{6}(kL)^2\right)\begin{bmatrix} 1 - \frac{1}{2}(kL)^2 & -1 \\ -1 & 1 - \frac{1}{2}(kL)^2 \end{bmatrix} \\
&\approx \frac{EA}{L}\begin{bmatrix} 1 & -1 \\ -1 & 1 \end{bmatrix} - \frac{EA(kL)^2}{L}\begin{bmatrix} \left(\frac{1}{2} - \frac{1}{6}\right) & \frac{1}{6} \\ \frac{1}{6} & \left(\frac{1}{2} - \frac{1}{6}\right) \end{bmatrix} \\
&= \mathbf{D}_{\mathrm{FE}}
\end{aligned} \tag{3.21}$$

As is seen, when L is small enough, the response of the system is the same as exact solution.

3.3 Simplified Model of Resonance Phenomena in Liquid Dampers

The modelling of sloshing phenomena in liquid dampers can be addressed at different levels of complexity, ranging from rigorous fluid–dynamic formulations to simplified mechanical analogies. In this section, these approaches are presented as successive levels of approximation forming a consistent modelling framework. At the most fundamental level, the fluid motion is described using linear potential flow theory, which provides an accurate representation of the sloshing dynamics through the solution of Laplace's equation with appropriate boundary conditions. This formulation leads to the classical dispersion relation and allows the identification of the natural sloshing frequencies. The fluid behaviour is reduced to an equivalent mechanical representation in the form of lumped mass–spring–damper systems. The parameters of this simplified model (modal masses, stiffness, and damping) are derived such that the fundamental dynamic characteristics—particularly the natural frequencies—match those predicted by the fluid model. Accordingly, the approaches presented in this section should be interpreted as a hierarchical transition from a physics-based fluid description to a reduced-order model suitable for structural dynamics and design purposes. In the following sections, the equivalent mechanical formulation is adopted as the primary modelling tool, while the fluid model serves as its theoretical foundation and validation reference.

Resonance phenomena in liquid dampers are central to their function in controlling structural vibrations. These systems exploit the dynamic properties of a fluid contained within a cavity to dissipate the kinetic energy induced by external forces such as wind, seismic activity, or mechanical operations. When the excitation frequency matches the natural frequency of the liquid oscillatory motion, resonance occurs, resulting in significant energy transfer from the host structure to the fluid, which can then be dissipated. Understanding and simplifying these resonance effects is critical in designing effective dampers. This theoretical background aims to develop and discuss simplified models of resonance phenomena in liquid dampers, drawing on principles of fluid-structure interaction, mechanical analogies, and classical sloshing theory. The discussion highlights key concepts, assumptions, governing equations, and applications in engineering design. There are three types of liquid dampers: (1) Tuned Liquid Dampers (TLDs), which are passive control devices that are based on the sloshing of surface waves within a container. The liquid absorbs structural energy at resonance; (2) Tuned Liquid Column Dampers (TLCDs), which incorporate vertical columns and air compression chambers, which offer better frequency adjustment and adaptability. (3) Hybrid Systems, which combine TLDs with baffles, viscoelastic membranes, or mechanical springs to broaden the damping bandwidth [110].

Liquid dampers, particularly TLDs and TLCDs, consist of a partially filled container with liquid. Their operation is based on the principle of sloshing, where the liquid undergoes an oscillatory motion when the container is excited. These oscillations induce hydrodynamic pressures and forces that act in opposition to the motion of the container, providing a damping effect. The efficiency of a liquid damper is maximized when its sloshing frequency is tuned to the natural frequency of the structure. In this resonance condition, energy transfer is optimal, and fluid motion can significantly reduce the amplitude of structural vibrations. The damping comes

primarily from: - viscous effects (fluid shear near walls), - wave breaking and turbulence (nonlinear effects), - momentum exchange (between fluid and structure) [210]. To analyze resonance phenomena, fluid motion is typically modeled using potential flow theory and linearized wave theory. For simplified models, sloshing is reduced to a mechanical analogy.

For a rectangular tank of length L, filled to height h with an inviscid, incompressible fluid and subject to horizontal oscillations, the elevation of the fluid-free surface can be modeled as follows [218].

$$\eta(x,t) = A\cos(kx)\cos(\omega t) \tag{3.22}$$

where $\eta(x,t)$ is the free surface displacement, A is the amplitude, $k = \frac{n\pi}{L}$ is the wave number (for mode n, ω is the angular frequency).

The natural sloshing frequency (for mode n) is [89]:

$$\omega_n = \sqrt{gk\tanh(kh)} \tag{3.23}$$

For the first-mode shallow-water approximation ($kh \ll 1$), it simplifies to:

$$\omega_1 \approx \frac{\pi}{L}\sqrt{gh} \tag{3.24}$$

where g is the gravitational acceleration, h is the depth of the fluid. This frequency is a critical parameter for tuning the damper.

To facilitate practical design, the fluid behavior is represented as a mass-spring-damper system:

$$m_f\ddot{u}(t) + c_f\dot{u}(t) + k_f u(t) = F(t) \tag{3.25}$$

with: m_f is equivalent sloshing mass, c_f: damping coefficient (from viscosity and turbulence), k_f sloshing stiffness, $u(t)$ displacement of fluid mass, $F(t)$ is input excitation from the host structure. This system exhibits resonance when the excitation frequency ω matches the natural frequency:

$$\omega_n = \sqrt{\frac{k_f}{m_f}} \tag{3.26}$$

At the fluid-structure interface, kinematic continuity ensures that the fluid velocity is equal to the structure velocity:

$$\mathbf{v}_f = \frac{\partial \mathbf{u}_s}{\partial t} \tag{3.27}$$

This condition ensures coupled motion and energy transfer. Similarly, dynamic continuity or traction balance states:

$$\boldsymbol{\sigma}_f \cdot \mathbf{n} = \boldsymbol{\sigma}_s \cdot \mathbf{n} \tag{3.28}$$

ensuring that the fluid and the structure exert equal and opposite stresses at their interface.

For a liquid damper to be effective, it must be tuned such that its sloshing frequency aligns with the dominant vibration frequency of the structure. In tall buildings, e.g., bridges and offshore structures, this frequency is often in the range

of 0.1 to 1 Hz. Real-world excitation may contain multiple frequency components. Thus, dampers are often designed with multiple chambers, baffles, or variable-depth tanks to broaden their effectiveness. While simplified models assume linear behavior, nonlinearities can arise from large wave amplitudes, tank geometry (curved or flat), and interaction with internal partitions or obstructions. Figure (3.2) shows experimental validation or CFD simulations often used in the final design stages [198].
Figure (3.3) shows a diagram of an equivalent mechanical model of a partially filled tank.

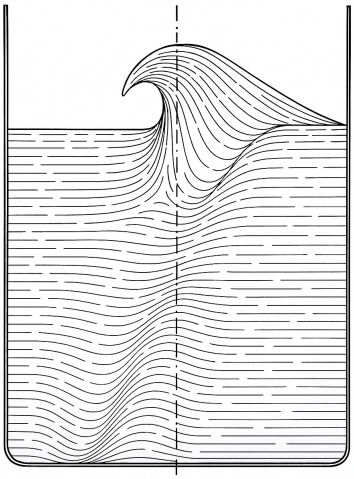

Figure 3.2: Sloshing impact of the tank in axial movement [198]

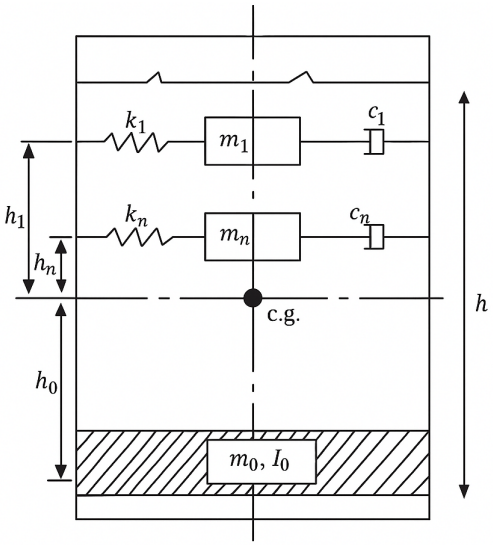

Figure 3.3: Simplified equivalent model (tank) as a damper in sloshing study [98]

The equivalent mechanical model shown in Figure 3.3 is described by a set of generalized coordinates representing the motion of the tank and the sloshing liquid masses. The impulsive component of the liquid, which moves together with the tank, is represented by the mass m_0, while the sloshing behaviour is modelled through a

set of n equivalent masses m_i connected to the tank by springs k_i and dashpots c_i. Consequently, the system possesses $n+1$ degrees of freedom, corresponding to the horizontal displacement of the tank and the relative motions of the sloshing masses. This model should satisfy the following conditions [98]:

$$m_F = m_o + \sum_{n=1}^{\infty} m_n \tag{3.29}$$

where m_F, m_0, and m_n are total fluid mass, rigid mass, and modal mass, respectively. Mass moment of inertia about the y-axis:

$$I_f = I_o + m_o h_o^2 + \sum_{n=1}^{\infty} m_n h_n^2 \tag{3.30}$$

The center of mass should be preserved:

$$m_o h_o - \sum_{n=1}^{\infty} m_n h_n = 0 \tag{3.31}$$

The following equation is obtained by writing the horizontal equilibrium of forces for the tank and the sloshing masses. Applying Newton's second law in the horizontal direction, the inertia forces associated with the rigid tank motion and the impulsive–convective sloshing components must balance the external excitation force F_x [98]. Therefore, force equilibrium is:

$$m_o(\ddot{x} - h_o\ddot{\psi}) + \sum_{n=1}^{\infty} m_n(\ddot{x}_n + \ddot{x} + h_n\ddot{\psi}) = -F_x \tag{3.32}$$

where: $\ddot{x}$ is the horizontal acceleration of the container, $\ddot{x}_n$ is the modal acceleration of the n-the sloshing mass, $\ddot{\psi}$ is the angular acceleration (e.g., pitch or roll), m_0 and h_0 are the mass and height of the base mass, m_n and h_n are the mass and height of each modal component, and F_x is external force in the direction x [98].
Sloshing equation of the nth mode is

$$m_n(\ddot{x} + \ddot{x}_n + h_n\ddot{\psi}) + K_n x_n + 2m_n\omega_n\zeta_n\dot{x}_n - m_n g\psi = 0 \tag{3.33}$$

where $K_n x_n$ is the restoring force, $2m_n\omega_n\zeta_n\dot{x}_n$ is the damping force (ζ_n is the damping factor of the equivalent dashpot) and g is the gravity acceleration.

The equivalent mechanical model described by Equation (3.33) represents the sloshing behaviour of the liquid through a set of lumped oscillators. The parameters of this model are selected such that the natural frequency of the mechanical oscillator reproduces the fundamental sloshing frequency of the fluid. This frequency can be obtained from linear potential flow theory.

Assuming the fluid to be incompressible and irrotational, the velocity field can be expressed in terms of a velocity potential ϕ such that

$$\mathbf{v} = \nabla\phi \tag{3.34}$$

Since the flow is incompressible, the velocity potential satisfies Laplace's equation

$$\nabla^2\phi = 0 \tag{3.35}$$

The fluid motion is subject to appropriate boundary conditions. At the rigid bottom of the tank, the no–penetration condition requires

$$\frac{\partial\phi}{\partial z} = 0 \qquad \text{at } z = -h \tag{3.36}$$

At the free surface, the linearized dynamic boundary condition gives

$$\frac{\partial^2\phi}{\partial t^2} + g\frac{\partial\phi}{\partial z} = 0 \qquad \text{at } z = 0 \tag{3.37}$$

Assuming a harmonic wave solution of the form

$$\phi(x, z, t) = A\cos(kx)\cosh[k(z + h)]e^{i\omega t} \tag{3.38}$$

and substituting this solution into the governing equations and boundary conditions leads to the classical dispersion relation for surface gravity waves

$$\omega^2 = gk\tanh(kh) \tag{3.39}$$

where g is the gravitational acceleration, k is the wavenumber and h is the fluid depth. For a rectangular tank of length d, the fundamental antisymmetric sloshing mode corresponds to the standing wave condition

$$k = \frac{\pi}{d} \tag{3.40}$$

Substituting this expression into the dispersion relation leads to the fundamental sloshing natural frequency

$$\omega_1 = \sqrt{gk\tanh(kh)} \tag{3.41}$$

which corresponds to Equation (3.33). The equivalent mechanical oscillator introduced in Equation (3.33) is therefore defined such that its natural frequency satisfies

$$\omega_n = \sqrt{\frac{K_n}{m_n}}, \tag{3.42}$$

ensuring that the simplified mechanical representation reproduces the sloshing dynamics predicted by the fluid model [98, 68].

This expression, derived from wave theory, defines the natural frequency of the lowest sloshing mode [58]. Only a portion of the fluid mass participates in the sloshing. For the first antisymmetric mode in a shallow tank:

$$m_s = \frac{4\rho dh}{\pi^2} \tag{3.43}$$

This is based on the kinetic energy equivalence between the fluid and the mechanical system [58, 236].

3.3.1 Inclusion of Damping

To incorporate damping in the proposed dynamic stiffness formulation, only the terms directly relevant to the mathematical model should be introduced. In the frequency domain, viscous damping is represented through a damping matrix $\mathbf{C}$, which enters the dynamic stiffness operator as

$$\mathbf{D}(\omega) = \mathbf{K} + i\omega\,\mathbf{C} - \omega^2\mathbf{M}, \tag{3.44}$$

as previously defined. Here, $\mathbf{C}$ is the equivalent linear damping contributions associated with the sloshing motion. In practice, this matrix accounts for all energy-dissipation mechanisms of the fluid–structure system—including boundary layer effects, turbulence, and surface deformation losses—through an equivalent viscous representation.

For a single sloshing mode, the equivalent viscous damping coefficient can be expressed in terms of the modal mass m_f, modal stiffness k_f, and damping ratio ζ as

$$c_f = 2\zeta\sqrt{m_f k_f}, \tag{3.45}$$

This equivalent formulation allows the damping of each sloshing mode to be included directly in Equation (3.44) through the modal contributions of $\mathbf{C}$.

3.4 Coupling of Periodic Liquid Dampers with Host Structures (Dynamic Stiffness Matrix Formulation)

The integration of periodic liquid dampers (LDs) into host structures has recently gained attention as an effective strategy for mitigating vibrations in structures and fluid-filled systems. Such configurations can exploit the combined benefits of fluid–structure interaction and periodicity to suppress undesirable dynamic responses and enhance overall structural performance. The key mechanism in coupling PLDs with host structures lies in the mutual interaction of fluid and structural motions. As periodic liquid chambers oscillate under structural excitation, they exert counteracting forces that can be tailored to suppress specific vibrational modes. This coupling becomes particularly effective when it is configured to take advantage of resonance mechanisms and band–gap formation due to periodicity, which together enable the selective attenuation of structural responses over targeted frequency intervals [94, 198]. When liquid dampers are arranged in a spatially periodic manner, the repeated configuration introduces wave interference phenomena such as Bragg scattering and local resonance, leading to the emergence of stop bands that hinder the propagation of vibrational energy [27, 94]. When coupled with host structures such as tanks or flexible-walled pipes containing liquid, these dampers serve to mitigate resonant amplification phenomena triggered by external excitations or seismic events. The slope in partially filled containers can induce significant hydrodynamic pressures and structural stresses [68]. The fluid-structure interaction (FSI) is exacerbated when the excitation frequency approaches the natural sloshing frequency of the tank, which can cause instability or structural failure [195]. In this context, periodic LDs are placed strategically to interrupt the fluid motion and

redistribute energy, thereby suppressing dominant sloshing modes. The resulting coupling effect originates from the dynamic interaction between the dampers and the host structure, which alters both the vibration characteristics of the container and the sloshing behavior of the enclosed liquid [225]. The periodic arrangement of the dampers plays a decisive role in shaping the overall dynamic response of the coupled system. In particular, the repeated configuration gives rise to band gaps - whose location and width can be typically tailored by modifying the spacing, mass, and stiffness of the dampers [116]. These gaps are particularly effective when the dominant sloshing frequencies falls within it, leading to significant attenuation [241]. Moreover, coupling periodic dampers directly with the structural walls of a tank or tube modifies the effective boundary conditions experienced by the liquid, altering its vibrational modal characteristics [130]. In these models, the host structure is often represented by shell or beam elements, while the fluid domain may be simulated using acoustic or potential flow elements [217, 161]. Periodic dampers are modeled as discrete mass-spring systems or homogenized as a metamaterial layer [147]. The fluid-structure interaction is incorporated through the interface coupling conditions, which account for pressure continuity and kinematic compatibility. Experimental and computational studies have demonstrated the effectiveness of this coupling strategy in suppressing sloshing and associated dynamic effects [40, 203]. The design optimization of such systems involves selecting the periodicity and material properties of the dampers to ensure that the band gaps align with the structural and fluid resonances. When well designed, PLDs not only reduce liquid motion but also lower transmitted forces to the support structure, improving overall system resilience [156].

In the following analysis, we introduce a simplified model that serves as a preliminary design and assessment tool. This model provides an insight into the system's behavior before incorporating more advanced features, such as full fluid–structure interaction, into the design process.

For the simple case, we calculate the shape function or modes of the rod including simple elements (mass and spring) by two simliar approaches, the Dynamic Stiffness Matrix (DSM) and the Transfer Matrix Method (TMM).

As already introduced, the DSM of a structural element can expressed as:

$$[\mathbf{D}]\mathbf{u} = \mathbf{F} \tag{3.46}$$

where $\mathbf{u}$ and $\mathbf{F}$ are the displacement and force vectors, respectively, at the node of each separated element. To calculate $\mathbf{D}$, we start from the exact equation of motion. In the following subsections, we calculate the DSM (Dynamic Stiffness Matrix) for 3 case of study.

3.4.1 Case 1: DSM for Rod Only

Consider Figure (3.4), in which a segment of a rod in axial movement is depicted.

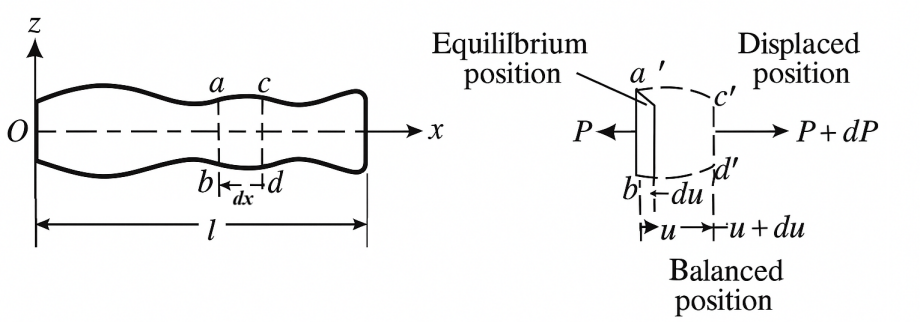

Figure 3.4: A segment of a rod element in axial motion, [175].

From the equilibrium equation,

$$\sum F_x = ma_x \rightarrow P + \frac{\partial P}{\partial x}\,dx - P = (\rho A\,dx)\frac{\partial^2 u}{\partial t^2} \tag{3.47}$$

On the other hand, for a linear material with constant cross section (A), since axial stress has a linear relation with the strain, one can write:

$$P = \sigma A = E\varepsilon A = EA\frac{\partial u}{\partial x} \quad \rightarrow \quad \frac{\partial P}{\partial x} = EA\frac{\partial^2 u}{\partial x^2} \tag{3.48}$$

From Equations (3.47) and (3.48), the governing equation is obtainable:

$$E\frac{\partial^2 u}{\partial x^2} - \rho\frac{\partial^2 u}{\partial t^2} = 0 \tag{3.49}$$

The solution of this problem can be presented in the following form (separation method):

$$u(x,t) = \{B_1\cos(kx) + B_2\sin(kx)\}\,\{B_3\cos(\omega t) + B_4\sin(\omega t)\} \tag{3.50}$$

or in short form (if we define $\{B_3\cos(\omega t) + B_4\sin(\omega t)\} = T(t)$):

$$u(x,t) = \{B_1\cos(kx) + B_2\sin(kx)\}\,T(t) \tag{3.51}$$

where $k = \frac{\omega}{c_L}$ is the wave number with $c_L = \sqrt{\frac{E}{\rho}}$. Based on Equation (3.48), the axial force can be calculated,

$$P(x,t) = EA\frac{\partial u}{\partial x} \rightarrow P(x,t) = EAk\,\{-B_1\sin(kx) + B_2\cos(kx)\}\,T(t) \tag{3.52}$$

Now an element of length L_e is examined separately (Figure (3.5))

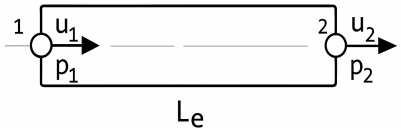

Figure 3.5: An element of a rod (discretized model)

P_1 and P_2 are the forces applied on two nodes (1 and 2). Four boundary conditions are as follow:

$$u_1 = u(0,t) = B_1T(t) \tag{3.53}$$

$$u_2 = u(L_e, t) = \{B_1 \cos(kL_e) + B_2 \sin(kL_e)\} T(t) \tag{3.54}$$

$$P_1 = P(0, t) = EAk \{B_2\} T(t) \tag{3.55}$$

$$P_2 = P(L_e, t) = EAk \{-B_1 \sin(kL_e) + B_2 \cos(kL_e)\} T(t) \tag{3.56}$$

We rewrite these formulae in the matrix form:

$$\begin{pmatrix} u_1 \\ u_2 \end{pmatrix} = \begin{bmatrix} 1 & 0 \\ \cos(kL_e) & \sin(kL_e) \end{bmatrix} \begin{pmatrix} B_1 \\ B_2 \end{pmatrix} T(t) \tag{3.57}$$

$$\begin{pmatrix} P_1 \\ P_2 \end{pmatrix} = \begin{bmatrix} 0 & -EAk \\ -(EAk)\sin(kL_e) & -(EAk)\cos(kL_e) \end{bmatrix} \begin{pmatrix} B_1 \\ B_2 \end{pmatrix} T(t) \tag{3.58}$$

From Equation (3.57):

$$\begin{pmatrix} B_1 \\ B_2 \end{pmatrix} = T(t) \begin{bmatrix} 1 & 0 \\ \cos(kL_e) & \sin(kL_e) \end{bmatrix}^{-1} \begin{pmatrix} u_1 \\ u_2 \end{pmatrix} \tag{3.59}$$

Now, substituting Equation (3.59) into Equation (3.58),

$$\mathbf{F} = T(t) \begin{bmatrix} 0 & -EAk \\ -(EAk)\sin(kL_e) & -(EAk)\cos(kL_e) \end{bmatrix} \begin{bmatrix} 1 & 0 \\ \cos(kL_e) & \sin(kL_e) \end{bmatrix}^{-1} \mathbf{u} \tag{3.60}$$

Finally, based on Equation (3.46), the DSM is obtained for an element of a rod:

$$\mathbf{D} = \frac{EAk}{\sin(kL_e)} \begin{bmatrix} \cos(kL_e) & -1 \\ -1 & \cos(kL_e) \end{bmatrix} \tag{3.61}$$

At this stage, the Dynamic Stiffness Matrix (DSM) formulation provides a frequency-dependent relation between nodal forces and displacements within a finite element framework. While DSM is particularly convenient for assembling global matrices and solving boundary value problems, an alternative and equally powerful approach for studying wave propagation in periodic systems is the Transfer Matrix Method (TMM).

3.4.2 Case 2: TMM for Infinite Rod with Spring-Mass Resonators

Unlike DSM, which relates forces and displacements at the same element, the Transfer Matrix Method directly connects the state variables (displacement and force) at one boundary of a segment to those at the other boundary. This formulation is especially advantageous for analyzing infinite or periodic structures, as it naturally lends itself to the study of wave transmission, reflection, and dispersion characteristics. For this reason, both methods are considered in the following sections, allowing a complementary interpretation of the dynamic behavior of the rod with periodically attached resonators. Consider an infinite rod in which the lumped mass (m_0) and a spring-mass (K_1 and m_1) elements are attached (Figure 3.6).

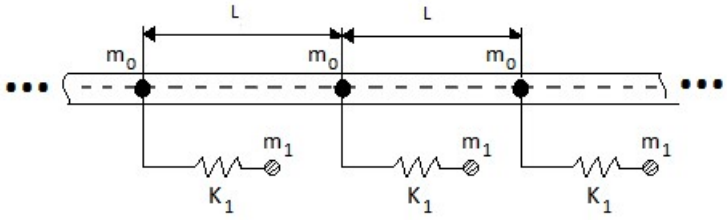

Figure 3.6: Repeated mass-spring element for a rod (1DoF)

To find the transfer matrix method, we first investigate a segment individually (Figure (3.7)).

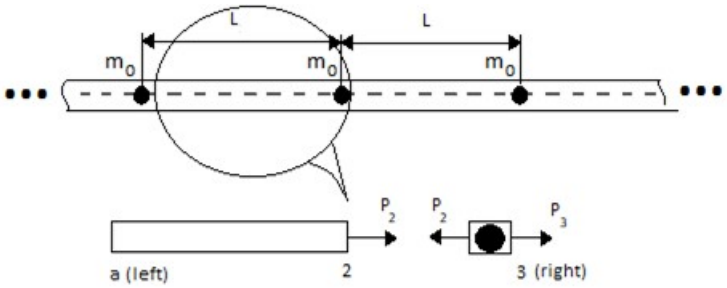

Figure 3.7: An infinite rod with lumped masses

The boundary conditions for the points (a) and (2) are the following:

$$\mathbf{u}_a = \mathbf{u}(0,t) = \mathbf{B}_1\mathbf{T}(t) \tag{3.62}$$

$$\mathbf{u}_2 = \mathbf{u}(L,t) = \{\mathbf{B}_1\cos(kL) + \mathbf{B}_2\sin(kL)\}\,\mathbf{T}(t) \tag{3.63}$$

$$\mathbf{P}_a = \mathbf{P}(0,t) = EAk\,\{\mathbf{B}_2\}\,\mathbf{T}(t) \tag{3.64}$$

$$\mathbf{P}_2 = \mathbf{P}(L,t) = EAk\,\{-\mathbf{B}_1\sin(kL) + \mathbf{B}_2\cos(kL)\}\,\mathbf{T}(t) \tag{3.65}$$

After elimination of the constant coefficients (B_1 and B_2), and writing the values in matrix form, we obtain the following:

$$\begin{pmatrix} u_2 \\ P_2 \end{pmatrix} = \begin{bmatrix} \cos(kL) & \dfrac{\sin(kL)}{EAk} \\ -(EAk)\sin(kL) & \cos(kL) \end{bmatrix} \begin{pmatrix} u_a \\ P_a \end{pmatrix} \tag{3.66}$$

thus, the TM for this segment is obtained. Now for convenient, we define $\mathbf{T}_1$ as:

$$\mathbf{T}_1 = \begin{bmatrix} \cos(kL) & \dfrac{\sin(kL)}{EAk} \\ -(EAk)\sin(kL) & \cos(kL) \end{bmatrix} \tag{3.67}$$

Now, to obtain the complementary matrix of TM, that is, T_2, we shift our focus to another part of the case: Resonator(s). Figure (3.8) shows the force diagram of the separated segment of the main structure.

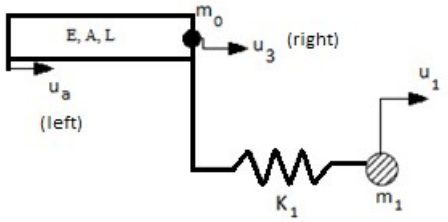

Figure 3.8: A segment of the structure

As is seen from Figure (3.7), the points 2 and 3 are the neighbors and based on the continuity of displacement, we have:

$$\mathbf{u}_3 = \mathbf{u}_2 \tag{3.68}$$

Figure (3.9) illustrates the force diagram of each mass individually.

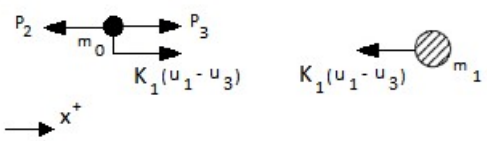

Figure 3.9: Force configuration of the segment

Applying the Second Newton Law for the two masses leads to the following:

$$\mathbf{P}_3 - \mathbf{P}_2 + K_1(u_1 - u_3) = m_0\ddot{u}_3 \tag{3.69}$$

$$-K_1(u_1 - u_3) = m_1\ddot{u}_1 \tag{3.70}$$

For the mass m_1, the solution can be suggested in the harmonic form by the separation method, that is,

$$u_1(x,t) = U(x)T(t) = U(x)\left\{C_1\cos(\omega t) + C_2\sin(\omega t)\right\} \tag{3.71}$$

By two times derivative of u_1 respect to time,

$$\ddot{u}_1 = -\omega^2 u_1 \tag{3.72}$$

Putting the quantity obtained from Equation (3.72) in (3.70) leads to:

$$u_1 = \left(\frac{K_1}{K_1 - m_1\omega^2}\right)u_3 \tag{3.73}$$

The same assumption can be made for the oscillation of mass m_0, which means harmonic solution. Thus:

$$\ddot{u}_3 = -\omega^2 u_3 \tag{3.74}$$

By imposing Equation (3.73) into Equation (3.69), we have the following.

$$P_3 = P_2 + \left(\frac{-(m_1+m_0)K_1\omega^2 + (m_1m_0)\omega^4}{K_1 - m_1\omega^2}\right)u_3 \tag{3.75}$$

In order to acquire T_2, the following matrices should be arranged:

$$\begin{pmatrix} u_3 \\ P_3 \end{pmatrix} = \begin{bmatrix} \frac{1}{K_1 - m_1\omega^2}\left[-(m_1+m_0)K_1\omega^2 + (m_1m_0)\omega^4\right] & 0 \\ 1 & 1 \end{bmatrix}\begin{pmatrix} u_2 \\ P_2 \end{pmatrix} \tag{3.76}$$

or

$$\begin{pmatrix} u_3 \\ P_3 \end{pmatrix} = \begin{bmatrix} \mathbf{N} & 0 \\ 1 & 1 \end{bmatrix}\begin{pmatrix} u_2 \\ P_2 \end{pmatrix} \tag{3.77}$$

where:

$$\mathbf{N} = \frac{(m_1m_0)\omega^4 - (m_1+m_0)K_1\omega^2}{-m_1\omega^2 + K_1} \tag{3.78}$$

or, in the dimensional form:

$$\mathbf{N} = \frac{\left(\frac{m_0}{\omega_1^2}\right)\omega^4 - (m_1+m_0)\omega^2}{-\left(\frac{1}{\omega_1^2}\right)\omega^2 + 1} \tag{3.79}$$

in which $\omega_1 = \sqrt{\frac{K_1}{m_1}}$ is the natural frequency of the resonator. For convenient, we define $\mathbf{T}_2$ as:

$$\mathbf{T}_2 = \begin{bmatrix} \mathbf{N} & 0 \\ 1 & 1 \end{bmatrix} \tag{3.80}$$

By re-writing Equation (3.76):

$$\begin{pmatrix} u_3 \\ P_3 \end{pmatrix} = \mathbf{T}_2 \begin{pmatrix} u_2 \\ P_2 \end{pmatrix} \tag{3.81}$$

Finally, we have the following relation between the degree of freedoms of points 3 and a (Note that $\mathbf{T}_1$ is calculated from Equation (3.67):

$$\begin{pmatrix} u_3 \\ P_3 \end{pmatrix} = \mathbf{T}_2\mathbf{T}_1 \begin{pmatrix} u_a \\ P_a \end{pmatrix} = \mathbf{T} \begin{pmatrix} u_a \\ P_a \end{pmatrix} \tag{3.82}$$

As a result, $\mathbf{T}$ (Transfer Matrix) is obtained:

$$\mathbf{T} = \begin{bmatrix} \cos(kL) - \dfrac{\sin(kL)}{EAk}\mathbf{N} & \dfrac{\sin(kL)}{EAk} \\ -(EAk)\sin(kL) - \cos(kL)\mathbf{N} & \cos(kL) \end{bmatrix} \tag{3.83}$$

3.4.3 Case 3: TMM for Infinite Rod with Spring-Mass-Dashpot Resonators

In this part, damped system denoting linear viscous damping coefficient (C_1) is considered (Figure (3.10)).

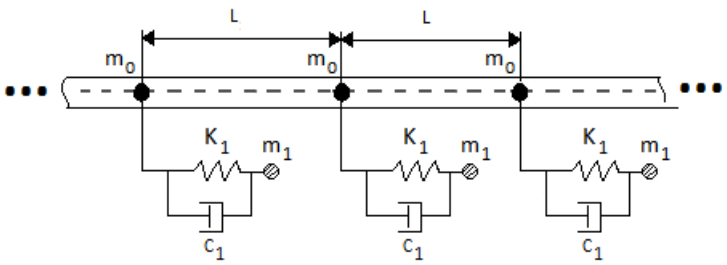

Figure 3.10: Repeated mass-spring-damper element for a rod (1DoF) [98]

Before proceeding to the next step, we evaluate the inherent damping due to viscosity for a rectangular tank. The damping ratio (ζ), in general, depends on the physical properties of the fluid (kinematic viscosity) and the geometry of the tank (diameter, especially the width of the tank for the rectangular cross section). Based on empirical and dimensional analysis, ζ has the general form [98]:

$$\zeta = G\left(\frac{\upsilon}{d^{3/2}\sqrt{g}}\right)^a \tag{3.84}$$

where d is the characteristic dimension of the tank, which is equal to the width of the rectangular container, υ is the kinematic viscosity, G and a are constants. By experimentally determining the values of the constant G and exponent a, the damping ratio can be calculated. For our case: G=1.0 and a=0.5 [98]. As it is calculated for TM of a simple spring-mass resonator, we wish to do the same work

here, that is, first, the force diagram of each mass is investigated separately (Figure (3.9)), and then we arrange the equations in matrix form.

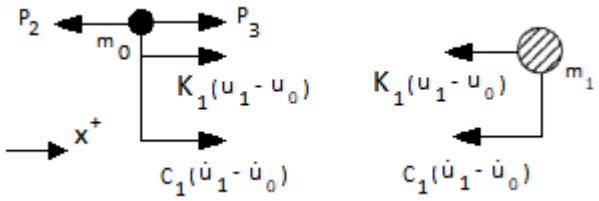

Figure 3.11: Force configuration of the segment in Figure (3.10)

Note that for two masses (m_0 and m_1) the harmonic oscillation is assumed;

$$u_0 = \mathbf{U}_0(\mathbf{x})e^{i\omega t} \tag{3.85}$$

$$u_1 = \mathbf{U}_1(\mathbf{x})e^{i\omega t} \tag{3.86}$$

As a result:

$$\dot{u}_0 = (i\omega)u_0 \tag{3.87}$$

$$\dot{u}_1 = (i\omega)u_1 \tag{3.88}$$

And:

$$\ddot{u}_0 = (-\omega^2)u_0 \tag{3.89}$$

$$\ddot{u}_1 = (-\omega^2)u_1 \tag{3.90}$$

Governing of the equation of motion is required to apply Newton Law, leading to:

$$-K_1(u_1 - u_0) - C_1(\dot{u}_1 - \dot{u}_0) = m_1\ddot{u}_1 \tag{3.91}$$

$$P_3 - P_2 + K_1(u_1 - u_0) + C_1(\dot{u}_1 - \dot{u}_0) = m_0\ddot{u}_0 \tag{3.92}$$

Inserting the value obtained from Equations (3.88) and (3.90) into (3.91) leads to the following:

$$u_1 = \left(\frac{K_1 + i\omega C_1}{K_1 + i\omega C_1 - m_1\omega^2}\right) u_0 \tag{3.93}$$

For the spring-mass-dashpot system in Figure (3.10),

$$C_{\text{cr1}} = 2m_1\omega_1 \tag{3.94}$$

where C_{cr1} are the critical damping coefficient. Also,

$$\zeta = \frac{C_1}{C_{\text{cr1}}} = \frac{C_1}{2m_1\omega_1} \tag{3.95}$$

So, we can obtain the dimensionless form of Equation (3.93),

$$u_1 = \left(\frac{1 + i\dfrac{2\zeta}{\omega_1}}{1 + i2\zeta\dfrac{\omega}{\omega_1} - \left(\dfrac{\omega}{\omega_1}\right)^2}\right) u_0 \tag{3.96}$$

Similarly, after substituting Equations (3.87) and (3.89) into (3.92), we reach the following.

$$P_3 = P_2 + \left(\frac{(m_1 m_0)\omega^4 - (m_1 + m_0) i C_1 \omega^3 - (m_1 + m_0) K_1 \omega^2}{-m_1\omega^2 + i C_1 \omega + K_1} \right) u_0 \tag{3.97}$$

In order to acquire the TMM for the system, the following matrices should be considered:

$$\begin{pmatrix} u_3 \\ P_3 \end{pmatrix} = \begin{bmatrix} \frac{(m_1 m_0)\omega^4 - (m_1+m_0) i C_1 \omega^3 - (m_1+m_0) K_1 \omega^2}{-m_1\omega^2 + i C_1 \omega + K_1} & 0 \\ 1 & 1 \end{bmatrix} \begin{pmatrix} u_2 \\ P_2 \end{pmatrix} \tag{3.98}$$

Or,

$$\begin{pmatrix} u_3 \\ P_3 \end{pmatrix} = \begin{bmatrix} R & 0 \\ 1 & 1 \end{bmatrix} \begin{pmatrix} u_2 \\ P_2 \end{pmatrix} \tag{3.99}$$

where:

$$R = \frac{(m_1 m_0)\omega^4 - (m_1 + m_0) i C_1 \omega^3 - (m_1 + m_0) K_1 \omega^2}{-m_1\omega^2 + i C_1 \omega + K_1} \tag{3.100}$$

Dimensionless form of R is:

$$R = \frac{\frac{m_0}{\omega_1^2}\omega^4 - \left(\frac{m_1+m_0}{\omega_1}\right) 2i\zeta\omega^3 - (m_1 + m_0)\omega^2}{-\frac{1}{\omega_1^2}\omega^2 + \frac{2i\zeta}{\omega_1}\omega + 1} \tag{3.101}$$

By re-writing Equation (3.98):

$$\begin{pmatrix} u_3 \\ P_3 \end{pmatrix} = \mathbf{T}_2 \begin{pmatrix} u_2 \\ P_2 \end{pmatrix} \tag{3.102}$$

In which $\mathbf{T}_2$ is the part of TM considering the resonator elements (spring, mass, and damper). Finally, we have the following relation between the degree of freedoms of points 3 (right) and a (left);

$$\begin{pmatrix} u_3 \\ P_3 \end{pmatrix} = \mathbf{T}_2 \cdot \mathbf{T}_1 \begin{pmatrix} u_a \\ P_a \end{pmatrix} = \mathbf{T} \begin{pmatrix} u_a \\ P_a \end{pmatrix} \tag{3.103}$$

Since k is the wave number, we define the wavelength ($\bar{\lambda}$) as: $\bar{\lambda}$=kL. For simplicity of notation, the dynamic contribution of the resonator is denoted by D, where D corresponds to the frequency-dependent term defined in Equation (3.83), so:

$$\mathbf{T} = \begin{bmatrix} \cos(\bar{\lambda}) - \dfrac{\sin(\bar{\lambda})}{EAk} R & \dfrac{\sin(\bar{\lambda})}{EAk} \\ -(EAk)\sin(\bar{\lambda}) - \cos(\bar{\lambda}) R & \cos(\bar{\lambda}) \end{bmatrix} \tag{3.104}$$

This part analyzes wave propagation in a periodic fluid–filled pipe system equipped with a series of rectangular tanks acting as local resonators. Each tank, partially filled with liquid, behaves as a multi–degree-of-freedom (MDOF) resonating substructure that introduces additional mass and stiffness to the host pipe through fluid–structure interaction. The dynamic coupling between the pipe wall and the internal sloshing modes modifies the effective impedance of the unit cell, thereby altering the global wave propagation characteristics. Following the formulation proposed by Xiao *et al.* [220], the governing equations are expressed in matrix form,

where the global mass and stiffness matrices of the unit cell include both the structural contribution of the pipe segment and the dynamic effects of the attached fluid domain. These additional degrees of freedom produce frequency-dependent effective parameters, which lead to pronounced dispersion phenomena typical of acoustic metamaterials. Applying the Bloch–Floquet periodic boundary condition, the spectral element (SE) formulation is employed to derive the complex dispersion relation of the infinite periodic pipe–tank system. The computed dispersion curves reveal distinct band-gap regions: the low-frequency gaps are governed by the local resonance of the liquid oscillations inside the tanks, while the higher-frequency gaps arise from Bragg scattering due to the periodic repetition of the unit cell. Such coupled configurations, which combine periodicity and local fluid resonance, significantly enhance vibration attenuation efficiency and enable tailored control of longitudinal wave transmission in fluid-filled structures [90, 41].

3.4.4 Case 4: DSM for Infinite Rod with N Spring-Mass Resonators

Consider a locally resonant metamaterial rod system composed of an infinitely long, uniform hollow rod with identical multi-degree-of-freedom (MDOF) resonators periodically attached to its interior (Figure 3.12). L is the spacing of the resonators. Each resonator consists of a series of springs k_i and masses m_i.

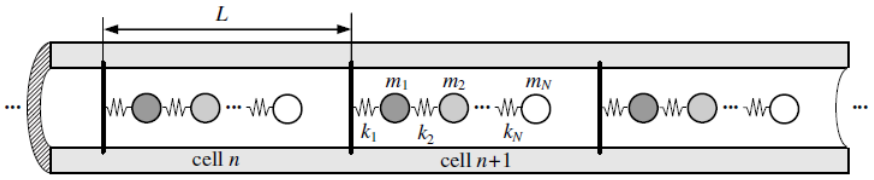

Figure 3.12: An infinite metamaterial-based rod with a periodic array of MDOF spring–mass resonators [220]

The equation of motion of the resonator can be written as [220]:

$$(\mathbf{K} - \omega^2 \mathbf{M})\mathbf{q} = \mathbf{F} \tag{3.105}$$

where the stiffness and mass matrices and the vectors of degrees of freedom and forces are [220]:

$$\mathbf{K} = \begin{bmatrix} k_1 & k_{1r} \\ \mathbf{k}_{r1} & \mathbf{k}_{rr} \end{bmatrix}, \quad \mathbf{M} = \begin{bmatrix} 0 & 0 \\ 0 & \mathbf{m}_{rr} \end{bmatrix}, \quad \mathbf{q} = \begin{Bmatrix} q_0 \\ \mathbf{q}_r \end{Bmatrix}, \quad \mathbf{F} = \begin{Bmatrix} F_0 \\ \mathbf{F}_r \end{Bmatrix}. \tag{3.106}$$

and:

$$\mathbf{k}_{\mathrm{rl}} = \mathbf{k}_{\mathrm{lr}}^{\mathrm{T}} = \begin{bmatrix} -k_1 \\ 0 \\ 0 \\ \vdots \\ 0 \end{bmatrix}, \quad \mathbf{k}_{\mathrm{rr}} = \begin{bmatrix} k_1 + k_2 & -k_2 & 0 & \cdots & 0 \\ -k_2 & k_2 + k_3 & -k_3 & \cdots & \vdots \\ 0 & -k_3 & \ddots & \ddots & 0 \\ \vdots & \vdots & \ddots & k_{N-1} + k_N & -k_N \\ 0 & \cdots & 0 & -k_N & k_N \end{bmatrix} \tag{3.107}$$

$$\mathbf{m}_{\mathrm{rr}} = \begin{bmatrix} m_1 & 0 & 0 & \cdots & 0 \\ 0 & m_2 & 0 & \cdots & 0 \\ 0 & 0 & \ddots & \ddots & \vdots \\ \vdots & \vdots & \ddots & m_{N-1} & 0 \\ 0 & 0 & \cdots & 0 & m_N \end{bmatrix}, \quad \mathbf{q}_{\mathrm{r}} = \begin{Bmatrix} q_1 \\ q_2 \\ \vdots \\ q_{N-1} \\ q_N \end{Bmatrix}, \quad \mathbf{F}_{\mathrm{r}} = \begin{Bmatrix} F_1 \\ F_2 \\ \vdots \\ F_{N-1} \\ F_N \end{Bmatrix} \tag{3.108}$$

q_0 is the displacement of the attachment point, q_i is the displacement of the ith mass, F_0 is the reaction force of the rod at the attachment point and F_i is the external force acting on the ith mass. If no external forces act on the masses so that $\mathbf{F}_{\mathrm{r}} = \mathbf{0}$, the displacement vector of the resonator, $\mathbf{q}_{\mathrm{r}}$, can be obtained. Equation (3.105) will be reduced to:

$$F_0 = D_0 q_0 \tag{3.109}$$

where D_0 is the dynamic stiffness of the resonator at the attachment point, which can be expressed as [220]:

$$D_0 = k_1 - \mathbf{k}_{\mathrm{lr}} \left(\mathbf{k}_{\mathrm{rr}} - \omega^2 \mathbf{m}_{\mathrm{rr}} \right)^{-1} \mathbf{k}_{\mathrm{rl}} \tag{3.110}$$

If an additional lumped mass, m_0, is mounted at the attachment point, the expression for D_0 should be modified by $D_0' = -\omega^2 m_0 + D_0$ to include the dynamic effects of the lumped mass. The longitudinal vibration of the finite rod in a unit cell can be represented using the Spectral Element (SE) method, which yields the corresponding SE matrix [124, 61].

$$\mathbf{D}_{\mathrm{rod}} = \begin{bmatrix} D_{11} & D_{12} \\ D_{21} & D_{22} \end{bmatrix} = EA\beta \begin{bmatrix} \cot(\beta L) & -\csc(\beta L) \\ -\csc(\beta L) & \cot(\beta L) \end{bmatrix} \tag{3.111}$$

where $\beta = \omega / c_0 = \omega / \left(\frac{E}{\rho} \right)^{1/2}$ is the wavenumber of longitudinal waves in the rod, c_0 is the wave speed, E and ρ are the Young's modulus and density of the rod material, and A is the cross-sectional area of the rod. Thus, the equation of motion for the entire unit cell of the infinite periodic system can be written as:

$$\mathbf{D}\mathbf{u}_{\mathrm{c}} = \mathbf{f}_{\mathrm{c}} \tag{3.112}$$

where:

$$\mathbf{u}_{\mathrm{c}} = \begin{Bmatrix} u_L \\ u_R \end{Bmatrix}, \quad \mathbf{f}_{\mathrm{c}} = \begin{Bmatrix} f_L \\ f_R \end{Bmatrix} \tag{3.113}$$

$$\mathbf{D} = \begin{bmatrix} D_{LL} & D_{LR} \\ D_{RL} & D_{RR} \end{bmatrix} = \begin{bmatrix} D_{11} + D_0 & D_{12} \\ D_{21} & D_{22} \end{bmatrix} = EA\beta \begin{bmatrix} \cot(\beta L) + \dfrac{D_0}{EA\beta} & -\csc(\beta L) \\ -\csc(\beta L) & \cot(\beta L) \end{bmatrix} \tag{3.114}$$

$\mathbf{D}$ is the dynamic stiffness matrix of the entire unit cell that includes the dynamic effects of the local resonator (represented by the arrows D_0), $\mathbf{u}_{\mathrm{c}}$ and $\mathbf{f}_{\mathrm{c}}$ are, respectively, the displacement vector and the loading force vector of the boundary of the unit cell, and the subscripts 'L' and 'R' denote the left and right sides of the unit cell. According to Bloch's theorem, wave propagation in an infinite periodic system follows the principle that:

$$u_{\mathrm{R}} = e^{\mu} u_{\mathrm{L}} \tag{3.115}$$

$$f_{\mathrm{R}} = -e^{\mu} f_{\mathrm{L}} \tag{3.116}$$

where μ is the propagation constant [139, 142, 49]. The real part of μ is the 'attenuation constant', and the imaginary part is the 'phase constant'. These quantities characterize the amplitude attenuation and the phase shift of wave motion between neighboring periodic unit cells, respectively. Note that the Bloch wave vector (also known as the Bloch wavenumber), $\boldsymbol{b}$, which is commonly used in studies of phononic crystal (PC), is related to the propagation constant by:

$$\mu = -i\boldsymbol{b}L \tag{3.117}$$

Consequently, the imaginary part of the Bloch wave vector, $\mathrm{Im}(\boldsymbol{b})$, which describes the exponential decay of the wave amplitude per unit length, is directly associated with the attenuation constant through the relation [220]:

$$\mathrm{Re}(\mu) = \mathrm{Im}(\boldsymbol{b}) \times L \tag{3.118}$$

Inserting Equation (3.115) into the first row of Equation (3.112) leads to the following relationship between f_L and u_L:

$$f_L = (D_{LL} + e^{\mu} D_{LR})\, u_L \tag{3.119}$$

Combining Equation (3.116) with the second row of Equation (3.112) produces the quadratic eigenvalue problem for e^{μ} [220]:

$$\left[D_{RL} + (D_{LL} + D_{RR})e^{\mu} + D_{LR}\, e^{2\mu}\right] u_L = 0 \tag{3.120}$$

One solution is as follows.

$$D_{RL} + (D_{LL} + D_{RR})e^{\mu} + D_{LR}\, e^{2\mu} = 0 \tag{3.121}$$

Substituting the elements of the dynamic stiffness matrix $\mathbf{D}$ into Equation (3.121) gives:

$$\cosh(\pm\mu) = \cos(\beta L) + \frac{\bar{D}}{2}\sin(\beta L) \tag{3.122}$$

where:

$$\bar{D} = \frac{D_0}{EA\beta} \tag{3.123}$$

$\bar{D}$ is the non-dimensional dynamic stiffness of the resonators. Equation (3.122) offers a direct method for determining the propagation constants, enabling the evaluation of the complex band structure of the infinite periodic system.

3.5 Modeling Periodic Boundary Conditions

Periodic boundary conditions (PBCs) are used in modeling systems that exhibit translational symmetry or repeating patterns. These conditions enable researchers to simulate infinite or large-scale systems using only a single or a few unit cells, drastically reducing computational demands while accurately capturing the global behavior of the system [141, 94]. PBCs are widely used in wave propagation, structural dynamics, fluid sloshing, heat transfer, and electromagnetic modeling, particularly in systems that can be characterized by spatial periodicity [129, 169]. In the context of sloshing and fluid-structure interaction (FSI), PBCs play an important

role in analyzing the dynamics of systems such as periodic arrays of liquid dampers, tank walls with repeating compartments, and acoustic-structural systems. The application of PBCs in such problems not only improves the efficiency of modeling but also allows the use of Bloch-Floquet theory to explore wave phenomena such as band gaps, pass bands, and resonance behavior [129, 169].
The basic concept of periodic boundary conditions is that the physical field under consideration (whether displacement, pressure, temperature, or potential) is repeated exactly after a certain spatial interval. Mathematically, for a one-dimensional problem, periodicity implies:

$$\mathbf{f}(x + L) = \mathbf{f}(x) \tag{3.124}$$

where f(x) is a scalar or vector-valued field variable (e.g., displacement or pressure), and L is the period of the unit cell. This condition ensures that the left and right boundaries of the unit cell behave identically, effectively modeling a seamless infinite array of repeating domains.
When dealing with harmonic wave propagation through periodic media, it is necessary to account for phase shifts across the boundaries. This leads to the Bloch-Floquet condition [219]:

$$\mathbf{f}(x + L) = \mathbf{f}(x)e^{ikL} \tag{3.125}$$

Here, $kL = \mu$ is the Bloch wave number, representing the phase change of the propagating wave between one cell and the next one.
To study stop-band formation and wave propagation in periodic media, it is essential to compute the dispersion relations that describe how waves travel through a repetitive structure [94]. A dispersion curve represents the relationship between the excitation frequency ω and the wavenumber k, which defines the spatial periodicity of the propagating wave. In the case of periodic structures, Bloch waves are considered and the propagation constant is used μ. Each branch of the dispersion diagram corresponds to a possible vibration mode of the periodic system, where the slope of the curve indicates the phase velocity of the wave. Frequency ranges where no real wavenumber exists correspond to band gaps in which wave propagation is inhibited. These frequency intervals arise either from Bragg scattering, due to destructive interference between waves reflected at the cell interfaces, or from local resonance effects when attached substructures exhibit their own dynamic response. An illustrative example is shown in Figure (3.13), where a one-dimensional beam carrying a periodic array of lumped masses exhibits alternating pass and stop bands, demonstrating the influence of periodicity on longitudinal wave transmission.

In a periodic beam subjected to axial or flexural vibration, the displacement, u, at one end of the unit cell is related to the other end by a complex factor. The resulting formulation helps identify pass bands (where waves propagate) and stop bands (where wave motion is suppressed due to destructive interference).

PBCs are particularly useful in our case for prediction vibration attenuation zones in periodic tank systems, such as rows of fluid-filled chambers or tuned liquid dampers arranged periodically along a structure. Instead of modeling the entire system, a single cell with appropriate boundary conditions can be used to predict how pressure waves and free surface motion propagate throughout the array [68, 98]. In such systems, both continuity of displacements and dynamic equilibrium (force or pressure matching) are enforced across periodic boundaries.

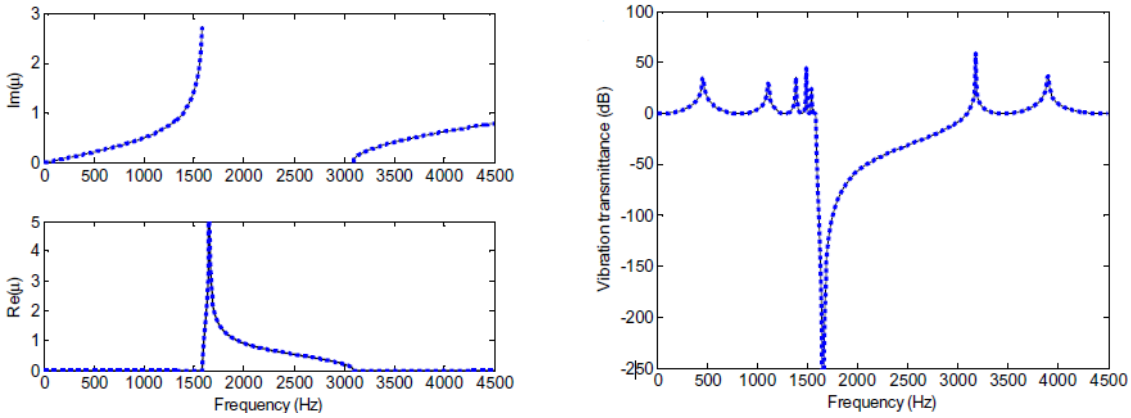

(a) (b)

Figure 3.13: Band gap characteristics of a rod with a periodic array of SDOF resonators: (a) Propagation constants/complex band structure of the system and (b) vibration transmittance of a finite system with eight unit cells [220]

In periodic tanks, the interaction between neighbouring chambers results in coupled sloshing modes, and the presence of periodic boundaries allows the study of how energy is transferred across units [218].

3.6 Effects of Periodicity and Resonances

Periodicity and resonance, as discussed earlier, can play an important role in determining the dynamic behavior of fluid–structure coupled systems in terms of vibration attenuation. The combined influence of periodicity and resonance governs the dynamic response of the pipe–tank system. In a periodically arranged structure, the repetition of identical unit cells introduces interference effects that modify the propagation of longitudinal waves along the host pipe. The fluid inside each tank behaves as a local resonator: the sloshing and compressional modes of the liquid which introduce additional inertia and stiffness, generating localized resonances that produce low-frequency band gaps. On the other hand, due to repetitive structure, we have Bragg band. When these two mechanisms coexist, their interaction can be tailored to enhance vibration attenuation over a wide frequency range.

The periodic configuration therefore affects both the stiffness and mass distribution of the host structure, producing a frequency-dependent impedance. This controls how energy is transmitted or reflected from cell to another cell. At specific frequencies, the waves reflected inside each unit cell interfere with one another in such a way that they cancel out. This destructive interference prevents the wave from propagating through the structure, creating what is known as a band gap (a frequency range where transmission is nearly zero). Conversely, at pass-band frequencies, the propagating modes remain in phase across the periodic interfaces, enabling efficient transmission of longitudinal motion along the structure.

To better understand the effect of periodic resonance and Bragg-type band gaps, both types of stop-bands are shown in Figure (3.14).

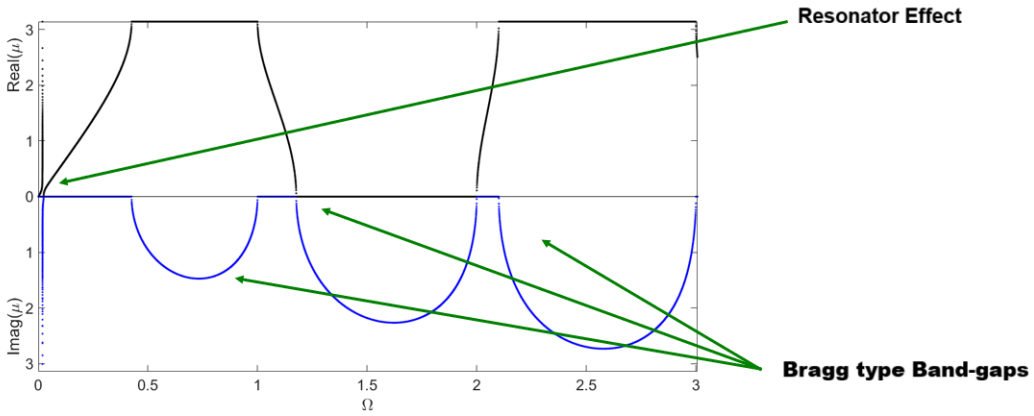

Figure 3.14: The Effects of Resonator and Bragg-Type on Band-Gap Formation

The resonance behavior of the liquid-filled tanks can also be used to adjust where the stop band appears, allowing the designer to shift the attenuation range to the desired frequencies. By changing the tank geometry, the height of the liquid or the stiffness of the connection, the natural frequencies of the local resonators can be adjusted so that their resonance coincides or complements the Bragg condition of structural periodicity. This combined mechanism forms the foundation of how the periodic liquid damper (PLD) works, with fluid sloshing and periodic scattering working together to reduce axial vibrations.

The influence of periodicity and resonance can be visualized through the dispersion relations, which relate the excitation frequency ω to the wavenumber k. The dispersion diagram illustrates how wave modes evolve across the frequency spectrum, highlighting the regions of propagating (real k) and evanescent (complex k) behavior.

In the present case, similar dispersion characteristics are obtained for the periodic pipe–tank system, confirming the formation of locally resonant and Bragg-type band gaps.
The quantitative effects of these mechanisms, along with their impact on the system's transmissibility, are examined in the next Subsection (3.6.1), where the proposed periodic liquid damper configuration is implemented in the reference pipe–tank model.

3.6.1 Dispersion Curves, Wavemodes, and Model Interpretation

To study wave propagation throughout the system including pipes and tanks, we focus on the equivalent one-dimensional structure. Each cell comprises a length structural segment L and a fluid-filled tank that acts as a locally resonant substructure, as illustrated in Figure (6.10).
The periodic repetition of these cells along the pipe gives rise to distinct wave propagation characteristics, which can be represented through the dispersion relation $k(\omega)$. This relation links the circular frequency ω to the wavenumber k and determines whether a wave can propagate or becomes evanescent within the structure. The dispersion curves are obtained by solving the eigenvalue problem derived from

the unit cell's dynamic stiffness matrix (DSM) under Bloch–Floquet boundary conditions:

$$\det[\mathbf{D}(\omega, k)] = 0,$$

where $\mathbf{D}(\omega, k)$ represents the dynamic stiffness of the coupled fluid–structure system. For a given wavenumber, the real roots of this equation correspond to propagating modes, whereas complex or imaginary wavenumbers indicate stop bands (frequency regions of attenuation). These band-gap regions emerge due to the combined effects of Bragg scattering - produced by the periodic geometry—and local resonance introduced by the sloshing motion of the internal fluid. Tuning can be achieved by modifying the length of the tank L, the depth of the fluid h, or adjusting the distribution of the damper units. The result is a controllable band gap structure that filters vibrations at selected frequencies [2].

Understanding the dispersion curves and the associated wavemodes is essential for interpreting the behaviour of the proposed PLD system. The spatial mode shapes along each branch show how the structural and fluid motions interact, indicating whether the response is dominated by the pipe, driven by fluid sloshing, or results from a hybrid coupling between the two domains.

Consider Figure (3.15) in which there is periodic system composed of identical unit cells. Each unit cell comprises a host segment of length L with a central fluid-filled container.

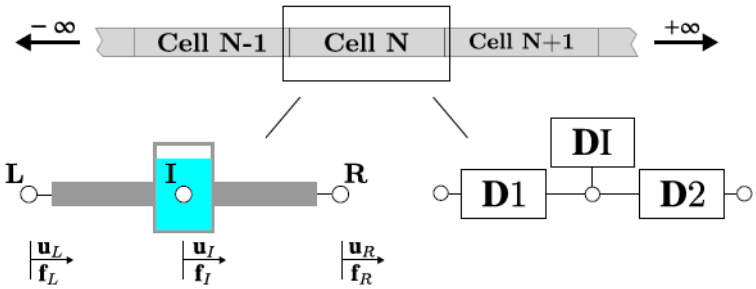

Figure 3.15: Illustration of the periodic fluid–structure system incorporating liquid dampers, including both the unit cell and its simplified model [12]

.

The equations of motion are derived using the dynamic stiffness matrix (DSM) method, which, in more advanced configurations, enables the combination of DSM and Finite Element (FE) techniques to construct and solve the equations of the global system. This approach also allows for the consideration of varying tank geometries. The formulation of the DSM for the unit cell in the above figure is given in Equation (3.126) [12]:

$$\begin{bmatrix} \mathbf{D}_{LL} & \mathbf{D}_{LI} & 0 \\ \mathbf{D}_{IL} & \mathbf{D}_{II} & \mathbf{D}_{IR} \\ 0 & \mathbf{D}_{RI} & \mathbf{D}_{RR} \end{bmatrix} \begin{Bmatrix} \mathbf{u}_L \\ \mathbf{u}_I \\ \mathbf{u}_R \end{Bmatrix} = \begin{Bmatrix} \mathbf{f}_L \\ 0 \\ \mathbf{f}_R \end{Bmatrix}. \tag{3.126}$$

The internal degrees of freedom are eliminated through dynamic condensation, resulting in a Dynamic Stiffness Matrix (DSM) that directly links the left and right

boundary states of the unit cell (Equation (3.127)).

$$\begin{bmatrix} \overline{\mathbf{D}}_{LL} & \overline{\mathbf{D}}_{LR} \\ \overline{\mathbf{D}}_{RL} & \overline{\mathbf{D}}_{RR} \end{bmatrix} \begin{Bmatrix} \mathbf{u}_L \\ \mathbf{u}_R \end{Bmatrix} = \begin{Bmatrix} \mathbf{f}_L \\ \mathbf{f}_R \end{Bmatrix} \tag{3.127}$$

where: $\overline{\mathbf{D}}_{LL} = \mathbf{D}_{LL} - \mathbf{D}_{LI}\mathbf{D}_{II}^{-1}\mathbf{D}_{IL}$, $\overline{\mathbf{D}}_{LR} = -\mathbf{D}_{LI}\mathbf{D}_{II}^{-1}\mathbf{D}_{IR}$; $\overline{\mathbf{D}}_{RL} = -\mathbf{D}_{RI}\mathbf{D}_{II}^{-1}\mathbf{D}_{IL}$, $\overline{\mathbf{D}}_{RR} = \mathbf{D}_{RR} - \mathbf{D}_{RI}\mathbf{D}_{II}^{-1}\mathbf{D}_{IR}$

Wave propagation within the periodic structure is analyzed using the Dynamic Stiffness Matrix (DSM) in conjunction with Floquet–Bloch theory. This methodology enables the computation of complex dispersion relations and wave modes by solving the associated quadratic eigenvalue problem:

$$\left[\lambda^2 \overline{\mathbf{D}}_{LR} + \lambda\left(\overline{\mathbf{D}}_{LL} + \overline{\mathbf{D}}_{RR}\right) + \overline{\mathbf{D}}_{RL}\right] \mathbf{u}_L = 0 \tag{3.128}$$

where $\lambda = e^{-i\mu}$ and μ is the propagation constant. Equation (3.128) is rewritten in the form of a linear eigenvalue problem to determine the left and right displacement fields, $\mathbf{u}_L$ and $\mathbf{u}_R$ [139, 15].

$$\left(\begin{bmatrix} \overline{\mathbf{D}}_{RL} & \overline{\mathbf{D}}_{RR} \\ \mathbf{0} & \mathbf{I} \end{bmatrix} - \lambda \begin{bmatrix} -\overline{\mathbf{D}}_{LL} & -\overline{\mathbf{D}}_{LR} \\ \mathbf{I} & \mathbf{0} \end{bmatrix} \right) \begin{Bmatrix} \mathbf{u}_L \\ \mathbf{u}_R \end{Bmatrix} = \begin{Bmatrix} \mathbf{0} \\ \mathbf{0} \end{Bmatrix}. \tag{3.129}$$

The solution of Equation (3.129) gives rise to two sets of eigenvalues, each associated with their corresponding right eigenvectors (λ^+) and (λ^-), representing waves propagating in the positive and negative directions. When no dissipation is considered, real and purely imaginary values of the propagation constant μ correspond to propagating and evanescent waves, respectively. In cases where μ is complex, its values appear as complex conjugate pairs, indicating the presence of a band gap. In the following, the imaginary component of μ is referred to as the attenuation constant, while the real component is called the phase constant.
Now, to evaluate wave propagation, we consider the following system in which nodal forces and displacements of the periodic structure can be expressed by the sum of positive end negative going waves of amplitudes a^+ and a^- [94] .

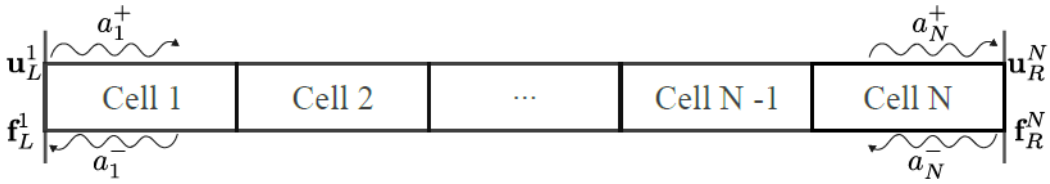

Figure 3.16: Illustrative diagram showing wave transmission and reflection in a finite structure made up of N repeating cells [94]

Based on the propagation constant, the relationship between wave amplitudes before and after passing through N cells (as illustrated in Figure (3.16)) is given by:

$$a_N^+ = \left(e^{-i\mu}\right)^N a_1^+; \qquad a_1^- = \left(e^{-i\mu}\right)^N a_N^- \tag{3.130}$$

Therefore, the corresponding nodal displacements and forces become the following:

$$\mathbf{u}_L^1 = \boldsymbol{\phi}_u^+ a_1^+ + \boldsymbol{\phi}_u^- \left(e^{-i\mu}\right)^N a_N^-; \qquad \mathbf{u}_R^N = \boldsymbol{\phi}_u^+ \left(e^{-i\mu}\right)^N a_1^+ + \boldsymbol{\phi}_u^- \bar{a}_N^-; \tag{3.131}$$

$$\mathbf{f}_L^1 = \boldsymbol{\phi}_f^+ a^+ + \boldsymbol{\phi}_f^- \left(e^{-i\mu}\right)^N a_N^-; \qquad \mathbf{f}_R^N = -\boldsymbol{\phi}_f^+ \left(e^{-i\mu}\right)^N a_1^+ - \boldsymbol{\phi}_f^- \bar{a}_N^-. \tag{3.132}$$

where ϕ_u^+ is the right-propagating eigenvector associated with the positive-direction travelling wave that comes from solving the Bloch–Floquet eigenvalue problem. ϕ_u^- is the corresponding eigenvector for a left-travelling wave (negative direction).

By merging Equations (3.131) and (3.132), the Dynamic Stiffness Matrix (DSM) representation for the entire periodic structure can be derived [142].

$$\mathbf{D} = \begin{bmatrix} \boldsymbol{\phi}_f^+ & \boldsymbol{\phi}_f^-(e^{-i\mu})^N \\ -\boldsymbol{\phi}_f^+(e^{-i\mu})^N & -\boldsymbol{\phi}_f^- \end{bmatrix} \begin{bmatrix} \boldsymbol{\phi}_u^+ & \boldsymbol{\phi}_u^-(e^{-i\mu})^N \\ -\boldsymbol{\phi}_u^+(e^{-i\mu})^N & -\boldsymbol{\phi}_u^- \end{bmatrix}^{-1} \tag{3.133}$$

Therefore, forces and displacements amplitudes at the two sides of the system are then given by:

$$\begin{bmatrix} \mathbf{D}_{11} & \mathbf{D}_{1N} \\ \mathbf{D}_{N1} & \mathbf{D}_{NN} \end{bmatrix} \begin{Bmatrix} \mathbf{u}_L^1 \\ \mathbf{u}_R^N \end{Bmatrix} = \begin{Bmatrix} \mathbf{f}_L^1 \\ \mathbf{f}_R^N \end{Bmatrix} \tag{3.134}$$

Assuming that the structure is excited by a harmonic force $\mathbf{f}_L^1$ at the left end and that no excitation is applied at the right end (i.e., $\mathbf{f}_R^N = 0$), the transmissibility between the two ends is given by the following [220]:

$$Tr = 20 \log \left(\left| -\mathbf{D}_{NN}^{-1} \mathbf{D}_{N1} \right| \right) \tag{3.135}$$

This quantity represents the ratio between the displacement amplitude at the right end of the structure, $\mathbf{u}_R^N$, and that at the left end, $\mathbf{u}_L^1$, where the external force is applied.

Vibration transmissibility is a valuable metric for characterizing the dynamic response of the structure. Specifically, vibration attenuation bands are identified in the frequency regions where $T_r < 0$. Consider Figure (3.17) in which Transmissibility (TR) (dB) and wave propagation characteristics are depicted [221].

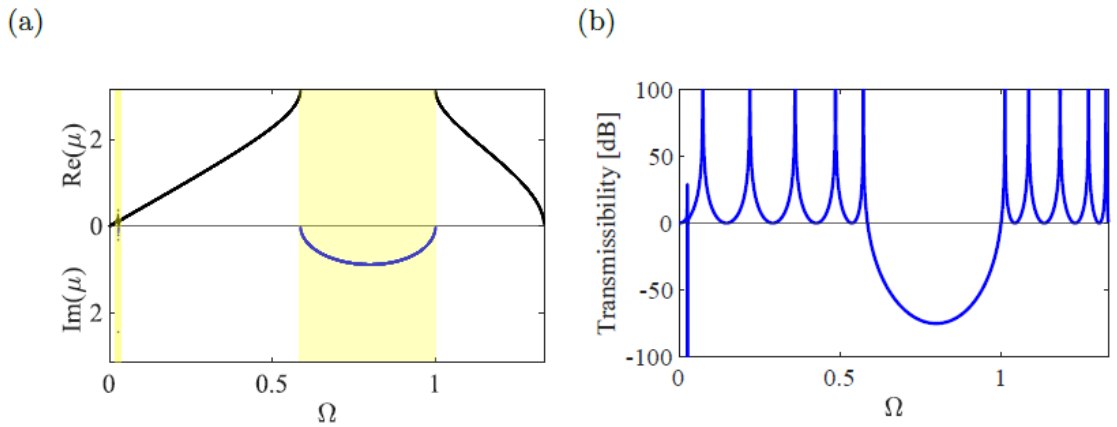

Figure 3.17: (a) Complex dispersion curves for waves propagating in the positive x direction. Black solid lines: pure propagating waves. Blue lines: evanescent waves. Yellow regions indicate band gaps. (b) Transmissibility - finite structure with five cells [221]

.

Note that the frequency Ω is dimensionless and defined by

$$\Omega = \frac{\omega L}{c_L} \tag{3.136}$$

where L is the length of a unit cell and c_L is the phase speed (that is, $c_L = \sqrt{\frac{E}{\rho}}$), respectively.

The lower branch corresponds to the fundamental longitudinal wave in the host structure, while higher branches represent modes dominated by the resonant dynamics of the fluid. Near the resonant frequencies of the liquid tanks, the interaction between the host structure and the fluid produces avoided crossings in the dispersion curves. These interactions generate low-frequency stop bands whose position can be tuned by adjusting the tank length L, the liquid height h, or the stiffness of the connection. The resulting dispersion features directly reveal the frequency regions where vibration transmission is either strongly suppressed or significantly enhanced. In the context of the periodic liquid damper (PLD), the identified stop bands correspond to frequency regions where the system naturally suppresses vibration propagation.

This chapter has presented a simplified analytical model of a tube with periodically attached liquid tanks, represented as an axially vibrating beam coupled with discrete resonators. Through the derivation of the Dynamic Stiffness Matrix (DSM) and the analysis of dispersion relations, the essential mechanisms of band gap formation, avoided crossings, and tunable stop bands have been identified. The results have clarified how periodicity and liquid-induced resonance interact to control vibration transmission within the proposed PLD configuration.

Although the analytical formulation provides valuable physical insight into wave propagation and resonance-induced attenuation, it is based on idealized mechanical representations of the fluid and its coupling with the host structure. A more rigorous treatment requires a formulation capable of directly incorporating fluid inertia, pressure fields, interface continuity conditions, and two-way coupling within a unified mathematical framework. For this reason, the following chapter introduces the finite element formulation of fluid–structure interaction problems. By expressing the governing equations in weak (variational) form, the analysis is extended to a multiphysics setting that enables consistent modelling of structural dynamics, acoustic fluid behaviour, and their coupled interaction in periodic liquid damper systems.

Chapter 4

Finite Element Formulation

In the field of structural dynamics, fluid-filled structures are found applications in numerous engineering applications, including aerospace tanks, nuclear reactors, and marine pipelines. These structures, when subjected to dynamic loads, can exhibit complex vibration behaviors due to interactions between the internal fluid and the host structure. Such vibrations, if not controlled, can lead to fatigue, resonance-induced failure, or long-term degradation of the system [182]. Therefore, vibration attenuation mechanisms have been intensively investigated, with Periodic Liquid Dampers (PLDs) emerging a possible passive control method. The design and analysis of such dampers is increasingly performed using Finite Element (FE) models, which offer a robust computational framework to capture the coupled dynamics of fluid and structure. When a structure containing fluid is subjected to external excitation, a fluid–structure interaction (FSI) takes place. In this process, the fluid mass responds to the motion of the structure and, in turn, imposes additional inertia forces and pressure loads back onto the container walls. This two-way coupling modifies the effective stiffness and damping properties of the structure. The structural formulation of FE models for fluid-filled systems with periodic liquid dampers (PLDs) integrates solid mechanics with fluid dynamics to simulate vibration attenuation mechanisms. The fluid within each damper is often modelled using a potential-based formulation depending on the frequency regime. The fluid-structure interaction is established through the continuity of normal velocities and the equilibrium of traction at the interface. The multiphysics FE formulation enables accurate prediction of dynamic responses, including natural frequencies, mode shapes, and attenuation bands in fluid-filled structures enhanced by PLDs.

In the Finite Element Method, the governing equations of motion are generally expressed in their weak form (also known as the variational formulation). This approach is not limited to a specific domain—such as the acoustic fluid—but is equally applicable to solid and fluid–structure interaction problems. The weak formulation is preferred over the strong form because many engineering problems involve discontinuities, complex geometries, or boundary conditions for which a classical (strong) solution may not exist. The weak formulation provides a mathematically consistent and computationally efficient foundation for both structural and acoustic analyses [246, 91, 16].

4.1 Solid Domain: Structural Dynamics FE Modelling

The Finite Element (FE) method is a cornerstone of modern computational mechanics, widely employed to analyze and predict the behavior of complex structural systems such as fluid-filled pipe–tank assemblies. The FE approach has become indispensable for studying the static and dynamic response of solids and coupled fluid–structure systems under various loading conditions. By discretizing a continuous domain into smaller, manageable subdomains—called elements—the method enables the accurate evaluation of stress, strain, pressure, and displacement fields, even in structures with irregular geometries or mixed boundary conditions.

In the context of the present research, which examines the dynamic behavior of fluid-filled periodic structures incorporating liquid tanks as passive dampers, the finite element (FE) formulation offers a systematic framework for accurately representing the interaction between the solid pipe walls and the internal fluid domain. The formulation is grounded in the principle of virtual work, which states that the virtual work performed by external forces must equal the corresponding internal and inertial virtual work. By discretizing the system, the structural and fluid domains are partitioned into finite elements, within which the displacement and pressure fields are approximated through suitable interpolation (shape) functions defined at discrete nodal points.

The resulting element matrices—including the stiffness, mass, coupling, and damping matrices—represent the relationships among nodal displacements, velocities, accelerations, and fluid pressures. These local matrices are then assembled into the global system of equations, which governs the coupled fluid–structure dynamics of the pipe–tank unit cell. To obtain the time-dependent response, numerical time-integration schemes such as the Newmark-β or Runge–Kutta methods are commonly employed [60].

The FE formulation begins from the strong form of the momentum equation [246]:

$$\rho\,\ddot{\mathbf{u}} - \nabla\cdot\boldsymbol{\sigma} = \mathbf{b} \quad \text{in } \Omega \tag{4.1}$$

where $\ddot{\mathbf{u}}$ is acceleration, $\mathbf{b}$ is the force of the body per unit volume (e.g. gravity), $\boldsymbol{\sigma}$ denotes the Cauchy stress tensor and Ω is the computational domain or the problem domain in the space over which the partial differential equations (PDEs) are defined. Apply the principle of virtual work:

$$\int_\Omega \delta\mathbf{u}^T\rho\ddot{\mathbf{u}}\,d\Omega + \int_\Omega \delta\boldsymbol{\varepsilon}^T\mathbf{D}\boldsymbol{\varepsilon}\,d\Omega = \int_\Omega \delta\mathbf{u}^T\mathbf{b}\,d\Omega + \int_{\Gamma_t}\delta\mathbf{u}^T\bar{\mathbf{t}}\,d\Gamma \tag{4.2}$$

where $\delta\mathbf{u}$ is the virtual displacement vector, the density of the material ρ, the acceleration $\ddot{\mathbf{u}}$, the strain ε, the constitutive matrix $\mathbf{D}$ (from Hooke's law), $\bar{t}$ traction on the Neumann boundary surface Γ_t.
The space over which the partial differential equations (PDEs) are defined is denoted by Ω.

The weak form can be specialized for one-dimensional structural elements, such as beams. To illustrate, consider the Euler–Bernoulli beam in transverse displacement $w(x,t)$. The corresponding strong form (governing differential equation) reads:

$$\rho A\frac{\partial^2 w(x,t)}{\partial t^2} + EI\frac{\partial^4 w(x,t)}{\partial x^4} = f(x,t) \tag{4.3}$$

where A is the cross-sectional area, E the Young's modulus, and I the second moment of area. To derive the weak form of Equation (4.3), we multiply both sides by the virtual displacement δw and integrate over the domain $\Omega = [0, L]$:

$$\int_0^L \delta w \, \rho A \ddot{w} \, dx + \int_0^L EI \, \frac{d^2 \delta w}{dx^2} \frac{d^2 w}{dx^2} \, dx = \int_0^L \delta w \, f(x,t) \, dx \tag{4.4}$$

Integration by parts of the second term reduces the derivative order and introduces boundary terms associated with bending moments and shear forces. This constitutes the weak (variational) form of the beam equation, suitable for finite element implementation.

In the finite element method, the field variable $w(x,t)$ and its virtual counterpart δw are approximated by shape functions $N_i(x)$ and nodal values $w_i(t)$:

$$w(x,t) = \sum_{i=1}^{n} N_i(x) \, w_i(t), \qquad \delta w(x,t) = \sum_{i=1}^{n} N_i(x) \, \delta w_i(t) \tag{4.5}$$

Substituting these approximations into Equation (4.4) and assembling over all elements yields the discrete FE equations of motion in matrix form:

$$\mathbf{M}\ddot{\mathbf{w}} + \mathbf{K}\mathbf{w} = \mathbf{F} \tag{4.6}$$

where $\mathbf{M}$ is the consistent mass matrix, $\mathbf{K}$ the stiffness matrix, and $\mathbf{F}$ the equivalent nodal force vector. This formulation establishes the link between the principle of virtual work and the finite element discretization.
By substituting the Hermite interpolation functions into the weak form (Equation 4.6), the governing equation can be expressed in matrix form as [175]:

$$\mathbf{M}_e \, \ddot{\mathbf{w}}_e + \mathbf{K}_e \, \mathbf{w}_e = \mathbf{F}_e,$$

where $\mathbf{M}_e$, $\mathbf{K}_e$ and $\mathbf{F}_e$ are the element mass, stiffness matrices, and force nodal, respectively, defined as

$$\mathbf{M}_e = \int_{\Omega_e} \rho A \, \mathbf{N}^T \mathbf{N} \, dx, \qquad \mathbf{K}_e = \int_{\Omega_e} EI \, \mathbf{B}^T \mathbf{B} \, dx,$$

with $\mathbf{N}$ representing the Hermite shape function matrix and $\mathbf{B} = \frac{d^2 \mathbf{N}}{dx^2}$ the corresponding strain–displacement matrix.

For a two-node Euler–Bernoulli beam element, the displacement field is interpolated as

$$w(x,t) = [N_1(x) \; N_2(x) \; N_3(x) \; N_4(x)] \begin{Bmatrix} w_1 \\ \theta_1 \\ w_2 \\ \theta_2 \end{Bmatrix},$$

where w_i and θ_i denote the transverse displacement and rotation at node i, respectively.

Substituting these shape functions into the above integrals yields the standard element stiffness matrix

$$\mathbf{K}_e = \frac{EI}{L^3} \begin{bmatrix} 12 & 6L & -12 & 6L \\ 6L & 4L^2 & -6L & 2L^2 \\ -12 & -6L & 12 & -6L \\ 6L & 2L^2 & -6L & 4L^2 \end{bmatrix},$$

and the consistent mass matrix

$$\mathbf{M}_e = \frac{\rho AL}{420}\begin{bmatrix} 156 & 22L & 54 & -13L \\ 22L & 4L^2 & 13L & -3L^2 \\ 54 & 13L & 156 & -22L \\ -13L & -3L^2 & -22L & 4L^2 \end{bmatrix}.$$

Where L is the length of the element. These matrices form the basis for assembling the global FE model of the beam and are widely used in vibration and modal analyses [167].

4.2 Fluid Domain: Acoustic FE Model

The fluid is considered incompressible because we are studying acoustic wave transmission, band gaps, or modal/harmonic pressure fields in the fluid. To capture sound wave propagation, the fluid must be modelled as incompressible, governed by the wave or Helmholtz equation (used in acoustic analysis) [18]. The formulation of acoustic finite elements is applied to model the propagation of sound waves. The acoustic wave equation, which describes sound wave propagation in a fluid, is given by [129]:

$$\nabla^2 p - \frac{1}{c^2}\frac{\partial^2 p}{\partial t^2} = 0 \tag{4.7}$$

where p is the acoustic pressure and c is the speed of sound. Weak formulation converts the strong form of the wave equation into its weak form by multiplying with a function and integrating over the domain.
In FE modelling of fluid-filled structures with periodic liquid dampers (PLDs), the weak formulation is employed in both the solid and fluid domains to ensure a consistent coupling of their governing equations. In the structural domain, it governs the elastic vibration equations, while in the fluid domain it is used to derive the acoustic or sloshing wave equations.

The weak form is particularly advantageous for fluid–structure interaction (FSI) problems, as it naturally enforces the continuity conditions at the fluid–structure interface. When the variational of the solid and fluid subdomains are combined, the integration introduces boundary terms that automatically impose the continuity of traction and normal velocity (or displacement) across the fluid–structure interface. This feature eliminates the need for separate constraint equations and provides a unified mathematical framework for coupling the two fields [18].

Discretization is applied to divide the domain into finite elements and the approximate measurement of the pressure field using shape functions:

$$p \approx \sum_i N_i p_i \tag{4.8}$$

where N_i are the shape functions and p_i are the nodal pressures In the finite element framework, the continuous pressure field $p(x,t)$ within each element is approximated by a weighted combination of nodal values through these interpolation functions. The choice of N_i depends on the element type (e.g., linear, quadratic) and determines the accuracy and continuity of the approximate solution.

The spatial discretization using shape functions transforms the governing partial differential equations into a system of ordinary differential equations of the form. This algebraic system is then solved using an appropriate time-integration scheme—such as the Newmark-β or Runge–Kutta methods—to determine the transient pressure or displacement response of the structure [246, 167].

4.2.1 Governing Fluid Equations and Simplified Acoustic Formulation

The motion of a viscous and incompressible fluid is governed by the Navier–Stokes equations, which represent the conservation of mass and momentum in the strong form:

$$\nabla \cdot \mathbf{u} = 0, \tag{4.9}$$

$$\rho \left(\frac{\partial \mathbf{u}}{\partial t} + \mathbf{u} \cdot \nabla \mathbf{u} \right) = -\nabla p + \mu \nabla^2 \mathbf{u} + \mathbf{f}, \tag{4.10}$$

where $\mathbf{u}$ is the velocity field, p the pressure, ρ the density, μ the dynamic viscosity, and $\mathbf{f}$ the body force per unit volume.

In a finite element framework, these equations are transformed into their weak (variational) form by multiplying the governing equations by suitable test functions and integrating over the domain [167]:

$$\int_\Omega q \, (\nabla \cdot \mathbf{u}) \, d\Omega = 0, \tag{4.11}$$

$$\int_\Omega \left[\rho \left(\frac{\partial \mathbf{u}}{\partial t} + \mathbf{u} \cdot \nabla \mathbf{u} \right) \cdot \mathbf{v} + \mu \, \nabla \mathbf{u} : \nabla \mathbf{v} - p \, (\nabla \cdot \mathbf{v}) \right] d\Omega = \int_\Omega \mathbf{f} \cdot \mathbf{v} \, d\Omega, \tag{4.12}$$

where $\mathbf{v}$ and q are the weighting functions (test functions) for the velocity and pressure fields, respectively. Also $\nabla \mathbf{u} : \nabla \mathbf{v}$ is a double contraction ($\nabla \mathbf{u} : \nabla \mathbf{v} = \sum_{i=1}^{3} \sum_{j=1}^{3} \frac{\partial u_i}{\partial x_j} \frac{\partial v_i}{\partial x_j}$).

The discretization of finite elements of $\mathbf{u}$ and p then converts these equations into a system of nonlinear algebraic equations that can be solved iteratively [246].

While the full Navier–Stokes formulation is necessary to capture strongly nonlinear flow phenomena (e.g., turbulence, large free-surface motion, or vortex formation), it is computationally demanding for large or periodic domains. In many engineering applications that involve small pressure oscillations and weak fluid motion—such as those encountered in fluid-filled periodic pipe–tank systems—the flow can be linearized around a quiescent reference state.

By assuming small perturbations of pressure and velocity and neglecting nonlinear convective and viscous terms, the Navier–Stokes equations reduce to the acoustic wave equation [170]. This linearized form accurately describes the propagation of pressure waves, resonances, and fluid–structure coupling effects under low-Mach-number conditions. This simplified acoustic formulation provides a computationally efficient yet physically consistent framework for modeling the dynamic interaction between the fluid and the structural walls of the periodic system [170, 16]. Acoustics can be derived by linearizing steady state for low Mach numbers and negligible mean flow.

Generally, if sloshing with large free-surface motion, vortices, nonlinear wave breaking are considered, we need Navier-Stokes (CFD/FSI). However, if we want pressure wave propagation, resonances, stop band diagrams, fluid-structure coupling with small oscillations, acoustic analysis is sufficient and much faster.

4.3 Fluid-Structure Coupling Techniques in FEA

Fluid-structure interaction (FSI) problems involve the mutual influence between deformable solid structures and surrounding or internal fluid. The interaction between the two analyses typically takes place at the boundaries that the mechanical model shares with the fluid model. These boundaries of interaction are called the fluid-structure interface. At this interface, the results of one analysis are passed on to the other analysis as loads [7]. In FEA, solving these problems requires simultaneous solutions of the fluid and solid subdomains, ensuring compatibility at their interface. In practice, fluid–structure interaction can be handled using either monolithic or partitioned coupling strategies. Each comes with its own strengths, and the choice between them usually depends on the level of nonlinearity in the problem, the stability needed, and the available computational resources. For the fluid domain, the Navier-Stokes equations are commonly used (Equations (4.9) and (4.10)).

In fluid–structure interaction (FSI) modelling, it is essential to define the appropriate reference frame in which the governing equations are formulated. The Lagrangian description is commonly adopted for the structural domain, where the mesh moves together with the material points, allowing the direct computation of displacements and stresses. Conversely, the Eulerian description is typically used for the fluid domain, where the mesh remains fixed in space while the fluid flows through it, making it convenient for tracking velocity and pressure fields.

However, in problems involving moving boundaries or large deformations—such as the oscillation of the free surface or wall motion in fluid-filled pipe–tank systems—the pure Lagrangian or Eulerian formulations become inefficient or inaccurate. To overcome these limitations, the Arbitrary Lagrangian–Eulerian (ALE) approach is employed. This hybrid approach captures the benefits of both descriptions. In practice, the mesh can move independently of the fluid itself, allowing it to track the deformation of the structure while still letting the fluid flow naturally within the domain.

The ALE framework is therefore particularly suited to fluid-filled periodic structures with internal liquid motion, as it ensures accurate representation of the fluid–structure interface, and facilitates stable numerical coupling between the two fields [16, 59].

For the solid domain, the dynamic equilibrium equation in total Lagrangian formulation is:

$$\rho_s \frac{\partial^2 \mathbf{u}_s}{\partial t^2} = \nabla \cdot \boldsymbol{\sigma}_s + \mathbf{f}_s \tag{4.13}$$

$\mathbf{u}_s$ is the displacement field, $\boldsymbol{\sigma}_s$ is the Cauchy stress tensor, ρ_s is solid density, and $\mathbf{f}_s$ are external forces.
At the fluid-structure interface Γ_{fs}, two essential continuity conditions must be enforced: 1) Kinematic compatibility (velocity continuity):

$$\mathbf{u}_f|_{\Gamma_{fs}} = \left.\frac{\partial \mathbf{u}_s}{\partial t}\right|_{\Gamma_{fs}} \tag{4.14}$$

2) Dynamic equilibrium (traction continuity):

$$\boldsymbol{\sigma}_f \cdot \mathbf{n}_f = \boldsymbol{\sigma}_s \cdot \mathbf{n}_s \tag{4.15}$$

This ensures that the fluid stresses are equal and opposite to structural stresses on the interface [215, 180]. As mentioned above, there are four coupling strategies. Here, we consider some points for each strategy.
1) Monolithic Approach: Solves the fluid and structure equations in a single system of equations. It ensures strong coupling and excellent stability for highly nonlinear problems but is computationally intensive and less modular [145].
2) Partitioned Approach: Solves fluid and solid equations separately using data exchange at the interface per time step. It is more flexible and allows using specialized solvers but may suffer from instabilities (e.g., added mass effect). Two types are: (a) Explicit partitioned: faster but less stable. (b) Implicit partitioned: more stable due to iterative sub-time step exchange [72].
3) Arbitrary Lagrangian-Eulerian (ALE) Formulation: Often used in monolithic and partitioned methods, ALE allows mesh deformation to track interface motion:

$$\frac{D\mathbf{u}}{Dt} = \frac{\partial \mathbf{u}}{\partial t} + (\mathbf{u} - \mathbf{u}_m) \cdot \nabla \mathbf{u} \tag{4.16}$$

where $\mathbf{u}_m$ is the mesh velocity [59].
4) Discretization: The Galerkin finite element formulation for the weak form of the structure reads [79]:

$$\int_\Omega \delta \mathbf{u}_s^T \left(\rho_s \frac{\partial^2 \mathbf{u}_s}{\partial t^2} - \nabla \cdot \boldsymbol{\sigma}_s \right) d\Omega = 0 \tag{4.17}$$

Coupled acoustic fluid-structural system with symmetric matrix equation for full harmonic analysis can be obtained by [7]:

$$\left(-\omega^2 \begin{bmatrix} [\mathbf{M}_S] & 0 \\ 0 & \frac{[\mathbf{M}_F]}{\overline{\rho}_0} + \frac{[\mathbf{S}_F]}{\overline{\rho}_0} \end{bmatrix} + j\omega \begin{bmatrix} [\mathbf{C}_S] & -[\mathbf{R}] \\ -[\mathbf{R}]^T & \frac{[\mathbf{C}_F]}{\overline{\rho}_0} \end{bmatrix} + \begin{bmatrix} [\mathbf{K}_S] & 0 \\ 0 & \frac{[\mathbf{K}_F]}{\overline{\rho}_0} \end{bmatrix} \right) \begin{Bmatrix} \mathbf{u}_e \\ \mathbf{q}_e \end{Bmatrix} = \begin{Bmatrix} \mathbf{f}_S \\ \frac{j f_F}{\omega \overline{\rho}_0} \tilde{\mathbf{f}} \end{Bmatrix} \tag{4.18}$$

where:

- $\omega = 2\pi f$ (where f is the frequency of oscillations of the pressure)
- $[\mathbf{M}_S]$ = mass matrix of the structure;
- $[\mathbf{M}_F]$ = mass matrix of the fluid;
- $\overline{\rho}_0$ = density of the structure (solid) in the reference configuration;
- $[\mathbf{S}_F]$ (added-mass-like matrix related to the interface (surface coupling)) $= \frac{\overline{\rho}_0}{g} \iint_{\Gamma_{SL}} \frac{1}{\rho_F} \{N\}\{N\}^T \, ds$ (where: ρ_F is fluid density, $\iint_{\Gamma_{SL}}$ is structural-liquid (fluid) interface boundary, N is shape functions employed to discretize the displacement components u, v, and w (obtained from the structural element);

- $j = \sqrt{-1}$;
- $[\mathbf{C}_S]$ = structural damping matrix;
- $[\mathbf{R}]^T$ (fluid-structure coupling matrix)
  $= \iint_{\Gamma_F} \{N\}\{\mathbf{n}\}^T\{N'\}^T\, ds$ (where Γ_F is fluid boundary, $\mathbf{n}$ is outward normal unit vector of fluid domain, ds is differential element of the surface area on the interface);
- $[\mathbf{K}_S]$ is stiffness matrix;
- $[\mathbf{K}_F]$ (fluid stiffness matrix (from Helmholtz/acoustic equation))
  $= \overline{\rho}_0 \iiint_{\Omega_F} \frac{1}{\rho_0} [\nabla N]^T [\nabla N]\, dv$ (where ρ_0 is local (possibly spatially varying) fluid density, Ω_F is fluid domain (volume integral), dv is differential volume element);
- $\mathbf{u}_e$ = structural nodal displacement vector;
- $\mathbf{q}_e$ = acoustic pressure degrees of freedom;
- $\mathbf{f}_S$ = structural external force vector;
- $\mathbf{f}_F$ = amplitude or magnitude of the fluid source excitation, such as a pressure load, an acoustic excitation, or a body force applied within the fluid domain;
- $\tilde{\mathbf{f}}$ = fluid excitation source (e.g., vibrating boundary or monopole).

4.4 Implementation in commercial and custom FE codes

Fluid–structure interaction (FSI) refers to the two–way coupling between a deformable or moving structure and the surrounding or internal fluid. From a numerical perspective, FSI problems are typically approached in two main ways: by using commercial multiphysics platforms—such as ANSYS, COMSOL Multiphysics, or Abaqus coupled with CFD solvers—or by developing custom, research–oriented codes that give the user more control and flexibility over the underlying formulation.

In commercial software, ANSYS performs FSI through its system coupling framework, which connects the structural solver (Mechanical) with the fluid solvers (Fluent or CFX). In this setup, the structure provides the fluid domain with displacements and velocities, while the fluid returns pressure and shear forces to the structure

[7]. Similar strong and weak coupling capabilities are available in other multiphysics platforms such as Abaqus–CFD, Siemens STAR-CCM+, Altair AcuSolve, ADINA, MSC Dytran-Nastran, Fluidyn-MP, and LS-DYNA.

Commercial FSI software offers several advantages. User–friendly graphical interfaces and built–in solver links simplify model setup and automate data exchange between fluid and structural domains. Verified workflows and benchmark examples further enhance reliability across a wide range of engineering applications. Moreover, these platforms include comprehensive physical models—such as turbulence, multiphase flow, and advanced material behaviour—which enable the simulation of complex and realistic fluid–structure interactions. However, commercial tools offer limited flexibility when it comes to developing new formulations or experimenting with unconventional coupling strategies. Key numerical controls—such as selecting between monolithic and partitioned schemes or modifying time–step synchronization—are typically restricted to predefined settings. As a result, while these platforms are highly reliable and convenient for practical engineering analyses, they are generally less suitable for exploratory research or the development of novel computational methods.

In ANSYS, fluid–structure interaction (FSI) and structural–acoustic coupling are implemented through solver frameworks that coordinate multiple physics within a unified environment. Depending on the required strength of the interaction, the software supports both partitioned and semi-monolithic strategies. Within the Workbench platform, FSI problems are commonly handled through the *System Coupling* module, which links ANSYS Mechanical for the structural domain with either Fluent or CFX for the fluid domain. For applications involving incompressible and inviscid fluids—where pressure-wave propagation is of primary interest—the ANSYS Acoustics module provides an efficient alternative.

In structural–acoustic analyses, such as the modal or harmonic study of a fluid-filled container, the fluid domain is often represented using the acoustic elements (FLUID220) and (FLUID221). These elements assume small pressure perturbations and are therefore suitable for modelling wave propagation, resonance, and coupled vibration modes. At the interface between the acoustic and structural domains, ANSYS automatically enforces continuity of normal acceleration and pressure, enabling fully bidirectional coupling without the computational cost associated with a full CFD simulation [7].

When combined with Fluent or CFX, FSI is generally solved using a partitioned time-stepping method. The fluid solver calculates pressure and shear forces on the structure, which are then transferred to the structural solver; the resulting displacements are subsequently used to update the fluid mesh. Mesh movement is managed through an Arbitrary Lagrangian–Eulerian (ALE) formulation, while free-surface movement, as seen in sloshing tank problems, is modeled using the volume of fluid (VOF) method. This framework provides a balance between computational efficiency and precision, making it suitable for a wide range of steady and transient problems [86].

This work uses ANSYS for its FSI implementation mainly because of the accessible student version and the wide availability of official documentation and tutorials. These features make ANSYS especially suitable for academic purposes, ensuring reproducibility of results and allowing validation of custom models against a well-established numerical platform. The reliability of its solvers, along with a simple

setup process, help integrate FSI simulations into broader research workflows while keeping computational accuracy.

Custom or research-focused implementations, on the other hand, are usually developed when greater control or flexibility is needed. In such cases, monolithic formulations can be used, where the governing equations for both fluid and structure are solved together within a single matrix system. Alternatively, partitioned schemes may be implemented through external coupling of solvers written in MATLAB, Python, or C++, allowing detailed management of time integration, mesh handling, and data exchange. These methods enable the exploration of innovative numerical techniques, reduced-order models, or unconventional physics couplings. However, their development demands more computational expertise and programming effort, along with thorough verification and validation to ensure stability and accuracy comparable to commercial software.

4.4.1 Fluid–Structure Interaction (FSI) Coupling in ANSYS

The finite element analyses presented in this work were conducted using the commercial multiphysics software ANSYS Workbench, operated under a *student license*. ANSYS offers an integrated computational framework combining Finite Element Analysis (FEA) for structural mechanics and Computational Fluid Dynamics (CFD) for fluid flow simulations. This integration allows for accurate modeling of complex Fluid–Structure Interaction (FSI) phenomena, which are essential for understanding systems where fluid motion and structural deformation are mutually dependent. Such interactions are especially relevant in the context of this research, which focuses on acoustic–structural coupling and the sloshing phenomena occurring in partially filled enclosures. In these coupled systems, the fluid exerts dynamic loads (such as pressure fluctuations and shear stresses) on the structural boundaries, inducing deformations and vibrations. Conversely, the structural motion alters the shape and dynamics of the fluid domain, giving rise to a bidirectional exchange of energy and momentum at the interface. Accurate numerical modeling of such processes requires the proper enforcement of coupling conditions that ensure the physical continuity between the two domains [7].

4.4.1.1 FSI Coupling Strategies in ANSYS

ANSYS offers various coupling strategies that vary in the level of interaction between the fluid and structural solvers and in their computational cost. These methods are outlined below.

(a) One-Way FSI Coupling

In the one-way coupling approach, the simulation is performed sequentially. The fluid domain is solved first to obtain the spatial distributions of pressure, velocity, or temperature, which are subsequently applied as external loads on the structural model. The structural response is then computed independently, without influencing the fluid solution.

This method is computationally efficient and appropriate for problems where structural deformations are minor and have negligible impact on fluid flow. Typical

examples include scenarios where acoustic pressure waves act on rigid cavity walls or when sloshing amplitudes are limited so that wall movement does not significantly alter the free surface dynamics [7].

(b) Two-Way FSI Coupling

The two-way coupling strategy captures the complete bidirectional interaction between the fluid and structure. In this method, the fluid-induced loads deform the structure, and the updated structural geometry is relayed back to the fluid solver, modifying the flow field. The data exchange occurs iteratively until both the pressure and displacement fields at the interface reach convergence. This approach is essential when structural deformations significantly alter the fluid dynamics, as occurs in sloshing within flexible-walled tanks or in acoustic–structural coupling problems where wall vibrations influence the internal pressure distribution. Although more computationally demanding, this method provides a physically consistent representation of the coupled behavior [7].

(c) System Coupling Framework

Within ANSYS Workbench, the System Coupling module provides an integrated environment for managing both one-way and two-way FSI simulations. It allows the automatic exchange of interface variables such as pressure, displacement, and velocity between the fluid solver (ANSYS Fluent) and the structural solver (ANSYS Mechanical). At each coupling step, System Coupling ensures temporal synchronization and energy consistency between the solvers through user-defined relaxation factors, time-step controls, and convergence criteria. This framework is especially effective for analysing multiphysics phenomena like the coupled sloshing and acoustic–structural interaction examined in this study. It offers a robust and flexible solution approach for problems where pressure fluctuations within the fluid domain and deformation of the confining structure are closely linked.

This chapter has established the finite element framework required for the rigorous modelling of fluid-filled structures equipped with periodic liquid dampers. Starting from the weak (variational) formulation of the governing equations, the structural, acoustic, and coupled fluid–structure interaction problems have been presented within a unified multiphysics setting. The enforcement of interface continuity conditions and the discussion of coupling strategies, including one-way and two-way FSI approaches in ANSYS, have provided the theoretical and computational basis for accurately simulating the bidirectional exchange of forces and kinematic quantities between fluid and structure.

Having defined the mathematical formulation and the numerical coupling procedures, the next step consists in applying this framework to the specific case of liquid damper systems. The following chapter therefore focuses on the detailed FE modelling of the tank–fluid assembly under external excitation. Through modal analysis and post-processing, the dynamic characteristics of the system are evaluated and the corresponding dynamic stiffness representation is extracted, enabling subsequent integration into periodic structural models for band gap assessment and optimisation.

Chapter 5

Liquid Dampers: FE Modeling

This chapter deals with the FE modeling of the liquid dampers, considering the structure (tank), the internal fluid and the fluid structure interaction. The structure is excited by an external force and the dynamic behavior of the system has been evaluated.
Through finite element analysis and postprocessing, this chapter aims to show a numerical example for modelling the dynamic behavior of LD systems. The system is studied under the hypothesis of small-amplitude oscillations. The linear modal approach allows identification of natural frequencies and pressure distributions while avoiding the complexity of transient free-surface simulations. The developed model enables the extraction and assessment of the dynamic stiffness matrix (DSM), which can be further integrated into periodic structural models for advanced analysis and optimisation of band gap characteristics.

5.1 Modeling of Liquid Sloshing

Liquid sloshing refers to the oscillatory motion of the free surface of a liquid in a partially filled container subjected to external excitations or disturbances. The prediction of sloshing frequencies and mode shapes can be used in the design of tanks, vessels, and structural systems containing liquids, where the dynamic interaction between the fluid and the structure may lead to large amplitude responses or resonance. Here, the sloshing problem is modeled in the frequency domain using the linearized potential flow theory and implemented through an acoustic finite element formulation. This approach allows for the efficient estimation of natural sloshing frequencies under small-amplitude oscillations.

Under the assumption of an incompressible, inviscid, and irrotational fluid, the motion of the liquid can be described by a velocity potential ϕ, satisfying the Laplace equation within the fluid domain Ω_f:

$$\nabla^2 \phi = 0 \quad \text{in } \Omega_f. \tag{5.1}$$

The tank walls can be assumed as flexible that impose FSI. In this context, the linear modal analysis simplifies to an eigenvalue problem whose solutions provide the natural frequencies and the corresponding pressure mode shapes that characterize the sloshing motion.

In the subsequent analysis, the acoustic approximation of the fluid domain was used, which solve for the acoustic pressure p as the primary variable. The study

was extended to include deformable walls and two-way coupling using compatible structural elements at the fluid–structure interface.

The liquid depth was chosen to ensure a partially filled configuration, typically corresponding to a filling ratio between 50% and 70% [88]. The fluid domain was discretized using a structured hexahedral mesh, refined near the free surface to improve the resolution of pressure gradients and ensure convergence of the computed sloshing frequencies.

The upper boundary representing the free surface is modeled as a pressure-release condition, $p = 0$, which permits free fluctuations of the pressure field and accurately captures the behavior of the air–liquid interface. Gravity is included to establish the initial hydrostatic pressure distribution, ensuring a physically consistent equilibrium state before performing the modal analysis.

In the present study, modal analysis has been carried out. The resulting eigenfrequencies correspond to the natural sloshing frequencies, and the associated eigenmodes represent the pressure distributions for each sloshing mode. The first few modes typically exhibit dominant free-surface oscillations, whereas higher modes involve more complex pressure fields and reduced surface deformation [68, 98].

5.1.1 Post-Processing

The pressure mode shapes obtained from the finite element analysis can be post-processed to interpret the sloshing behavior in physical terms and to extract quantities relevant for subsequent dynamic characterization. The computed acoustic pressure fields were first used to reconstruct the motion of the free surface, allowing visualization of the characteristic sloshing modes and their spatial distribution. The corresponding free-surface elevation η is obtained from the pressure field p using the linearized dynamic boundary condition,

$$\eta = -\frac{p}{\rho g}, \tag{5.2}$$

which relates the pressure fluctuation at the free surface to the associated vertical displacement under small-amplitude oscillations. This relationship establishes a clear connection between the acoustic results and the actual deformation of the liquid surface, allowing both qualitative and quantitative comparison with the corresponding analytical mode shapes.

For quantitative assessment, the harmonic pressure field can be employed to evaluate the equivalent dynamic stiffness of the fluid domain. A unit harmonic displacement is imposed at the interface boundary, and the resulting complex reaction forces are integrated over the wetted surface to obtain the frequency-dependent dynamic stiffness matrix (DSM). The resulting includes the inertia effects of the fluid in a compact frequency-domain form [94].

This reduced-order representation of the liquid domain enables efficient coupling with structural or periodic models, eliminating the need to explicitly discretize the fluid in subsequent simulations. In the context of the present work, the extracted DSM could be used to represent the sloshing contribution within periodic fluid–structure systems, facilitating the analysis and tuning of their vibroacoustic band-gap characteristics.

5.2 Modeling of Liquid Sloshing in a Rectangular Tank Using ANSYS

5.2.1 Element Choice

In this study that involves a FSI (tank connected to pipe), when investigating sloshing and wave propagation, the choice of finite elements are critical for ensuring both accuracy and computational efficiency. For the structural domain (pipe and tank walls), shell elements (e.g. SHELL181 in ANSYS) are often preferred when the walls are thin relative to other dimensions. Shell elements reduce computational cost while accurately capturing the behavior of the structure. However, if the geometry is thick or requires detailed stress analysis, solid elements (e.g., SOLID185 or SOLID186) may be more appropriate. For the fluid domain, the type of element depends on the type of simulation. In acoustic analysis, we use FLUID30 (2D) or FLUID220/221 (3D) to model incompressible fluids, suitable for modal and harmonic pressure wave studies. When performing FSI simulations, it is essential to ensure that the fluid–structure interface is meshed appropriately to allow accurate data transfer. Using shared topology or a conformal mesh greatly improves the quality of the coupling, particularly in system coupling configurations. The correct choice of elements ensures physical fidelity, stable convergence, and meaningful predictions of wave or resonance behavior. For this study, we chose the shell element. This element is a 4-node structural shell with the following DoFs: UX, UY, UZ, ROTX, ROTY, ROTZ (Figure 5.1).

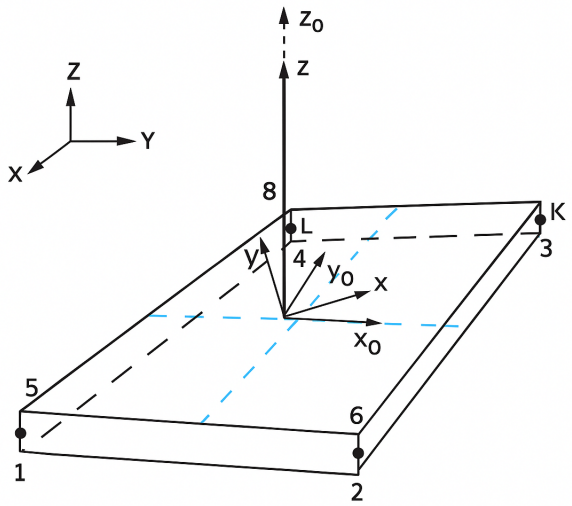

Figure 5.1: Shell element code 181 in ANSYS [7]

5.2.2 Acoustic Fluid

Acoustic fluid refers to a simplified representation of a fluid domain used in numerical simulations to model the propagation of pressure waves without considering actual fluid flow. The fluid is treated as incompressible, inviscid, and irrotational, with all dynamics governed by pressure fluctuations described by the Helmholtz equation or the linearized wave equation [149]. This method is widely applied when analyzing acoustic resonance, pressure wave transmission, structure–fluid coupling, or

vibration behavior in enclosed or bounded fluids [170]. In commercial solvers such as ANSYS, the acoustic fluid domain assumes zero mean flow and neglects shear effects, focusing solely on scalar acoustic pressure as the field variable. Boundary conditions can include rigid walls, impedance interfaces, or coupling surfaces to solid structures. This approach is especially valuable in simulations of sloshing tanks, fluid-filled pipes, and metamaterial-based periodic structures, where linear, small-amplitude oscillations dominate [31]. Compared to full CFD models, acoustic fluid models are computationally efficient and accurate for high-frequency wave behavior, provided that free surface effects and turbulence are not dominant [43].

5.2.3 Free Surface

A free surface refers to the interface between a fluid and another medium (typically a gas like air) where the pressure is constant and equal to atmospheric pressure. In engineering applications, the free surface is not fixed and can oscillate or deform in response to motion, gravity, or external forces. In the context of sloshing dynamics, the behavior of the free surface is critical, as it governs the sloshing modes, wave elevation, and fluid–structure interaction [58]. Modeling the free surface accurately requires solving the Navier–Stokes equations with appropriate boundary conditions to capture its dynamic movement [68]. For small-amplitude oscillations, simplified assumptions (e.g., linear sloshing theory) can model the free surface as a moving boundary governed by potential flow theory [98]. The inclusion of a free surface is essential in problems involving sloshing tanks, seismic fluid dynamics, or propellant management systems, where fluid movement due to container acceleration or vibration leads to significant surface deformation and dynamic pressure forces.

5.2.4 Fluid Structural Interaction (FSI)

FSI refers to the mutual interaction between a fluid and a solid structure, where the fluid flow induces forces on the structure and the deformation of the structure, in turn, affects the fluid flow. This coupled phenomenon is crucial in many engineering systems, including sloshing tanks, aerospace structures, marine vessels, pipelines, and biomechanical devices [18]. In FSI, both the fluid and structural domains are solved either separately but coupled (partitioned approach) or together (monolithic approach), depending on the complexity and stability required. In applications such as sloshing, the dynamic pressure exerted by the moving fluid on the tank walls causes significant structural vibrations, especially during seismic or base excitations. These vibrations, change the container's geometry, thereby influencing the fluid motion, a classical two-way coupling problem [98, 223]. FSI becomes even more critical in lightweight or flexible structures, where structural displacements are large enough to significantly alter fluid flow patterns. In computational tools like ANSYS Workbench, FSI is implemented through System Coupling, where solvers such as ANSYS Mechanical (for structures) and ANSYS Acoustic (for fluids) exchange data at each time step. The fluid solver provides pressure or viscous forces on the interface, and the structural solver returns displacements or velocities. The interface must satisfy two primary conditions: 1. Kinematic compatibility (continuity of velocity/displacement) 2. Dynamic equilibrium (continuity of traction or stress). For an accurate simulation, mesh conformality or interpolation algorithms

are required at the fluid–structure interface. When dealing with sloshing tanks, free surface modeling (e.g., volume of fluid method) is also integrated to capture wave elevation and its effect on walls [68]. FSI problems can be linear or nonlinear, steady or transient, and weakly or strongly coupled. Weak coupling is used when structural deformation has minimal effect on the fluid (e.g. rigid tanks), while strong coupling is necessary for systems where the feedback between the fluid and the structure is significant, such as in flexible structures, bio-fluid mechanics, or aeroelasticity [71]. In the context of periodic systems with sloshing (e.g., tank-pipe units), FSI analysis helps reveal coupled vibration modes, resonance frequencies, and wave attenuation mechanisms, which are crucial for metamaterial design, vibration isolation, and seismic protection [203, 38].

5.2.5 Mesh Convergence Study

A mesh convergence study is conducted to ensure the numerical precision and stability of the finite element model. As the mesh is refined, the difference between the successive results will decrease. The coarse mesh significantly underestimated the peak response due to spatial discretization error, while the fine mesh provided a more accurate solution at a higher computational cost. The quality of the mesh is also verified through the aspect ratios of the elements, ensuring that there are no severely distorted elements. This convergence study confirms that the chosen mesh resolution adequately captures the physics of the problem without introducing significant numerical artifacts.

The type of mesh is chosen as linear quadratic. The size of the mesh is $\lambda_{min}/20$ (λ_{min} is the wavelength of the maximum frequency to be analyzed) [246, 7]. Therefore,

$$\Delta x \leq \frac{\lambda_{\min}}{20} \quad \text{where} \quad \lambda_{\min} = \frac{c_f}{f_{\max}} \tag{5.3}$$

c_f is the speed of sound in the medium. Δx is the maximum element size.

5.2.6 Type of Analysis

We selected acoustic analysis for the study of wave propagation in FEM. Harmonic acoustic analysis is a frequency-domain method that is used to evaluate the steady-state acoustic response of a system when subjected to harmonic (sinusoidal) excitations. This type of analysis is crucial for predicting how pressure waves propagate and interact with structures and fluids, especially in systems where resonances and sound transmission are of interest. The analysis is governed by the Helmholtz equation, derived from the linearized form of the wave equation assuming time-harmonic behavior. The pressure field $p(\mathbf{x}, t)$ is assumed to vary sinusoidally as $p(\mathbf{x}, t) = \hat{p}(\mathbf{x})e^{j\omega t}$, where ω is the angular frequency and $\hat{p}$ is the complex pressure amplitude. Substituting this into the linear acoustic wave equation leads to:

$$\nabla^2 \hat{p} + k^2 \hat{p} = 0 \tag{5.4}$$

where $k = \omega/c$ is the acoustic wavenumber, and c is the speed of sound in the medium.

5.3 Numerical Example

This section introduces the modeling tank partially filled with fluid, which is considered to act as a Liquid Damper (LD) (Figure 5.2). The performance of LD depends on the tank geometry, type and level of the liquid, which influences the sloshing behavior of the system.
In ANSYS, the sloshing response of a partially filled tank is modeled using either acoustic or two-way FSI coupling. For small-amplitude free-surface motion, the fluid domain is represented by acoustic elements (FLUID220/221), which assume inviscid and incompressible behavior governed by the Helmholtz equation. The coupling with the structural walls is achieved through the continuity of normal acceleration and pressure at the interface. For larger nonlinear free-surface oscillations, ANSYS employs the Volume of Fluid (VOF) method in Fluent within the System Coupling environment [7]. The present analysis adopts the acoustic formulation, consistent with the linear potential-flow model introduced in Chapter 4, to capture the fundamental sloshing modes and their coupling with the structure.

Choosing the configuration of the pipe and tank depends on the objective of the study. When the focus is on wave propagation and stop-band behavior, the geometry must be periodically arranged with consistent dimensions to satisfy Bloch–Floquet periodicity. The tank height and fluid depth should be defined to permit representative sloshing motion, while the pipe cross-section governs the waveguiding and coupling characteristics. A smooth transition at the pipe–tank junction helps to minimize spurious wave reflections and ensures proper continuity of both the acoustic and structural fields. These dimensions are chosen to balance physical concept, computational efficiency, and the accurate capture of coupled acoustic–structural phenomena.

Finite Element (FE) modeling is a powerful tool to analyze and optimize the design of LD, providing data on the dynamic interactions between the liquid and the structure. FEM allows for the simulation of liquid sloshing dynamics within tank geometries of arbitrary shapes. This enables the identification of design parameters, such as tank shape, liquid depth, and placement, to enhance the overall performance of the damper [132]. Figure (5.2) shows a representation of a rectangular tank used in the analysis.

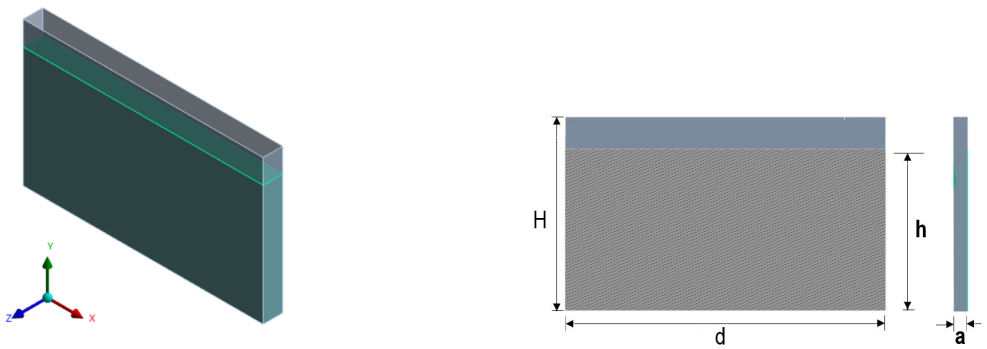

(a) (b)

Figure 5.2: Schematic view of the tank: (a) 3D view; (b) 2D view with geometric parameters

The material of the structure is assumed to be HDPE (High-Density Polyethylene); the fluid here considered is water. Material properties are given in Table (5.2), while geometric parameters are given in Table (5.1).

Table 5.1: Geometric parameter of the LD

Parameters	H	h	d	a	t (thickness)
Values	1.08m	0.9m	1.8m	0.15m	0.0015m

Table (5.2) shows the material characteristics of the system.

Table 5.2: Material properties of the LD

Properties	ρ	E	ν	ρ_f	c_f
Values	935 kg/m^3	10^9 Pa	0.4	$1000kg/m^3$	$1450m/s$

Here, ρ, E and ν are the density, Young modulus, and Poisson's ratio of the structure, respectively. While c_f and ρ_f are the speed of sound and the density of the fluid, respectively.

5.3.1 Axial Vibration Loadings

In the case of axial vibration, we restricted the entire structure in the Y and Z directions (zero displacement). Figure (5.3) and Table (5.3) show these boundary conditions.

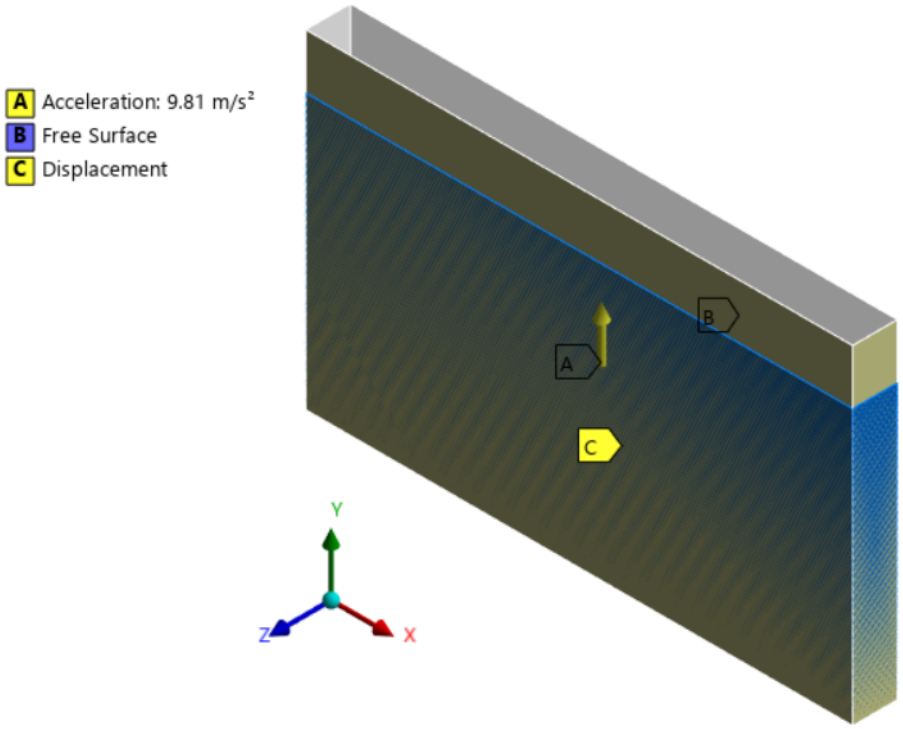

Figure 5.3: Loading conditions for the tank in free axial movement

Table 5.3: Boundary Conditions of the Structure in Axial Vibration

DoFs	U_x	U_y	U_z	θ_x	θ_y	θ_z
Values	Free	0	0	Free	Free	Free

Other conditions that are applied in the FE model include:
(a) FSI (Fluid Structure Interaction): by selecting the surfaces of the structure that have a common surface with fluid;
(b) Free surface: the surface of the fluid that represents the sloshing (B in Figure (5.3));
(c) Acceleration gravity: to apply the free surface effect, g is activated (A in Figure (5.3.))

5.3.2 Loading Conditions (Forced Vibration)

When there are loads in the system, the frequency of the load plays a key role in obtaining the equation of motion. By analyzing the problem in the harmonic acoustic module, we reach the critical frequency, which should be avoided. Figure (5.4) depicts these loadings and conditions.

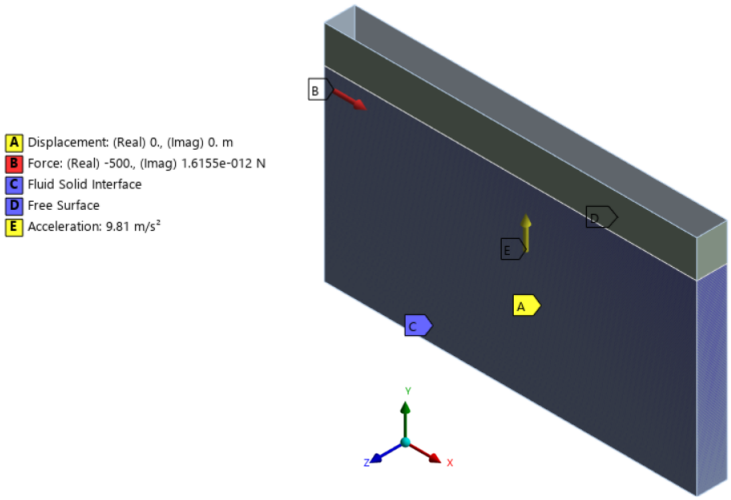

Figure 5.4: Loading conditions for the tank in forced axial movement

5.4 Comparison and Verification with Simplified Mechanical Model

Consider the movement of the free surface of the fluid (Figure (3.2)). Simplified mechanical models are widely used to represent sloshing dynamics in liquid-filled containers, particularly in the context of minimizing structural vibrations using liquid dampers (LD). These models replace the complex fluid-structure interaction with a reduced-order analog, typically comprising lumped masses, springs, and dampers that mimic the convective motion of the fluid and its associated inertial and dissipative effects [98, 58]. Verification of these models involves comparing their predictions with experimental observations and numerical simulations, such as Computational Fluid Dynamics (CFD) or full Navier–Stokes solvers. Key quantities assessed include

the natural sloshing frequency, the modal mass, the damping ratio, and the dynamic pressure distribution exerted on the container walls. For many practical tank geometries, especially shallow and rectangular tanks, the first sloshing mode dominates the dynamics and can be captured effectively by a single degree of freedom (SDOF) mechanical analog. Studies have shown that the resonant frequencies predicted by these simplified models closely match those obtained through linear potential theory and validated experiments [198, 210]. The accuracy of simplified models generally diminishes when the liquid motion involves large amplitudes, where nonlinear effects such as wave breaking, vortex shedding, and strong fluid–structure interaction become significant. Nevertheless, these simplified mechanical models remain valuable tools because of their computational efficiency and their ability to capture the dominant dynamic features of sloshing. Their usefulness in preliminary design and control studies makes them widely adopted in engineering practice, provided that they are properly validated against experimental benchmarks [98, 236].

Table 5.4: First Four Natural Frequencies of a Tank with Fluid in Axial Movement

Analytical (Hz)	0.63	0.93	1.14	1.31
FEM (Hz)	0.65	0.93	1.17	1.32

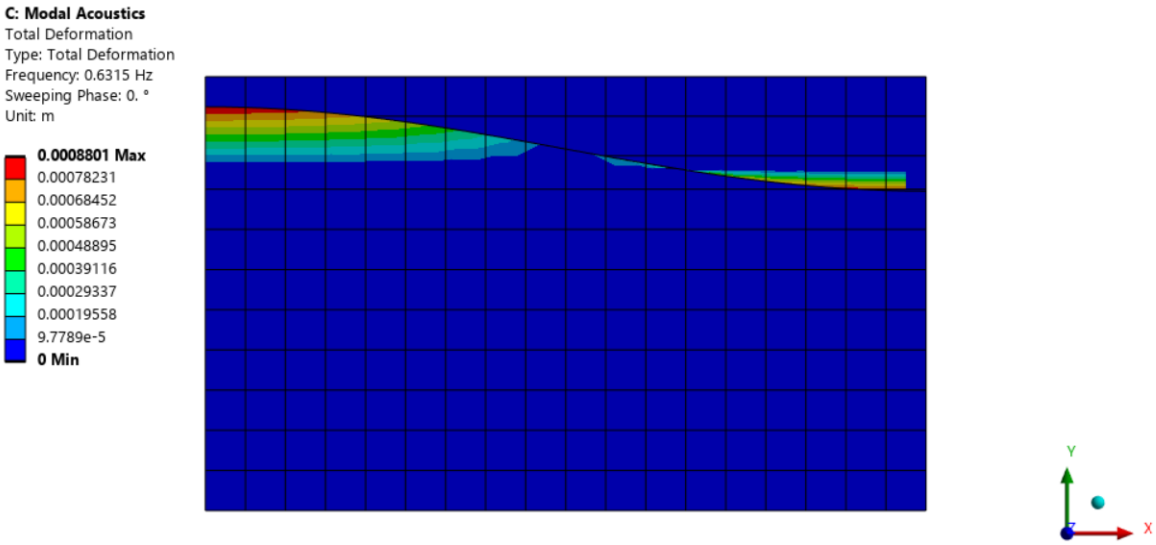

Figure 5.5: Mode shape (1st) for 1 tank with fluid

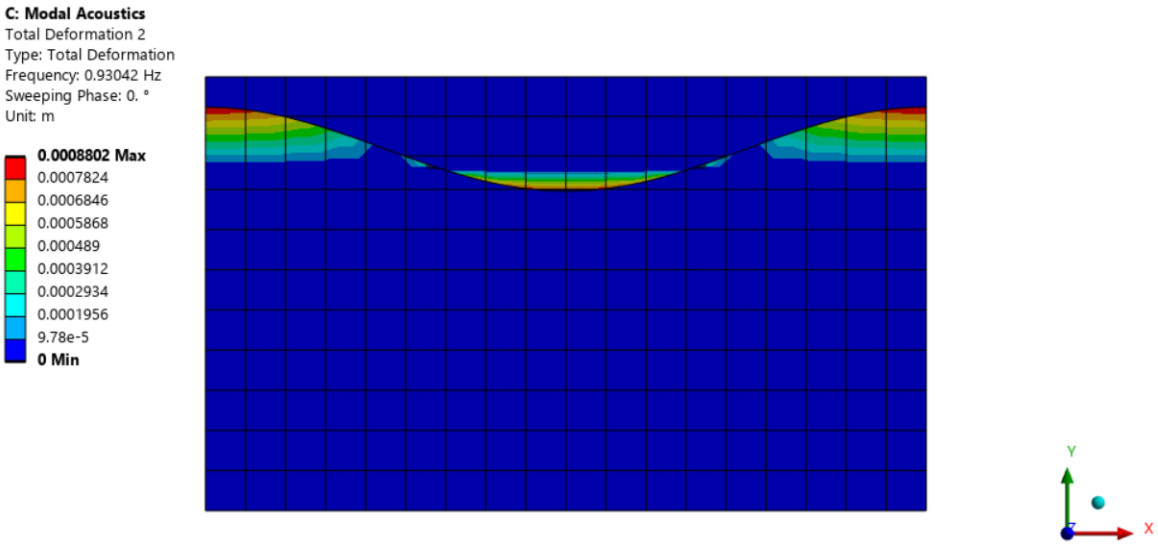

Figure 5.6: Mode shape (2nd) for 1 tank with fluid

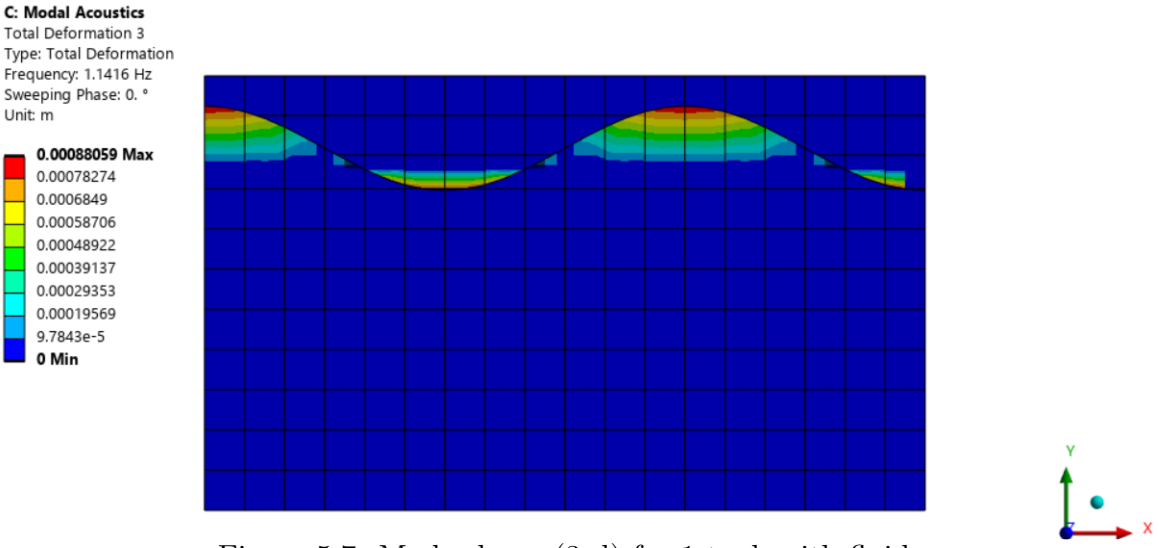

Figure 5.7: Mode shape (3rd) for 1 tank with fluid

This chapter has presented the finite element modelling of a liquid damper system, including the structural tank, the internal fluid domain, and their coupled fluid–structure interaction. Under the assumption of small-amplitude oscillations, a linear modal framework has been adopted to identify natural frequencies, pressure distributions, and dominant sloshing modes. The numerical model has enabled the extraction of the dynamic stiffness matrix (DSM), providing a compact representation of the coupled tank–fluid dynamics suitable for integration into periodic structural analyses. In addition, simplified mechanical analogues of sloshing have been discussed and validated against established theoretical and numerical references, highlighting their effectiveness in capturing the primary dynamic characteristics under linear conditions.

Having established and verified the FE model for an isolated liquid damper, the following chapter extends the investigation to configurations relevant to the proposed periodic liquid damper (PLD) concept. The focus shifts toward the numerical evaluation of the coupled pipe–tank unit cell and multi-cell assemblies, allowing assessment of how periodicity modifies resonance behaviour, wave propagation, and

vibration transmissibility. This progression enables a systematic examination of the mechanisms responsible for attenuation and stop-band formation in periodic fluid–structure systems.

Chapter 6

Numerical Results and Analysis

In this chapter, the focus is placed on the numerical results obtained for the fluid–structure systems. The discussion is directed toward the specific configurations relevant to the proposed periodic liquid damper (PLD) concept. The numerical analyses presented here allow us to examine the dynamic behavior of the tank acting as a resonator, the coupled pipe–tank unit cell, and the multi-cell configuration used to evaluate the influence of periodicity.

The simulations provide the essential quantities needed to characterize the system response, including free-surface motion, pressure fields, and structural deformations. These outputs enable identification of the dominant sloshing modes and their coupling with the axial vibration of the pipe. Particular attention is given to how resonance mechanisms evolve when moving from a single tank to a periodic arrangement, and how the number of liquid-filled cells affects wave propagation and attenuation.

The results presented in this chapter therefore form the basis for assessing the effectiveness of the periodic liquid damper. By comparing the isolated tank, the single unit cell, and the five-cell configuration, we illustrate how periodicity modifies the transmissibility, introduces stop-bands, and alters the energy distribution along the structure. This targeted analysis allows the reader to clearly understand the dynamic mechanisms that the subsequent chapters explore in greater theoretical and parametric detail.

6.1 Axial Vibration Analysis of the Host Structure without Fluid

For a linearly elastic bar (length L, area A, Young's modulus E, density ρ), the axial displacement $u(x,t)$ satisfies

$$\rho A \frac{\partial^2 u}{\partial t^2} = \frac{\partial}{\partial x}\left(EA\frac{\partial u}{\partial x}\right), \qquad 0 < x < L. \tag{6.1}$$

For uniform EA:

$$\frac{\partial^2 u}{\partial t^2} = c^2 \frac{\partial^2 u}{\partial x^2}, \qquad c = \sqrt{\frac{E}{\rho}} \quad \text{(longitudinal wave speed)}. \tag{6.2}$$

Assuming a separable solution $u(x,t) = \phi(x)\, q(t)$, substitution into Equation (6.2) yields the pair of ordinary differential equations

$$\phi''(x) + \beta^2 \phi(x) = 0, \qquad \ddot{q}(t) + \omega^2 q(t) = 0, \qquad \beta = \frac{\omega}{c}, \tag{6.3}$$

from which the general spatial mode shape becomes

$$\phi(x) = C_1 \cos(\beta x) + C_2 \sin(\beta x). \tag{6.4}$$

To verify the analytical formulation, we consider the axial vibration of the host structure, modelled here using a FEA.

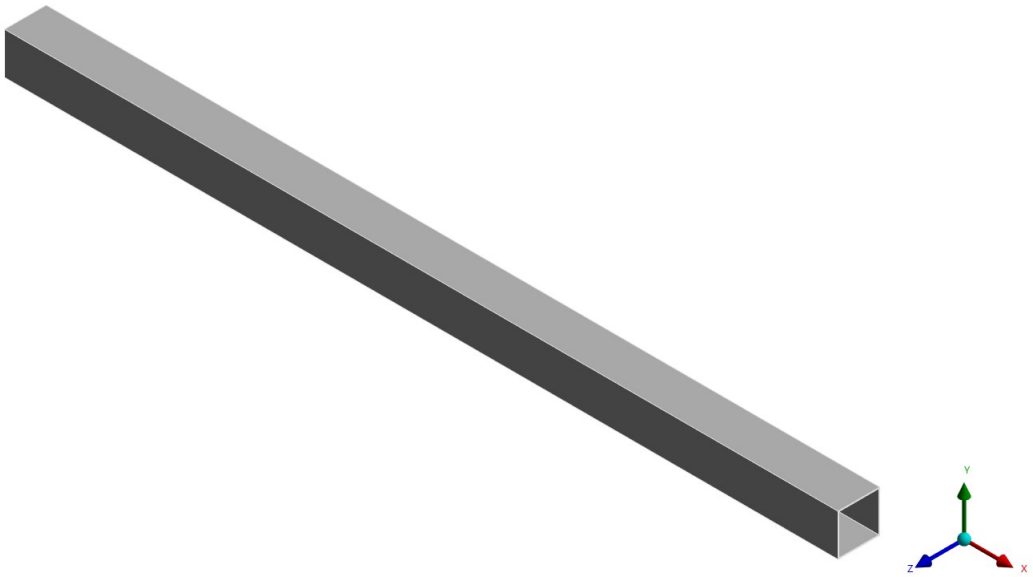

Figure 6.1: Schematic view of the pipe

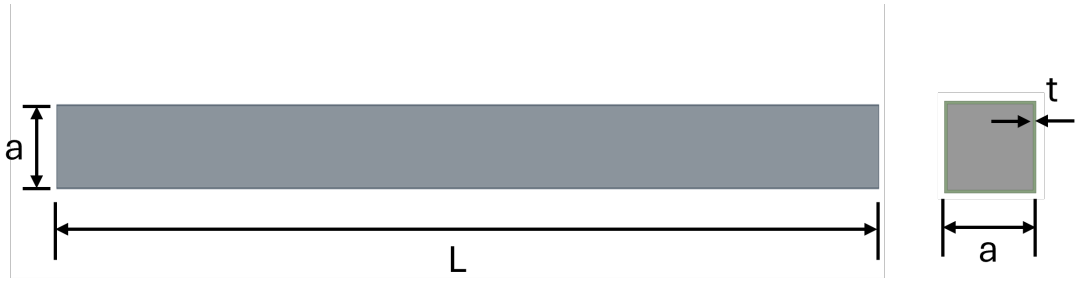

Figure 6.2: Dimensions of the pipe

For this case, the geometrical parameters are $L = 3\,\text{m}$, $a = 0.15\,\text{m}$, and wall thickness $t = 0.0015\,\text{m}$. These values are used consistently in both the analytical model and the finite element (FE) model to ensure a direct comparison between the two approaches.
Table (6.1) reports the first three natural frequencies obtained analytically and using the FE model.
The comparison demonstrates very good agreement: the FEM values differ from the analytical predictions by approximately 7% or less for all three modes. This level of deviation is expected, mainly due to the slight differences introduced by the

Table 6.1: First three natural frequencies of a pipe without fluid in axial movement

Model	Mode 1	Mode 2	Mode 3
Analytical (Hz)	301.7	582.3	867.7
FEM (Hz)	280.3	560.6	840.9

discretization and the 3D representation of the pipe in the FE model. The close correspondence of the results verifies the correctness of the analytical formulation and confirms that the FE mesh, boundary conditions, and material properties are appropriately defined. The gradual increase in natural frequency across the three modes reflects the expected behaviour of axial vibration in a uniform elastic member, where higher modes involve more nodal points and steeper gradients of deformation.

The mode shapes obtained from the FE analysis provide additional insight into the deformation pattern of each natural frequency. Figures (6.3) to (6.5) show the total deformation distributions.

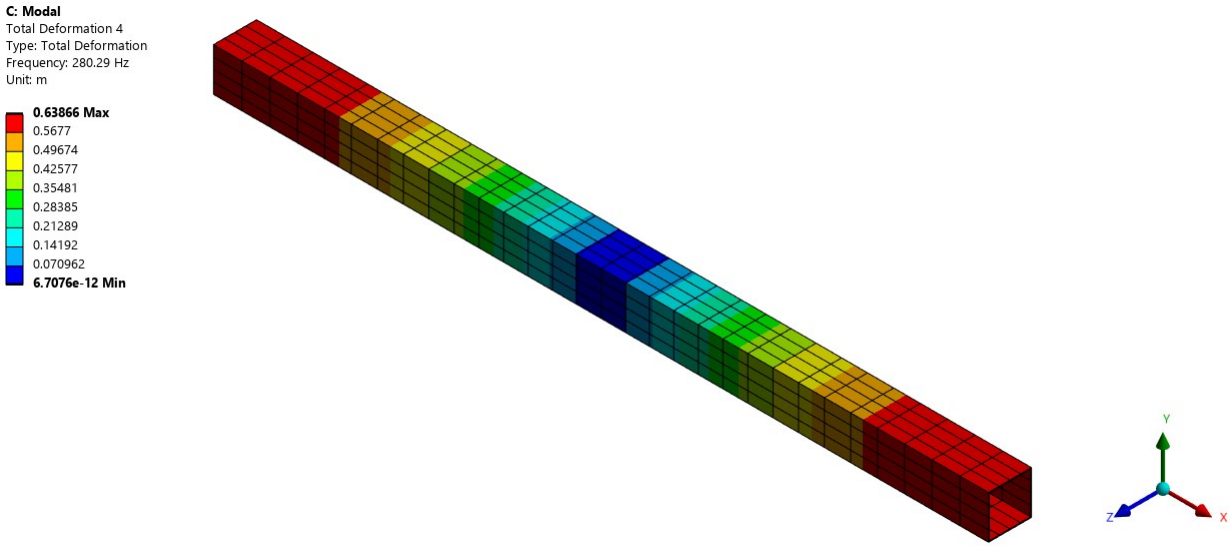

Figure 6.3: First natural frequency of the pipe without fluid

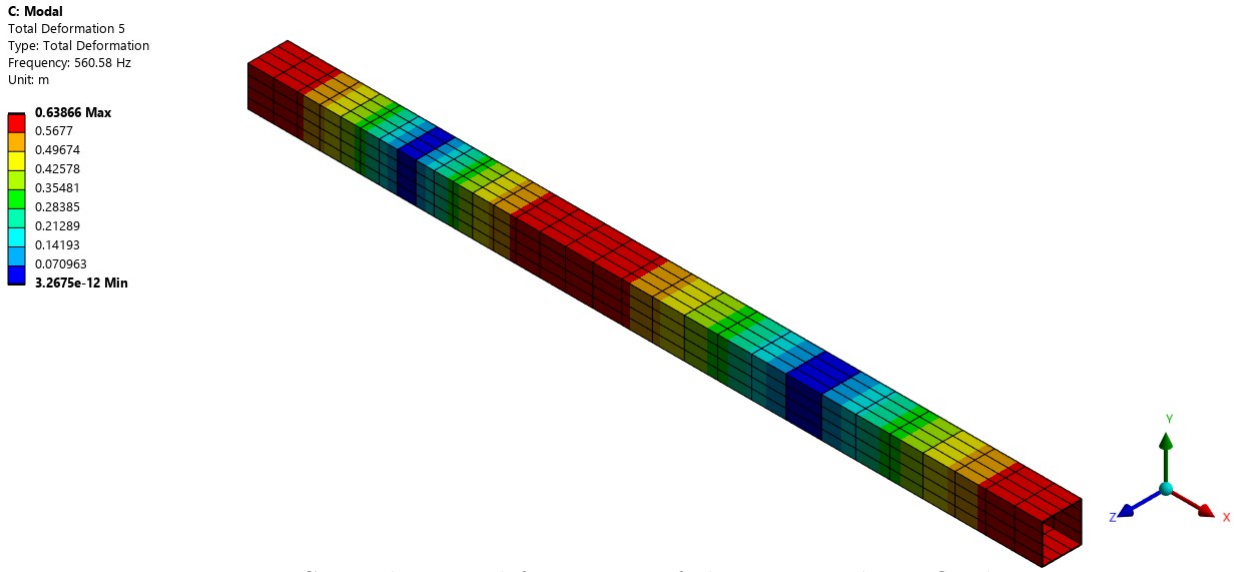

Figure 6.4: Second natural frequency of the pipe without fluid

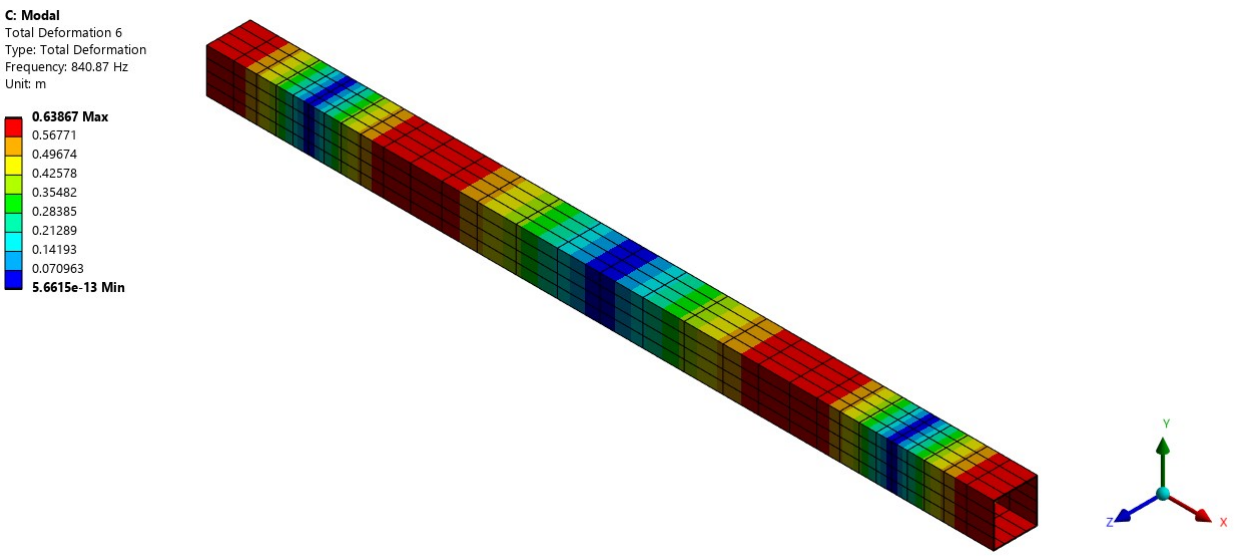

Figure 6.5: Third natural frequency of the pipe without fluid

Figure (6.3) illustrates the first axial mode, characterized by a uniform extension–contraction pattern. This mode shows the entire pipe oscillating in phase, as expected for the fundamental longitudinal mode. The deformation increases steadily toward the free end, reflecting the classical sine-shaped distribution of axial displacement.
Figure (6.4) displays the second axial mode, where a single internal node appears along the pipe length. In this case, one segment of the pipe moves in the opposite phase with respect to the other, producing a deformation shape consistent with the analytical second mode. The presence of the internal node is a key indicator of higher-order axial behaviour.
Figure (6.5) shows the third axial mode, which presents two internal nodes. The deformation alternates across three segments of the pipe, and the associated mode shape exhibits a higher curvature and a shorter wavelength. This progression from one to two nodes confirms the correct modal evolution and provides additional confidence in the accuracy of the FE model.

Together, the frequency comparison and the visualization of the FE mode shapes demonstrate that the analytical and numerical approaches are fully consistent. These results form the basis for the subsequent extension of the model to include fluid loading, periodic tank attachments, and coupled fluid–structure interaction effects in later sections.

6.2 Axial Vibration Analysis of the Host Structure with Fluid Inside

The free vibration analysis of a completely filled horizontal tube with water is essential in the study of fluid–structure interaction (FSI) in pipelines, heat exchangers, and nuclear fuel rods. The dynamics of a fully water-filled tube is influenced by the internal fluid inertia, which couples with the structural deformation modes of the tube wall. This interaction reduces the natural frequencies and modifies the mode shapes compared to an empty configuration [203, 38].

Consider Figure (6.6), which illustrates the hollow pipe serving as the host structure and the water completely occupying its interior.

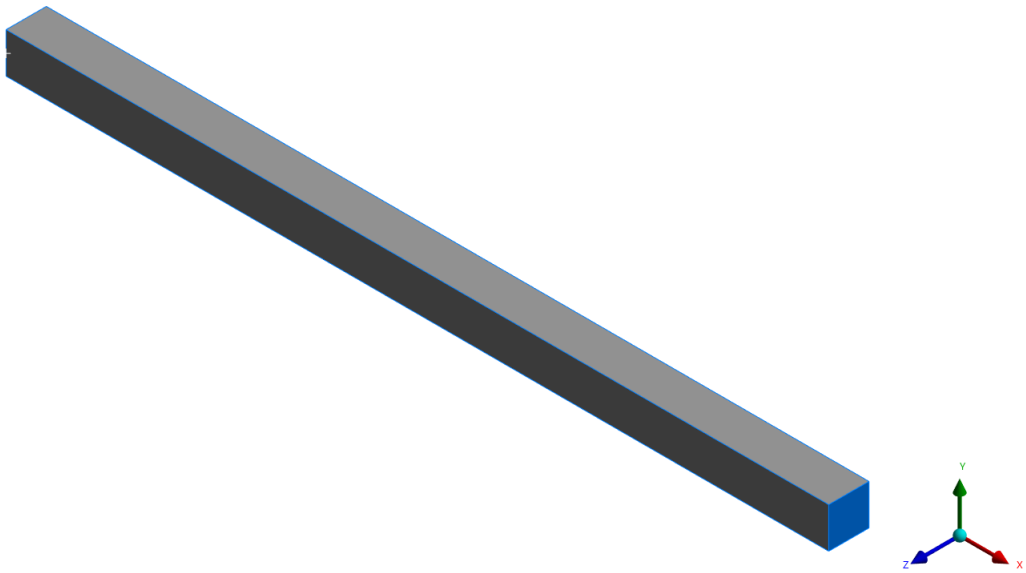

Figure 6.6: Free vibration of a pipe filled with water

Since the pipe is fully filled with water, no free surface exists, and the fluid contributes only through its inertia. For axial vibration of a pipe of length L, cross-sectional area A_s, Young's modulus E, pipe density ρ_s, wall thickness t, and water density ρ_f, the natural frequencies are given by [98]:

$$f_n = \frac{n}{2L}\sqrt{\frac{EA}{M_{\text{eff}}}}, \tag{6.5}$$

where $n = 1, 2, 3, \ldots$ denotes the mode number, $M_{\text{eff}} = \rho_s A_s + \rho_f A_f$ is the effective mass per unit length (including the pipe material and the internal fluid), A_s is the cross-sectional area of the solid wall, and A_f is the cross-sectional area of the fluid (inner pipe area).

The first three natural frequencies obtained analytically and via finite element modelling (FEM) are summarized in Table (6.2).

Table 6.2: First 3 natural frequencies of a pipe with fluid in axial movement

	Mode 1	Mode 2	Mode 3
Analytical (Hz)	172.36	344.70	517.09
FEM (Hz)	194.20	389.73	494.04

The results show a consistent trend: the FEM frequencies are slightly higher for the first two modes and slightly lower for the third mode. These differences stem from modelling assumptions. The analytical model simplifies the pipe as a perfect bar with uniform properties, while the FEM model captures mesh discretization, geometric effects, and the more realistic fluid mass distribution. Nevertheless, the agreement remains acceptable, confirming that the analytical expression provides a reliable baseline for validation.

To visualize the deformation characteristics, Figures (6.7) to (6.9) display the mode shapes at the first three natural frequencies.

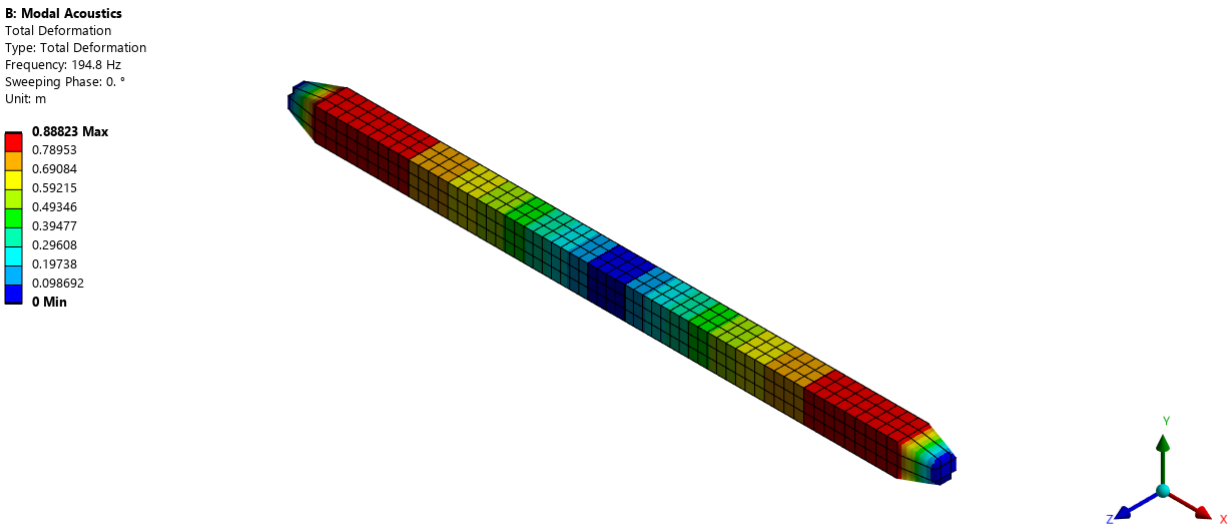

Figure 6.7: First natural frequency of the pipe with fluid inside

At the first mode, the deformation shape corresponds to a half-wavelength axial mode, with the entire pipe undergoing a smooth extension–contraction pattern. The presence of the internal fluid increases the effective inertia, causing the deformation to appear slightly damped and more distributed compared to the empty-pipe case.

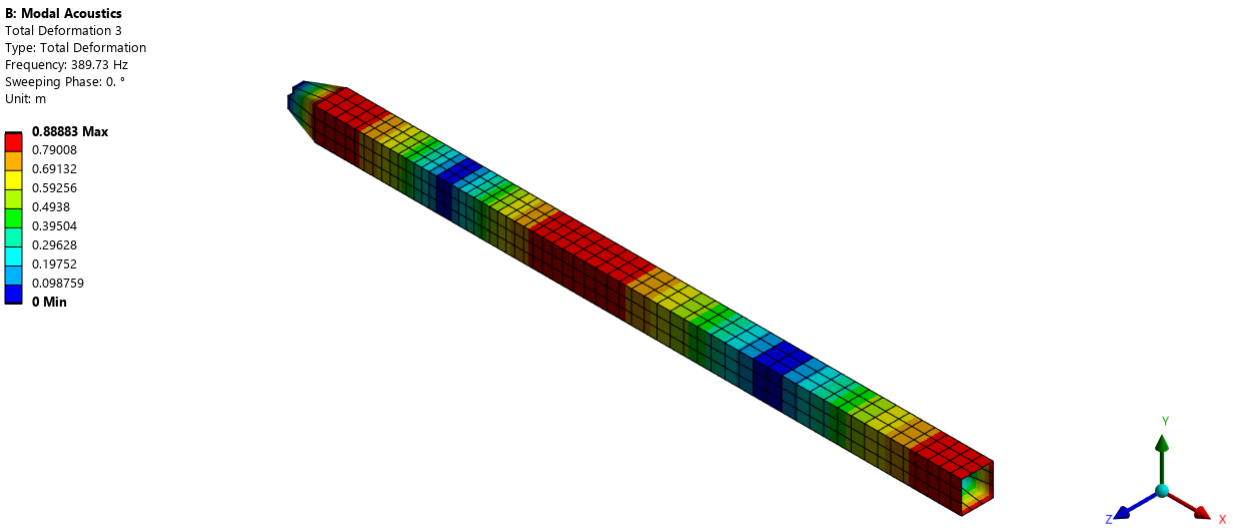

Figure 6.8: Second natural frequency of the pipe with fluid inside

The second mode exhibits one internal node along the pipe length, creating two symmetric axial deformation lobes. The added fluid mass again alters the stiffness-to-mass ratio, shifting the nodal position slightly and reducing the curvature intensity in each segment.

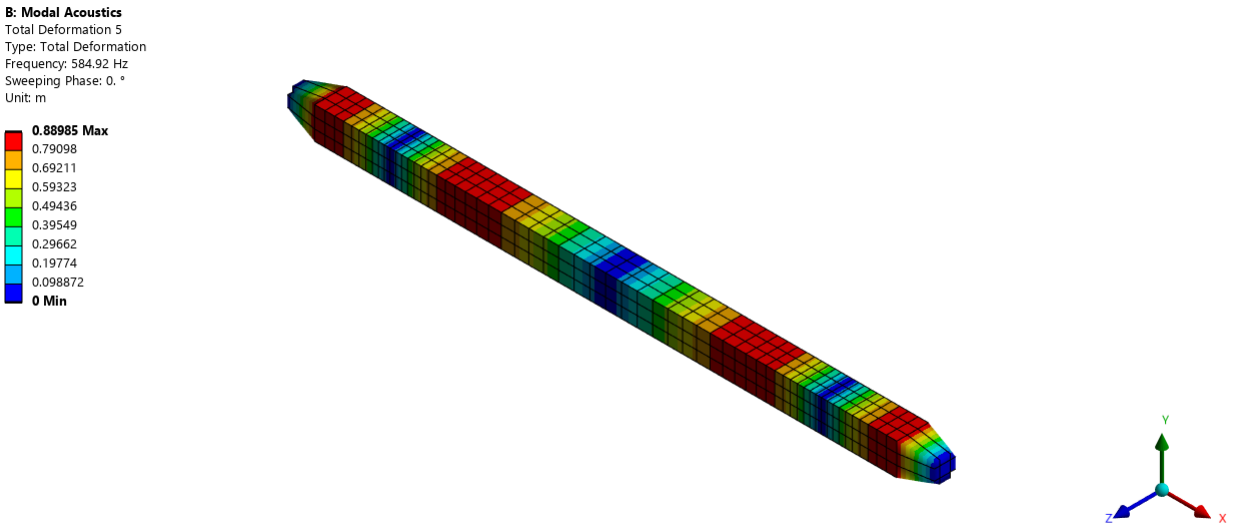

Figure 6.9: Third natural frequency of the pipe with fluid inside

In the third mode, two internal nodes are observed, and the pipe deforms with three axial wave segments. The internal fluid inertia has a stronger influence at higher modes, resulting in a noticeable smoothing of deformation gradients and slightly lower FEM frequency compared to the analytical prediction. This mode also demonstrates how fluid–structure coupling becomes increasingly significant with increasing mode order.

6.3 Comparison Between the Analytical Formulation and Full FSI Finite Element Models (Unit Cell and Five Cells)

When periodic liquid dampers (PLDs) are incorporated into a structural system, the resulting dynamic response is influenced by a combination of structural flexibility, fluid motion, and their interaction. Even in simplified configurations, the coupling between the liquid damper cavities, the host structure, and the internal fluid can cause complex dynamic effects—especially when fluid–structure interaction (FSI) becomes important. In such cases, the overall behaviour cannot always be understood solely from the damper or the structure itself.
Periodic arrangements of cavities can influence wave propagation in the supporting structure through mechanisms such as periodic scattering. However, when the cavities contain liquid, additional sloshing modes and hydrodynamic pressures modify the effective mass and stiffness experienced by the host structure. This alters both the structural vibration modes and the fluid response, and the combined behaviour is generally sensitive to geometric parameters, fill levels, and boundary conditions.
Due to this complexity, an analytical model—although useful for parametric studies and physical interpretation—must be validated against a more comprehensive numerical representation that explicitly considers the coupled fluid–structure domain. Finite element (FE) simulations serve as such a reference, enabling the interaction between the damper cavities, the host structure, and the fluid to be captured without the simplifying assumptions necessary in the analytical approach. Comparing both methods clarifies the range of validity of the analytical model and emphasises the impact of coupling mechanisms that may only be partially represented in simplified theories.

6.3.1 FE Transmissibility and Parametric Study of Unit Cell (Force Excitation)

Finite element–based transmissibility analysis provides a practical tool for evaluating how dynamic disturbances propagate through periodic structures that include fluid-filled cavities or liquid dampers. In these systems, a unit cell typically consists of a finite segment of the host structure—such as part of a tank wall or a tube— together with the contained liquid and any attached damping or resonant components. The transmissibility quantifies the ratio between the response at the downstream boundary of the cell and the response at the upstream boundary, under steady-state harmonic loading.
When sloshing is present, this response is influenced not only by the structural dynamics but also by the hydrodynamic pressure field generated by the moving fluid. As a result, the transmissibility captures both the resonant behaviour of the structure and the additional mass, stiffness, and coupling effects introduced by fluid–structure interaction (FSI). The excitation may arise from harmonic base motion or from fluid-induced forces, and the resulting frequency-domain response can be obtained by solving the coupled dynamic equilibrium:

$$(\mathbf{K} - \omega^2\mathbf{M})\mathbf{q} = \mathbf{F}, \tag{6.6}$$

where **K** and **M** are the global stiffness and mass matrices of the unit cell, including contributions from the liquid domain—**q** is the nodal displacement vector, and **F** represents the external structural or fluid-induced forcing [246, 38].

Using the analytical model related to the periodic system, to characterize wave attenuation, Bloch-Floquet boundary conditions can be applied at the unit cell interfaces. These conditions relate the degrees of freedom at the left and right boundaries of the unit cell via a complex exponential term e^{μ}, where μ is the Bloch propagation constant. Solving the eigenvalue problem under these boundary conditions provides information on attenuation (real part of μ) and phase change (imaginary part), which directly influences transmissibility [139, 220]. A parametric study is typically performed to assess how various physical parameters, such as liquid height, sloshing mass distribution, tank stiffness, damping coefficients, or resonator properties, affect the transmissibility. For example, increasing the depth of the fluid can change the location and width of the band gaps where wave propagation is suppressed [90, 194, 213].

Consider a cell that includes the pipe and tank as in Figure (6.10).

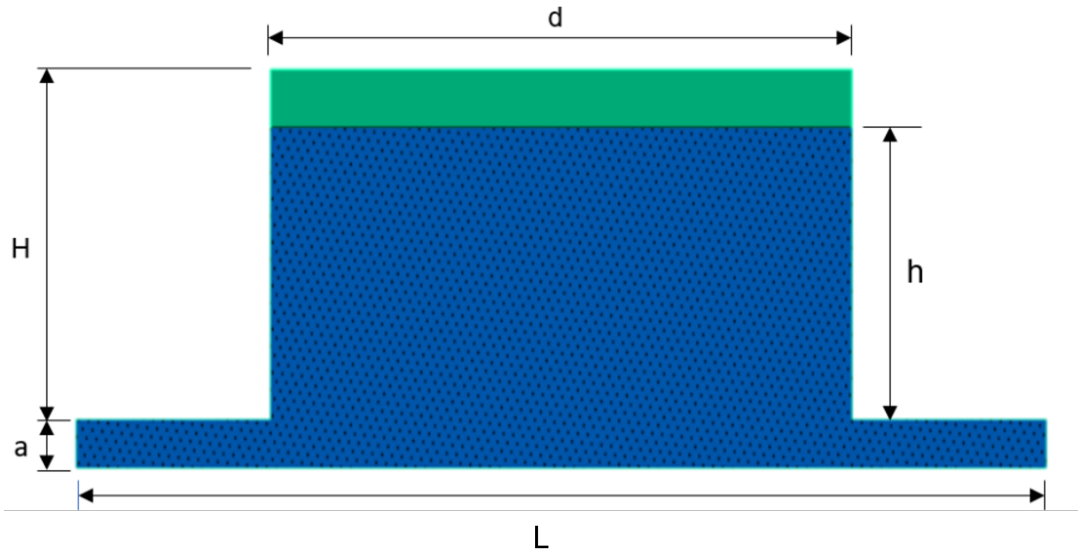

Figure 6.10: One unit cell

The data for this case of study are:

Table 6.3: Dimensions of unit cell

Parameters	L	d	H	h	a	t
Values (m)	3	1.8	1.08	0.9	0.15	0.0015

Based on Equation (3.29) to Equation (3.32), we can obtain the transmissibility of the system. The loading and boundary conditions are depicted in Figure (6.11). Harmonic excitation is assumed as:

$$F(t) = F_0 e^{i\omega t} \tag{6.7}$$

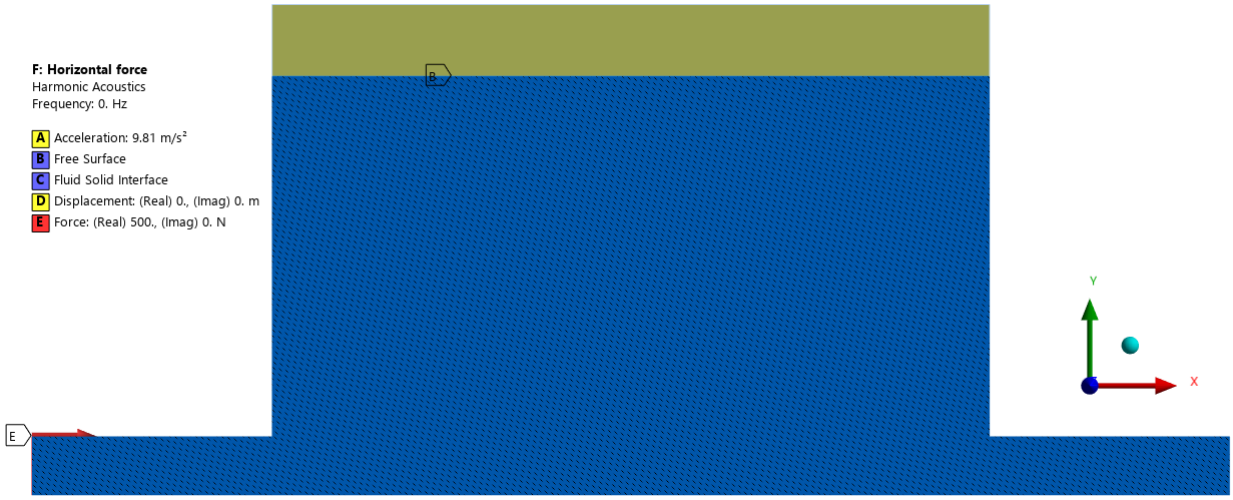

Figure 6.11: Loading conditions for unit cell (force case)

Force is applied as a pressure on the whole section area on the left side. Transmissibility is defined as:

$$TR = 20 \log_{10}\left(\frac{x_i}{x_o}\right) \tag{6.8}$$

where x_o and x_i are the displacements of the inlet (left side) and outlet (right side) of the structure (Figure (6.12)). More generally, transmissibility expresses the ratio between the displacement amplitude at the right boundary of the structure and the corresponding displacement at the left boundary, where the external excitation is applied. The transmissibility function is a useful indicator of the system's dynamic behavior. Frequency ranges in which $TR < 0$ correspond to attenuation regions, indicating reduced vibration transmission through the structure.

Figure 6.12: Positions of x_o and x_i in a unit cell

Figures (6.13a) and (6.13b) illustrate the transmissibility of a single periodic cell under harmonic excitation. In Figure (6.13a) two clear resonant peaks appear

around 0.7 Hz and 1.2 Hz, marking the frequencies where the axial vibration is strongly amplified. Between these peaks, a pass-band region is observed, while the areas immediately outside show a reduced response, indicating incipient stop-band behavior. Figure (6.13b) extends the range to 50 Hz, highlighting a dominant resonance near 20 Hz, followed by a gradual decay of transmissibility. In both plots, the FE model slightly overestimates the peak levels compared to the analytical curve, but the overall trend remains consistent.

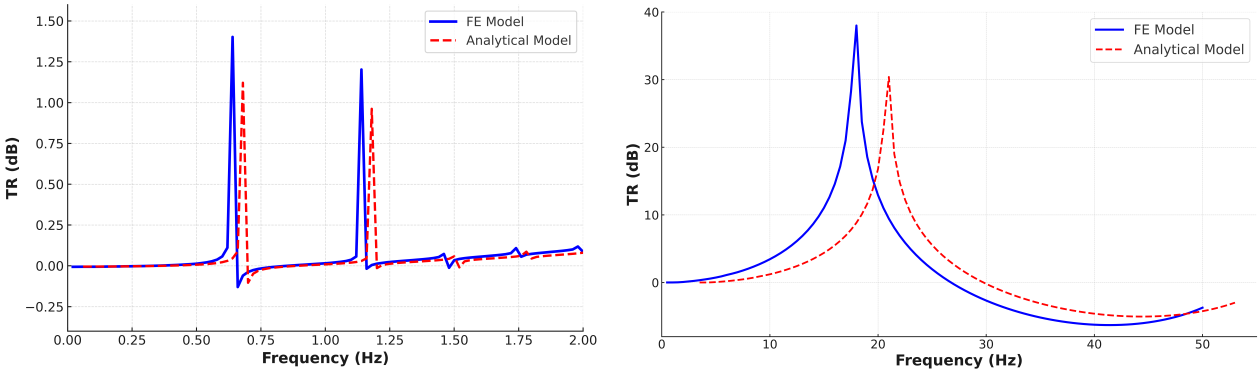

(a) (b)

Figure 6.13: Transmissibility of one unit cell (force case): (a) 0-2 Hz, (b) 0-50 Hz

The rightward shift of the FE resonant features in the figure is primarily due to the modelling of the pipe–tank connection. In the FE model, the interface is enforced via bonded contact, which imposes a strong kinematic constraint and effectively stiffens the junction region compared with the idealised coupling assumed in the analytical formulation. This increase in effective coupling stiffness raises the natural frequencies of the coupled modes, resulting in resonance peaks occurring at slightly higher frequencies in the FE response. Minor additional contributions may arise from 3D constraint effects at the junction that are not represented in the 1D analytical model. Importantly, the observed offset is limited and does not alter the identification of the main attenuation regions (pass-band/stop-band limits), but only produces a small frequency shift of the resonant features.

Figures (6.14) and (6.15) show the contours of the cell displacements at 20 Hz (pass band) and 40 Hz (stop band).

Figure 6.14: Total displacement contour at 20 Hz (pass band)

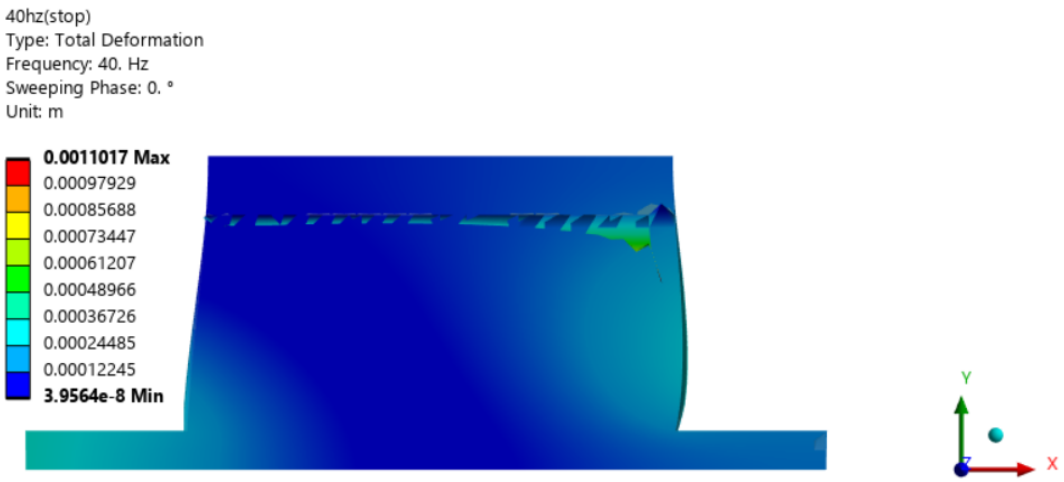

Figure 6.15: Total displacement contour at 40 Hz (stop band)

At 20 Hz (pass band), the displacement contour shows significant deformation along the tank wall, indicating wave propagation through the structure. Conversely, at 40 Hz (stop band), the deformation magnitude is markedly reduced, demonstrating vibration attenuation and localization. This confirms the formation of a stop band where energy transmission is inhibited, consistent with the band-gap behavior of the periodic system, effectively isolating vibrations at higher frequencies.

6.3.2 FE Transmissibility and Parametric Study of 5 Cells (Force Excitation)

To evaluate the effect of the number of cells on the response of the system, we consider a finite structure of five cells. Consider the places of 6 points in the system and the loadings Figures (6.16) and (6.17).

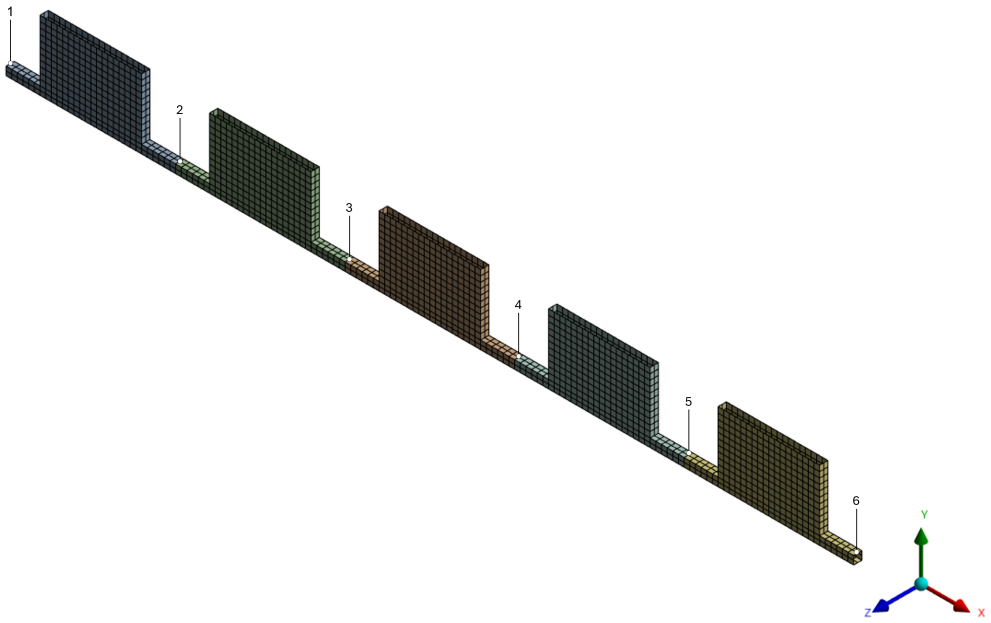

Figure 6.16: Six studied points in the 5-cell case

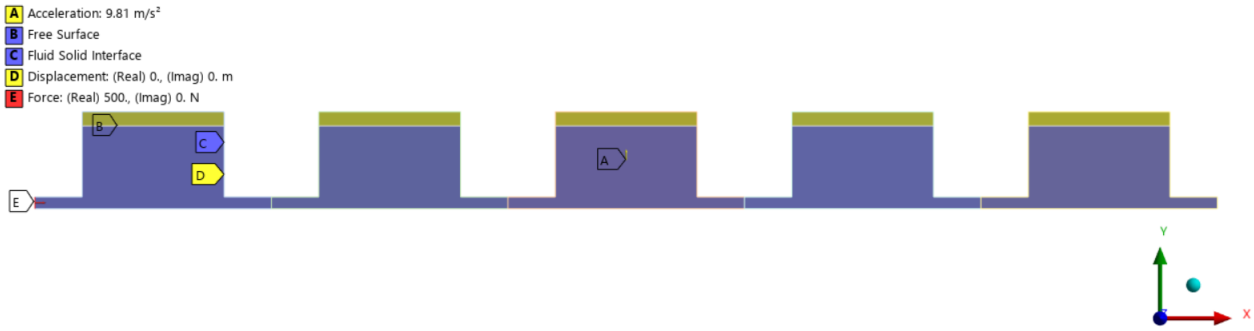

Figure 6.17: Loading conditions of 5-Cell case (force excitation)

By definition of:

$$TR1 = 20\log_{10}\left(\frac{x_2}{x_1}\right) \tag{6.9}$$

$$TR2 = 20\log_{10}\left(\frac{x_3}{x_1}\right) \tag{6.10}$$

$$TR3 = 20\log_{10}\left(\frac{x_4}{x_1}\right) \tag{6.11}$$

$$TR4 = 20\log_{10}\left(\frac{x_5}{x_1}\right) \tag{6.12}$$

$$TR5 = 20\log_{10}\left(\frac{x_6}{x_1}\right) \tag{6.13}$$

we can compare the transmisibility at each point and evaluate the effect of the number of cells on the stop/pass band.

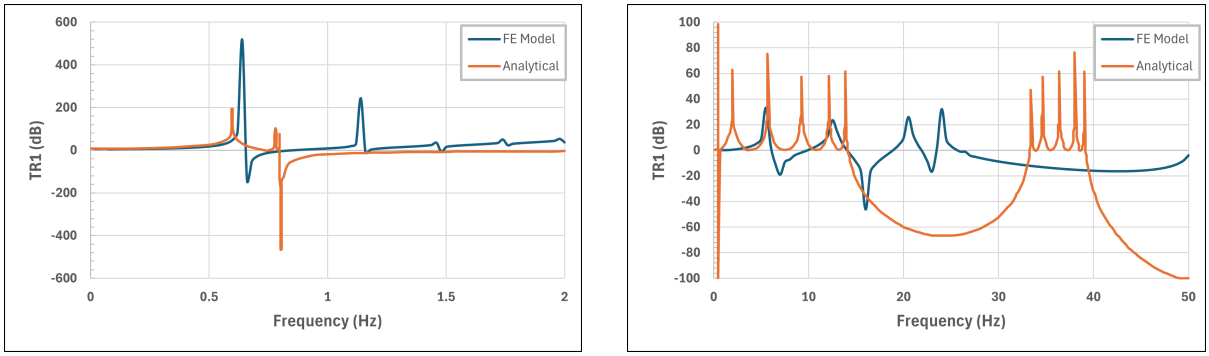

(a) (b)

Figure 6.18: Transmissibility (TR1) of the 5-cell case (force excitation): (a) 0-2 Hz, (b) 0-50 Hz

The transmissibility (TR1) curve of the 5-cell configuration under force excitation illustrate the dynamic response and the agreement between the FE and analytical models. In the low-frequency band (0–2 Hz), both models display marked resonance peaks linked to the global and local vibration modes of the liquid dapers. When extended to the full range (0–50 Hz), several attenuation zones appear, confirming the presence of stop bands resulting from periodicity. The difference in the results is because the analytical solution predicts the main band-gap locations for a simplified and infinite periodic structure, while the FE model provides a more detailed

response, capturing higher-order effects, damping influence, and the additional resonant interactions introduced by fluid–structure coupling phenomena for a finite structure of five cells.

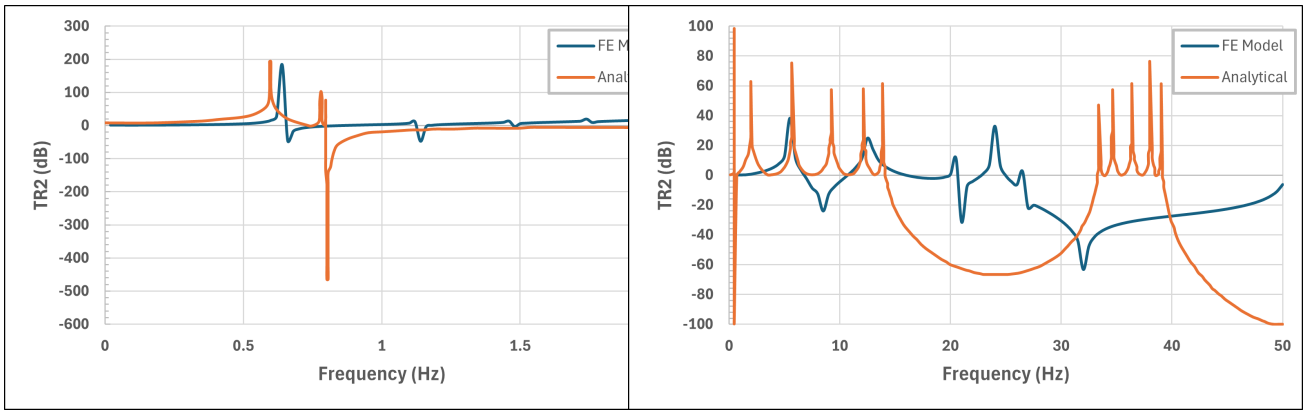

(a) (b)

Figure 6.19: Transmissibility (TR2) of the 5-cell case (force excitation): (a) 0-2 Hz, (b) 0-50 Hz

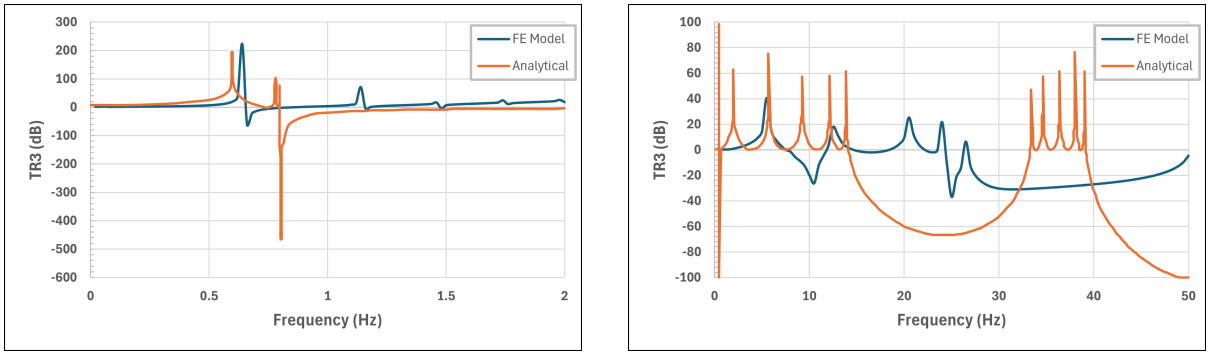

(a) (b)

Figure 6.20: Transmissibility (TR3) of the 5-cell case (force excitation): (a) 0-2 Hz, (b) 0-50 Hz

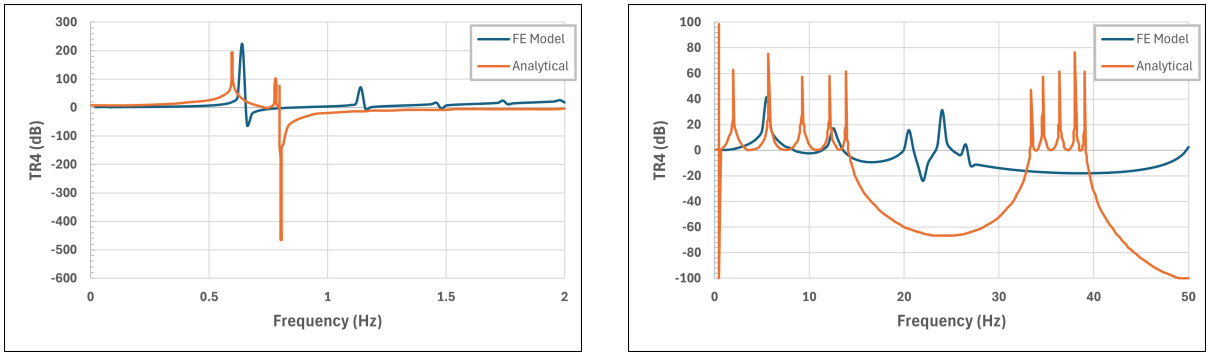

(a) (b)

Figure 6.21: Transmissibility (TR4) of the 5-cell case (force excitation): (a) 0-2 Hz, (b) 0-50 Hz

Figures (6.19), (6.20), and (6.21) illustrate the transmissibility responses (TR2, TR3, and TR4) of the five-cell configuration subjected to harmonic force excitation,

providing a direct comparison between the Finite Element (FE) simulations and the corresponding analytical predictions. These results clearly highlight how the gradual addition of periodic cells influences the periodicity effect. In the low-frequency range (0–2 Hz), both models exhibit almost identical trends, with sharp resonance peaks that correspond to the fundamental vibration modes. These peaks are mainly governed by the overall stiffness and distributed mass of the structure, where the fluid behaves as a nearly rigid body, resulting in large displacement amplitudes and a transmissibility ratio approaching 0 dB.

As the excitation frequency increases toward the higher range (up to 50 Hz), the influence of periodicity, and fluid–structure interaction in the FE model, becomes evident. Distinct attenuation regions emerge, corresponding to stop bands or band gaps where the propagation of elastic waves is attenuated. Within these intervals, the transmissibility magnitude decreases drastically, typically by 40–60 dB, indicating efficient vibration isolation. The analytical model successfully predicts the main band-gap boundaries, while the FE simulations capture additional physical effects such as damping, energy leakage, and minor coupling asymmetries caused by finite boundary conditions [98].

Moreover, adding more periodic cells makes the attenuation zones both sharper and wider, demonstrating the combined influence of Bragg scattering and resonance hybridization that is typical of periodic structures. The interaction between adjacent cells leads to phase opposition and destructive interference, which amplify the attenuation capability of the structure. Overall, these results validate the correspondence between analytical theory and FE modeling, demonstrating the ability of the simplified model to capture the main dynamics of the system. The analysis also shows that increasing the number of periodic liquid damper cells effectively broadens the stop-band range and improves the global vibration-mitigation performance.

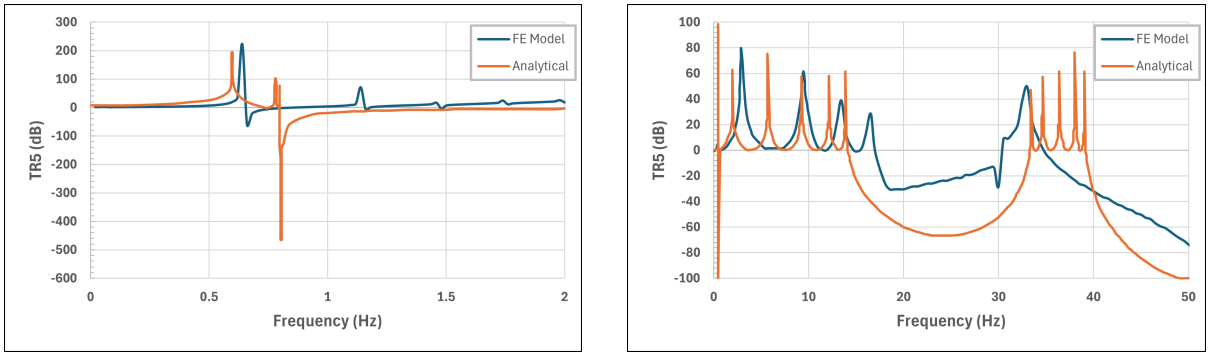

(a) (b)

Figure 6.22: Transmissibility (TR5) of the 5-cell case (force excitation): (a) 0-2 Hz, (b) 0-50 Hz

Figure (6.22) presents the transmissibility response (TR5) of the five-cell. This case exhibits the closest agreement between the formulations. In the low-frequency range (0–2 Hz), both approaches yield nearly identical curves, capturing the dominant global vibration mode of the system. The resonance amplitude at approximately 0.7 Hz remains moderate, and the displacement magnitude is consistent with those obtained in the previous configurations, confirming stable global dynamics as the number of cells increases.

The most significant advancement appears in the mid-frequency range (17–

30 Hz), which was previously not well represented in the 2-, 3-, and 4-cell cases. Within this band, the FE and analytical models show remarkable consistency in both amplitude and frequency trend. Distinct attenuation regions appear between 18 Hz and 28 Hz, indicating the development of a wide stop band where vibration transmission is suppressed. The FE model predicts a transmissibility reduction of approximately 50–60 dB within this range, while the analytical solution provides a nearly matching attenuation, with discrepancies below 5–10% in amplitude. Such an agreement validates the analytical formulation in predicting the attenuation zones and local resonances in the low frequency regime.

At higher frequencies (30–50 Hz), the FE response becomes slightly smoother due to the inclusion of damping and boundary losses, while the analytical curve retains sharper resonant peaks. In conclusion, the five-cell configuration demonstrates enhanced attenuation capability, wider band-gap formation, and good correlation between numerical and analytical models, confirming convergence of both approaches for periodic liquid damper systems.

Figures (6.23) and (6.24) compare pass (at frequency 5 Hz) and stop band (at 30 Hz) displacement contours.

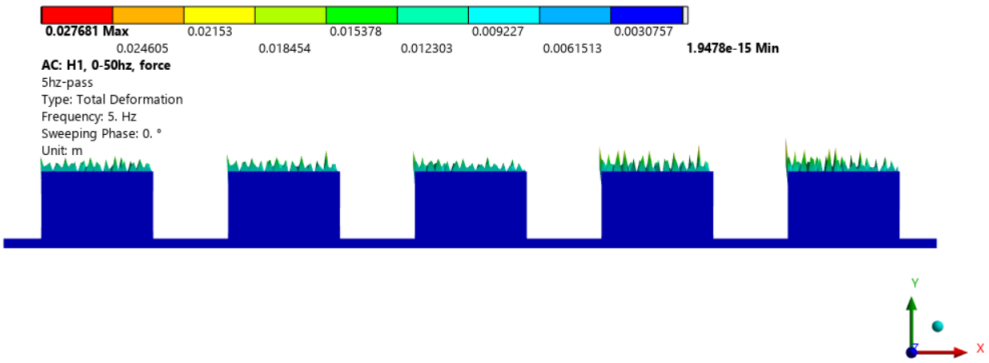

Figure 6.23: Total displacement contour at 5 Hz (pass band)

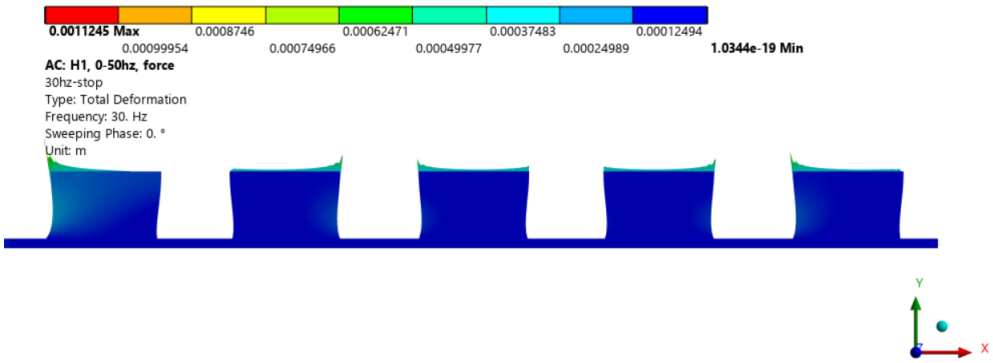

Figure 6.24: Total displacement contour at 30 Hz (stop band)

Figure (6.23) shows the total displacement contour of the system at when harmonically excited in a pass-band. It can be seen that the vibrational energy propagates efficiently through all five periodic cells. The deformation field extends continuously along the structure, confirming that the excitation frequency coincides with one of the propagating modes of the coupled pipe–tank system. The maximum total deformation reaches approximately 0.0277 m, while the minimum value,

around zero. It occurs near the place where motion is fully constrained. Intermediate regions exhibit displacement levels between 0.003 m and 0.021 m, indicating the gradual transmission of wave energy across successive cells. The patterns seen at the free surface do not indicate real fluid turbulence; instead, they arise from localized oscillations and amplified surface waves produced by the harmonic interaction between the liquid and the structural walls. These oscillations are further emphasized by the mesh discretization, the contour scaling, and the coupling at the fluid–structure interface. Such irregular contours indicate regions of high mobility, where the structural deformation and the free-surface sloshing move in phase, leading to noticeable surface motion even under small external excitations. At 5 Hz, the system clearly behaves in a pass-band regime: the wave energy propagates with little attenuation, the resonant motion builds up coherently across all unit cells, and the displacement levels remain high throughout the structure—consistent with freely propagating vibration modes below the first stop-band frequency.
At the excitation frequency of 30 Hz the system responds in a stop band region. The total displacement contour shown in Figure 6.24 clearly show a vibration attenuation condition of the periodic liquid damper system. In this frequency, wave propagation through the periodic arrangement of tanks and connecting pipes is strongly attenuated due to destructive interference and localized resonant effects. The overall deformation pattern demonstrates reduction in displacement amplitude along the structure, confirming that the system operates within a band gap where vibrational energy is reflected rather than transmitted. The maximum total deformation is approximately 0.00112 m, while the minimum value drops to about zero (1.03×10^{-19} m) near the fully confined boundary which illustrates an attenuation level exceeding four orders of magnitude compared with the 5 Hz pass-band case. Intermediate regions show displacement magnitudes between 0.00025 m and 0.00087 m, indicating that the vibrational energy rapidly decays as it moves from one cell to the next. This attenuation behavior is a defining feature of the stop-band mechanism, produced by the combined action of Bragg scattering and local resonance within the coupled fluid–structure system. In contrast to the 5 Hz contour, the 30 Hz response exhibits minimal surface undulations at the free liquid levels. The previously observed "turbulence-like" oscillations have vanished, replaced by smooth, nearly quiescent surfaces. This occurs because, at stop-band frequencies, the standing-wave fields confine motion locally at the first cells, preventing the phase propagation of waves across the periodic domain.

The contour clearly demonstrates that at 30 Hz, the system behaves as an efficient vibration barrier. The deformation field remains spatially confined, the free surfaces remain nearly still, and the transmitted motion between consecutive cells is negligible. This confirms the analytical prediction of a major stop band between approximately 17 Hz and 30 Hz, validating the Finite Element representation of wave attenuation and highlighting the remarkable energy isolation capability of the periodic liquid damper configuration.

This chapter has presented the numerical results obtained for the proposed periodic liquid damper configurations, examining the dynamic behaviour of the isolated tank, the coupled pipe–tank unit cell, and multi-cell periodic assemblies. Through contour plots, displacement distributions, and transmissibility analysis, the simulations have demonstrated the transition between pass-band and stop-band regimes. At low excitation frequencies, coherent wave propagation across successive cells con-

firms the presence of freely propagating modes, whereas at higher frequencies within the predicted band gap, strong attenuation and spatial confinement of motion are observed. The comparison between the 5 Hz pass-band response and the 30 Hz stop-band response clearly illustrates the combined effects of Bragg scattering and local resonance in suppressing vibration transmission.

These results validate the analytical dispersion predictions and confirm the effectiveness of the finite element modelling framework in capturing wave attenuation mechanisms in periodic fluid–structure systems. Having established both the physical interpretation and the numerical verification of the PLD concept, the final chapter synthesizes the main findings of the thesis, highlighting the methodological contributions and outlining potential directions for future research.

Chapter 7

Application and Case Study

Sloshing plays an important role in the design and safety assessment of many engineering systems. Understanding and controlling sloshing behavior is vital to ensure structural integrity, dynamic stability, and functional performance of containers, vehicles, and systems subjected to motion or excitation [97].

7.1 Application to Building Structures

In civil engineering, sloshing is not merely a fluid dynamic concern; it is an effective mechanism for passive energy dissipation and vibration control, especially when utilized through engineered devices such as Tuned Liquid Dampers (TLDs) and Tuned Liquid Column Dampers (TLCDs). The concept is related to the inertia and natural frequency of the moving liquid to counteract structural motions, thereby enhancing stability and comfort in tall and flexible structures. In structures such as water towers, rooftop storage tanks, and swimming pools, the fluid can interact with structural motion to exacerbate or mitigate the dynamic response. For example, during seismic loading, the resonance between the sloshing modes of the contained fluid and the fundamental structural mode can induce large lateral forces and overturning moments [210]. These interactions, if not taken into account properly, can lead to structural damage, tank failure, or excessive discomfort for the occupant.
An illustrative example is the 1994 Northridge earthquake in California, where several water tanks experienced severe sloshing, resulting in structural cracking and failure [73]. This highlighted the need to include sloshing effects in seismic design codes such as Eurocode 8 and API 650, which now require modal analysis of both structural and fluid systems. Tuned liquid dampers are passive control devices that consist of a container partially filled with liquid, typically placed at the top of a building. When the building undergoes movement (due to wind or seismic loads, for example), the sloshing liquid inside the TLD moves in the opposite direction, generating a counteracting force due to its inertia. The damping effect is enhanced by wave break, turbulence, and viscous dissipation [198]. The Kyobashi Seiwa Building in Tokyo is one of the first real-world applications of TLDs in buildings. Installed in the 1980s, the roof-mounted TLD successfully reduced wind-induced sway, improving comfort without the need for active energy input [202].
Some TLDs consist of U-shaped columns filled with fluid, where the liquid oscillates back and forth through a narrow orifice. The orifice provides controllable hydraulic damping, making more adaptable. Their simplicity, tunability, and large energy

dissipation capabilities have made them popular in bridge pylons, chimneys, and towers [134]. An example of practical implementation is the Kyobashi twin towers, where multiple TLCD units were installed to suppress lateral motion induced by wind. The researchers reported a 30-40% reduction in peak displacement [209]. Modeling sloshing in building-mounted dampers requires coupling fluid dynamics with structural motion. For rectangular tanks, the Navier-Stokes equations can be linearized and solved using potential flow theory. However, for high-amplitude or resonant sloshing, nonlinear models, including Volume of Fluid (VOF) and Smooth Particle Hydrodynamics (SPH), are used in computational tools such as ANSYS Fluent or OpenFOAM [114]. For practical design, simplified mechanical analogues, such as mass-spring-dashpot systems, are used to represent sloshing tanks behavior [236]. In seismic of buildings, sloshing dampers offer a cost-effective solution. They are particularly suited to flexible frame structures, where modal energy is concentrated in the first few modes. Case studies such as TLC towers in Korea and Taipei 101 demonstrate how liquid damping mechanisms can be tailored to specific seismic performance targets [95]. Experimental validation through shaking table tests and real-time hybrid simulations confirms the effectiveness of sloshing dampers in reducing both acceleration and drift.
Despite their advantages, sloshing-based devices face several limitations [96]:
1- Temperature sensitivity of damping (due to fluid viscosity),
2- Sensitivity to adjustment to structural frequency shifts due to damage or aging,
3- Complexity in modeling nonlinear wave breaking.
Innovations to overcome these include the use of magnetorheological fluids for adaptive damping [239], multi-directional TLCD arrays to suppress torsional modes [110], and coupled metafluidic dampers utilizing local resonances [240].
Beyond performance, sloshing dampers can be integrated into building. This duality is leveraged in projects like the Marina Bay Sands SkyPark, where pool levels on the roof contribute to mass damping. In addition, TLDs can serve sustainability goals by combining rainwater harvesting with structural control. This integration of sloshing mechanisms into eco-design is gaining popularity in green building certifications. The future of sloshing-based control systems in building structures lies in intelligent materials, intelligent monitoring, and adaptive control [97]. Recent research has explored the use of real-time feedback systems that adjust liquid levels or geometry in TLDs to maintain resonance with shifting building frequencies caused by temperature, aging, or seismic damage [40]. Integration of sensors and actuators within the damping unit enables real-time tuning, effectively transforming passive systems into semi-active or active sloshing dampers. Another emerging trend is the modularization of TLD and TLCD systems, which enables flexible designs based on prefabricated units that can be quickly configured and installed in practical engineering applications. This is especially promising for existing infrastructure in earthquake-prone regions where conventional base isolation is not feasible [156]. Moreover, multi-physics modeling platforms now allow simulation of fluid-structure interaction under coupled thermal, seismic, and aerodynamic loads. This computational capability supports the optimization of hybrid systems that combine sloshing dampers with tuned mass dampers (TMD) and viscous wall dampers, thus improving robustness [243]. As sustainability and resilience become central themes in modern structural engineering, the use of sloshing-based technologies is expected to evolve into a standard feature of smart, adaptable, and environmentally conscious

building systems.

7.2 Application to Aerospace or Marine Systems

In aerospace and marine systems, where vehicles undergo multidirectional acceleration, rapid movement, or external excitations such as waves or turbulence, sloshing becomes a crucial fluid-structure interaction (FSI) problem. Sloshing can cause unwanted dynamic effects, such as a shift of the center of mass, impact pressure on the walls, loss of control stability, and even structural failure if not adequately controlled [97, 58]. Consequently, understanding, modeling, and mitigating sloshing is fundamental to ensure the stability and safety of launch vehicles, spacecraft, ships, submarines, and offshore platforms. In aerospace systems, sloshing is most prominent in liquid propellant tanks during launch, stage separation, and orbital maneuvering. During vertical launch, the combination of thrust, vibration, and g-loading causes sloshing that leads to dynamic loads on the tank walls, which may excite structural modes or interact with guidance systems [68]. For example, the Apollo program encountered significant coupling between sloshing motion and autopilot dynamics, requiring tailored damping strategies to mitigate attitude instability [62]. The liquid inside the tank acts as a moving mass, and its momentum transfer affects the vehicle's pitch, yaw, and roll. Mechanical analog models, representing sloshing as spring–mass–damper systems, are commonly used in control system simulations to approximate the dynamic behavior [236]. These models provide engineers with transfer functions that can be incorporated into the guidance algorithms to predict and correct for slosh-induced torque. In spacecraft and satellites, sloshing becomes particularly critical when attitude control is sensitive to small angular disturbances, such as in microgravity environments. Another example is related to propellant management systems (PMS) that include bladders, diaphragms, or vortex suppressors to eliminate free surfaces and minimize sloshing [177]. Sloshing can also degrade the performance of the reaction control system (RCS) or induce jitter in inertial navigation systems [40]. Moreover, spacecraft maneuvering with low-thrust propulsion systems (e.g., ion engines) often operates over extended durations, during which low-frequency, long-duration slosh can accumulate and drift the spacecraft off-course [25]. Numerical simulations using computational fluid dynamics (CFD) coupled with finite element structural models help estimate the unsteady forces and moments transmitted through the tank walls and mounting supports [223].

In marine systems, sloshing is prominent in Liquefied Natural Gas (LNG) carriers, where cargo is stored in large partially filled membrane or spherical tanks. When the vessel is subjected to slam, roll, or pitch movements on rough seas, liquid cargo reacts with violent sloshing that can induce hydrodynamic impact pressures, also known as sloshing loads, on the tank walls [114]. These transient impacts can cause local structural damage. To manage this, classification societies such as DNV and ABS require detailed sloshing model tests and simulations under anticipated sea states. Experimental studies often employ scaled tanks using Froude scaling, while numerical models use Volume-of-Fluid (VOF) or Smoothed Particle Hydrodynamics (SPH) to capture free surface deformation and impact phenomena [40]. Partially filled ballast tanks and fuel tanks contribute to free surface effects, reducing transverse metacentric height, and thereby ship stability. In rough seas, the movement

of liquid in these tanks can resonate with the natural rolling frequency of the ship, amplifying roll motion and possibly leading to capsizing [97]. This phenomenon is particularly problematic in fishing boats, coasters, and tankers during partial loading. Anti-slosh baffles are used to divide into discrete tanks and suppress wave formation, while modern ship designs integrate tuned liquid dampers (TLDs) within superstructures to attenuate excessive vibrations or sway [210, 199]. In cruise ships and offshore platforms, passive damping strategies improve passenger comfort and extend the lifespan of equipment. High-fidelity simulations in both aerospace and marine contexts often use CFD–FEM coupling to model the interaction between fluid sloshing and flexible tank walls. Programs such as ANSYS Fluent, LS-DYNA, and STAR-CCM+ are widely adopted to resolve nonlinear free surface motion, turbulence, and pressure distribution over time [156]. In the marine industry, Reynolds Average Navier-Stokes (RANS) and Large Eddy Simulation (LES) models capture the turbulent energy of impact events with greater accuracy. For linear sloshing scenarios, modal decomposition is often used. Natural sloshing frequencies and mode shapes are computed by solving the Laplace equation with free surface boundary conditions, typically generating Bessel functions in cylindrical tanks or Fourier series in rectangular tanks [68]. These frequencies are then used to assess resonance risks in structural designs. Experimental studies are critical in validating numerical models. In the aerospace domain, parabolic flight tests have been conducted to assess sloshing dynamics under microgravity [242]. In marine environments, sloshing impact experiments are carried out in wave tanks with 1:10 or 1:20 scaled cargo models. Sensors measure wall pressures and accelerations to assess sloshing-induced loads under simulated sea conditions [162]. In addition, shake-table testing replicates the combined effects of seismic excitation and sloshing for naval platforms and offshore structures. These tests help refine design standards and code provisions, such as Eurocode 8 and API RP 2A for offshore installations.

The Ariane 5 upper stage extensively used dampers and baffles to mitigate propellant sloshing that affected attitude control. Likewise, SpaceX's Falcon 9 relies on high-fidelity simulations to manage sloshing-induced loads during stage separation and engine shutdown. The launch vehicle also underwent extensive testing to assess how sloshing could damage its internal insulation. The study resulted in the application of reinforced membranes, flexible insulation, and new loading protocols for partial fill operations [114]. Future research focuses on machine learning-assisted sloshing modeling, which allows real-time estimation of sloshing forces from sensor data [243]. Furthermore, the use of metafluidic systems, with engineered sloshing responses, may offer customized mitigation strategies in next-generation vehicles [239].

Chapter 8

Conclusion and Future Work

This thesis has investigated the dynamic behaviour of fluid-filled structures equipped with Periodic Liquid Dampers (PLDs), with the objective of understanding and predicting their vibration-attenuation mechanisms under axial excitation. A combined analytical and numerical strategy was developed, integrating Dynamic Stiffness Matrix (DSM) formulations with fully coupled Finite Element (FE) fluid–structure interaction (FSI) models. The work established a consistent modeling approach capable of capturing the main dynamic features of periodic fluid–structure systems, including sloshing effects, local resonances, and bandgap formation. The analytical DSM formulation clarified the fundamental role of both fluid properties and periodic layout in shaping wave-propagation behavior, while the FE models provided a detailed multiphysics validation of these predictions.

The results show that periodic configuration of liquid dampers can reduce axial vibration transmission in fluid-filled structures through the combined effects of fluid-structure coupling, local resonances, and periodicity effects. A major contribution of the work is the evaluation of the Dynamic Stiffness Matrix (DSM) analytical formulation's capabilities and limitations for predicting these effects in vibration mitigation. The DSM approach, derived from the exact formulation of the equations of motion, provided a simplified model for interpreting how structural stiffness, fluid inertia, and free-surface sloshing modes interact within a periodicity. Its predictions successfully identified the formation of frequency band gaps, distinguishing the roles played by fluid height, density, free-surface conditions, and geometric periodicity.

A central objective of this research was to examine the validity of these analytical predictions when compared with detailed multiphysics models. The coupled finite element (FE) simulations developed in ANSYS reproduced the system's fundamental structural and fluid modes, including free-surface oscillations and fluid–structure interaction. The transmissibility analyzis of both unit cells and multi-cell assemblies showed attenuation behavior consistent with that predicted by the DSM, with only minor frequency shifts attributable to damping assumptions and mesh discretization. This agreement confirms that the DSM can provide a sufficient reliable and computationally efficient tool for preliminary analyzes and parametric investigations of periodically coupled fluid–structure systems at low frequency.

The FE modal also offered clear insight into the evolution of mode shapes, revealing hybridization phenomena in which sloshing modes and axial structural modes interact near resonance. These observations support the interpretation of sloshing resonances as local resonant mechanisms analogous to those found in acoustic

metamaterials. From a practical viewpoint, the combined analytical and numerical results demonstrate that periodic liquid dampers can be used to generate low- and mid-frequency band gaps, thereby offering a passive means of controlling vibration propagation in slender fluid-filled structures. Although the study focuses on simplified geometries, the underlying mechanisms identified here provide a foundation for further investigation of periodic fluid-based damping devices.

In the following, the key contributions and findings of the thesis are presented through a structured overview of each chapter.

Chapter 1 — Introduction. Chapter 1 outlined the motivation for studying vibration mitigation in fluid-filled structural components, especially in systems such as pipelines, storage tanks, and aerospace structures where axial vibrations can propagate efficiently and compromise structural reliability. The chapter identified the need for modeling approaches that can account simultaneously for periodicity, sloshing behaviour, and fluid–structure coupling. The research objectives were defined as: (i) developing a simplified yet physically grounded analytical formulation based on the DSM approach, (ii) constructing detailed FE–FSI models for validation and deeper insight, and (iii) comparing the two sets of predictions to clarify the role of fluid parameters, geometry, and periodicity.

Chapter 2 — Literature Review. Chapter 2 presented a review of the state of the art on vibration control, tuned liquid dampers, fluid–structure interaction modeling, and periodic or locally resonant metamaterials. The chapter highlighted a research gap: while sloshing-based dampers and periodic metamaterial concepts have been independently studied, very few works have examined their combined effect in fluid-filled periodic structures, and even fewer have validated simplified analytical models against full FSI simulations. This gap motivated the modeling strategy adopted in the thesis.

Chapter 3 — Simplified Model. Chapter 3 developed the analytical model based on the Dynamic Stiffness Matrix approach. Starting from the governing equations of the coupled fluid–structure unit cell, the frequency-dependent dynamic stiffness is formulated. Applying Bloch periodicity enabled the computation of dispersion curves and the identification of both sloshing-driven local resonance band gaps and Bragg-type gaps associated with periodicity. The chapter showed that the DSM method can provides a clear physical interpretation of how fluid height, density, and free-surface conditions affect the lower-frequency regime, whereas cell length and structural mass influence the higher-frequency behavior. Importantly, the DSM formulation proved capable of predicting the main attenuation zones with minimal computational cost, making it a practical tool for parametric studies and preliminary design.

Chapter 4 — Finite Element Formulation. Chapter 4 established a high-fidelity finite element formulation to model the same system in a fully coupled fluid–structure interaction environment. The FE model combined structural elements with an acoustic fluid domain and included appropriate interface conditions to enforce pressure–displacement continuity. Special attention was given to the representation of the free surface and to the mesh refinement strategies ensuring numerical stability. The chapter detailed the implementation of periodic boundary conditions and validated the model by comparing structural and sloshing modes with analytical expectations. This chapter provided the numerical results to validate the DSM formulation and to observe the system's full multiphysics response.

Chapter 5 — Liquid Dampers: FE modeling. Chapter 5 analyzed the isolated behavior of the host structure, first empty and then filled with fluid, establishing the modifications induced by fluid–structure interaction even before periodicity is introduced. The results clearly showed the role of fluid inertia and internal pressure fields on shifting natural frequencies and altering modal patterns. These findings were useful for interpreting the hybrid modes observed in the subsequent investigations.

Chapter 6 — Numerical Results and Analysis. Chapter 6 presented the central results of the thesis. FE–FSI simulations of periodic systems, both single-cell and multi-cell, were performed under harmonic excitation and compared directly with DSM-based transmissibility predictions. The comparison revealed excellent consistency in identifying the locations and widths of the bandgaps. Lower-frequency gaps were driven by sloshing-induced local resonances, whereas higher-frequency gaps reflected Bragg scattering. Differences between analytical and numerical results were minor and confirmed the validity of the simplified model. Mode-shape visualisations clarified the hybridisation between fluid sloshing and structural axial modes, providing the first multiphysics confirmation of the mechanisms hypothesised in the analytical formulation.

Dissemination of Results

Part of the work developed in this thesis has been presented through two peer-reviewed international conference publications, which showed preliminary findings and supported the progressive development of the research. A first contribution was presented at the *RASD 2024 – International Conference on Structural Dynamics* [51], where an initial DSM-based analytical framework was introduced to investigate band-gap formation in fluid-filled periodic structures. In that work, the focus was placed on the simplified mechanical representation of the unit cell and on the role of fluid sloshing as a local resonance mechanism capable of generating low-frequency stop bands. The study demonstrated the feasibility of using the Dynamic Stiffness Matrix approach to characterize dispersion behavior and provided the first parametric insights into how fluid height and tank geometry influence attenuation characteristics.

A second contribution was later presented at the *COMPDYN 2025 – International Conference on Computational Methods in Structural Dynamics and Earthquake Engineering* [52]. This work extended the preliminary analysis by coupling the DSM predictions with full finite element models, including fluid–structure interaction, thereby validating the analytical framework proposed in the earlier study. The conference paper showcased the hybridization phenomena between structural and sloshing modes, confirmed the emergence of both local-resonance and Bragg-type band gaps, and demonstrated the effectiveness of periodic liquid dampers for axial vibration attenuation.

The findings developed in this thesis have also laid the groundwork for further progress within another PhD poject at the Doctoral School of Industrial Engineering of the University of Parma. Building on the analytical and numerical frameworks established here, and the insights into band-gap formation in periodic liquid-filled systems, a further PhD project is in progress to extend and deepen the investigation. This forthcoming research will explore more advanced configurations, multi-

directional wave propagation, and experimental validation.

Future Work

The assumptions identified in this thesis suggest several promising directions for further research. A natural extension of the present work concerns broadening the wave propagation analysis beyond the longitudinal motion considered here to include transverse and coupled multi-directional wave propagation. Incorporating flexural and transverse dynamics would allow investigation of richer dispersion phenomena, including directional stop-band formation, mode conversion, and coupling between longitudinal and transverse wave modes. Such an extension could provide deeper insight into the mechanisms governing complete band-gap formation and reveal additional opportunities for enhanced vibration attenuation through wave-mode interactions.

Another development involves extending the study to transient and broadband excitations. While the present analysis has focused primarily on harmonic steady-state responses, practical systems are often subjected to impulse-type loads, shocks, or broadband disturbances. Investigating the response of periodic liquid damper systems under transient excitations would provide a more comprehensive assessment of attenuation performance and the robustness of the predicted band gaps under realistic loading conditions.

Finally, future work should pursue experimental verification. Laboratory tests on periodic tank–pipe prototypes, using displacement measurement, pressure sensors, and free-surface tracking, would provide crucial validation of both the DSM formulation and the FE–FSI numerical predictions. Such experiments would also guide the refinement of the models and support the eventual development of engineering design guidelines for periodic LDs in practical applications.

Bibliography

[1] H. N. Abramson. *The Dynamic Behavior of Liquids in Moving Containers (NASA SP-106)*. NASA, 1966.

[2] L. Airoldi and M. Ruzzene. "Design of tunable acoustic metamaterials through periodic arrays of resonant shunted piezoelectric patches". In: *New Journal of Physics* 13 (2011), p. 113010.

[3] Mohammed Al Rifaie, Hasanain Abdulhadi, and Ahsan Mian. "Advances in Mechanical Metamaterials for Vibration Isolation: A Review". In: *Advances in Mechanical Engineering* 14.3 (2022), pp. 1–20. DOI: 10.1177/16878132221082872.

[4] Adnan Ali, Anirban Mitra, and Brahim Aïssa. "Metamaterials and metasurfaces: A review from the perspectives of materials, mechanisms and advanced metadevices". In: *Nanomaterials* 12.6 (2022), p. 1027. DOI: 10.3390/nano12061027.

[5] J.-F. Allard and N. Atalla. *Propagation of Sound in Porous Media: Modelling Sound Absorbing Materials*. 2nd ed. Wiley, 2009. DOI: 10.1002/9780470747339.

[6] Marco Amabili. *Nonlinear Vibrations and Stability of Shells and Plates*. Cambridge: Cambridge University Press, 2008.

[7] ANSYS Inc. *ANSYS Documentation*. 2025.

[8] N. Aquelet, M. Souli, and L. Olovsson. "ALE formulation for fluid–structure interaction problems in liquid-filled tanks under impact". In: *Computer Methods in Applied Mechanics and Engineering* 195.37–40 (2006), pp. 4797–4819. DOI: 10.1016/j.cma.2005.10.020.

[9] R. J. Astley. "Infinite elements for wave problems: Fundamentals and applications". In: *Journal of Computational Acoustics* 8.1 (2000), pp. 1–28. DOI: 10.1142/S0218396X00000016.

[10] N. Atalla and F. Sgard. *Finite Element and Boundary Methods in Structural Acoustics and Vibration*. CRC Press, 2015. DOI: 10.1201/b18613.

[11] H. Bachmann, W. Ammann, and F. Deischl. "Human comfort and liquid dampers in buildings". In: *Structural Engineering International* 5.2 (1995), pp. 109–118. DOI: 10.2749/101686695780601019.

[12] J. R. Banerjee. "Dynamic stiffness formulation for structural elements: A general approach". In: *Computers and Structures* 63.1 (1997), pp. 101–103. DOI: 10.1016/S0045-7949(96)00326-4.

[13] P. Banerji and M. Murudi. “Seismic vibration control of buildings using tuned liquid dampers”. In: *Earthquake Engineering and Structural Dynamics* 25.6 (1996), pp. 659–674. DOI: 10.1002/(SICI)1096-9845(199606)25:6<659::AID-EQE567>3.0.CO;2-L.

[14] P. Banerji, M. Murudi, and A. H. Shah. “Implementation of tuned liquid column dampers in buildings in India”. In: *Journal of Structural Engineering* 126.3 (2000), pp. 281–288. DOI: 10.1061/(ASCE)0733-9445(2000)126:3(281).

[15] P. Banerji and A. Samanta. “Response of multi-degree-of-freedom structures with multiple tuned liquid dampers”. In: *Earthquake Engineering and Structural Dynamics* 30.5 (2001), pp. 745–763. DOI: 10.1002/eqe.35.

[16] K.-J. Bathe. *Finite Element Procedures*. Prentice Hall, 1996.

[17] H. F. Bauer. “Coupled vibrations of fluid-filled elastic containers”. In: *Journal of Fluids and Structures* 13.5 (1999), pp. 561–579. DOI: 10.1006/jfls.1999.0212.

[18] Yuri Bazilevs, Kenji Takizawa, and Tayfun E. Tezduyar. *Computational fluid-structure interaction: Methods and applications*. Chichester: Wiley, 2013.

[19] F.-X. Bécot and N. Atalla. “Finite element modeling of poroelastic materials in acoustics”. In: *Journal of the Acoustical Society of America* 116.4 (2004), pp. 1995–2005. DOI: 10.1121/1.1783532.

[20] T. Belytschko and J. M. Kennedy. “Finite element methods for fluid–structure interaction in tanks under impulsive loading”. In: *Journal of Pressure Vessel Technology* 100.3 (1978), pp. 213–220. DOI: 10.1115/1.3454465.

[21] T. Belytschko, W. K. Liu, and B. Moran. *Nonlinear Finite Elements for Continua and Structures*. Wiley, 2000.

[22] A. Bermúdez et al. “Perfectly matched layers for time-harmonic acoustic wave propagation”. In: *SIAM Journal on Scientific Computing* 29.2 (2007), pp. 617–645. DOI: 10.1137/050646421.

[23] K. Bertoldi et al. “Flexible mechanical metamaterials”. In: *Nature Reviews Materials* 2 (2017), p. 17066. DOI: 10.1038/natrevmats.2017.66.

[24] Robert D. Blevins. *Formulas for Natural Frequency and Mode Shape*. Van Nostrand Reinhold, 1984.

[25] Christophe Bonnal, Jean-Michel Ruault, and Marie-Christine Desjean. “Propellant management in microgravity: Review and prospects”. In: *Acta Astronautica* 66.5–6 (2010), pp. 811–822.

[26] L. Brillouin. *Wave Propagation in Periodic Structures: Electric Filters and Crystal Lattices*. Dover Publications, 1953.

[27] M. Brun, S. Courrech du Pont, and A. Maurel. *Phononic Crystals: Wave Propagation and Resonance in Periodic Structures*. Wiley–VCH, 2012.

[28] M. Brun, S. Guenneau, and A. B. Movchan. “Achieving control of in-plane elastic waves”. In: *Applied Physics Letters* 94.6 (2009), p. 061903. DOI: 10.1063/1.3079673.

[29] T. R. Buckel and J. S. Kim. “Active vibration isolation in aerospace structures”. In: *Journal of Guidance, Control, and Dynamics* 9.2 (1986), pp. 185–191.

[30] W. Cai and V. M. Shalaev. *Optical Metamaterials: Fundamentals and Applications*. Springer, 2010. DOI: 10.1007/978-1-4419-1151-3.

[31] Y. Cai, X. Zhang, and X. Li. “Acoustic wave propagation in periodic liquid-filled structures”. In: *Journal of Sound and Vibration* 478 (2020), p. 115329. DOI: 10.1016/j.jsv.2020.115329.

[32] C. Caloz and T. Itoh. *Electromagnetic Metamaterials: Transmission Line Theory and Microwave Applications*. Wiley, 2006. DOI: 10.1002/0471784192.

[33] S. K. Chakrabarti. *Hydrodynamics of Offshore Structures*. Springer, 1987. DOI: 10.1007/978-94-009-3295-2.

[34] S. K. Chakrabarti and K. T. Ma. “Dynamic response of liquid-filled offshore caissons”. In: *Ocean Engineering* 26.7 (1999), pp. 635–659. DOI: 10.1016/S0029-8018(98)00012-0.

[35] A. R. Chandrasekaran and N. J. Gardner. “Seismic performance of elevated water tanks with flexible staging”. In: *Earthquake Engineering & Structural Dynamics* 23.5 (1994), pp. 507–522. DOI: 10.1002/eqe.4290230505.

[36] C. C. Chang. “Analytical design procedures for tuned liquid dampers”. In: *Journal of Engineering Mechanics* 124.4 (1998), pp. 449–456. DOI: 10.1061/(ASCE)0733-9399(1998)124:4(449).

[37] C. C. Chang and C. T. Hsu. “Applications of tuned liquid dampers to high-rise buildings”. In: *Structural Engineering and Mechanics* 6.4 (1998), pp. 391–403.

[38] T. Chen and D. C. Wiggert. “Dynamic behavior of fluid-filled cylindrical shells”. In: *Journal of Applied Mechanics* 41.2 (1974), pp. 403–408. DOI: 10.1115/1.3423311.

[39] W. Chen and M. A. Haroun. “Nonlinear sloshing and dynamic pressures in flexible tanks”. In: *Journal of Engineering Mechanics* 120.11 (1994), pp. 2310–2326. DOI: 10.1061/(ASCE)0733-9399(1994)120:11(2310).

[40] W. C. Chen and W. L. Chiang. “Dynamic pressure effects of sloshing under harmonic excitation”. In: *Journal of Pressure Vessel Technology* 136.1 (2014), p. 011204. DOI: 10.1115/1.4025431.

[41] Y. Chen and T. Wang. “Periodic liquid damper effects on cylindrical shells: FE modeling and vibration attenuation”. In: *International Journal of Mechanical Sciences* 169 (2020), p. 105298.

[42] Z. Chen, Y. Guo, and G. Hu. “Low-frequency band gaps in periodic fluid–solid systems”. In: *Wave Motion* 89 (2019), pp. 72–83. DOI: 10.1016/j.wavemoti.2019.03.001.

[43] Y. Cheng and Z. Liu. “Acoustic metamaterials: From local resonances to broad-band sound attenuation”. In: *Physical Review B* 81.17 (2010), p. 174303. DOI: 10.1103/PhysRevB.81.174303.

[44] S. K. Cho and S. H. Kwon. "Nonlinear sloshing effects in LNG storage tanks". In: *Ocean Engineering* 21.7 (1994), pp. 701–718. DOI: 10.1016/0029-8018(94)90005-1.

[45] A. K. Chopra. *Dynamics of Structures: Theory and Applications to Earthquake Engineering*. Prentice Hall, 2001.

[46] J. Christensen and F. J. García de Abajo. "Anisotropic metamaterials for full control of acoustic waves". In: *Physical Review Letters* 108.12 (2012), p. 124301. DOI: 10.1103/PhysRevLett.108.124301.

[47] S. Colwell and B. Basu. "Tuned liquid column-gas dampers for vibration control of structures". In: *Engineering Structures* 31.12 (2009), pp. 2930–2942. DOI: 10.1016/j.engstruct.2009.07.008.

[48] A. Craggs. "Sound transmission through a finite element model of an enclosure". In: *Journal of Sound and Vibration* 16.3 (1971), pp. 321–330. DOI: 10.1016/0022-460X(71)90453-7.

[49] L. Cremer, M. Heckl, and B. A. T. Petersson. *Structure-borne sound: Structural vibrations and sound radiation at audio frequencies*. 3rd ed. Berlin: Springer, 2005.

[50] S. A. Cummer, J. Christensen, and A. Alù. "Controlling sound with acoustic metamaterials". In: *Nature Reviews Materials* 1 (2016), p. 16001. DOI: 10.1038/natrevmats.2016.1.

[51] F. Dall'Olio et al. "A Preliminary Study on Band-Gaps Formation in Fluid-Filled Structures with Periodic Liquid Dampers". In: *Proceedings of the RASD 2024 – International Conference on Structural Dynamics*. 1-3 July 2024, University of Southampton, UK, 2024.

[52] F. Dall'Olio et al. "Wave Propagation and Sloshing Interactions in Structures with Periodic Liquid Dampers". In: *Proceedings of COMPDYN 2025 – 10th ECCOMAS Thematic Conference on Computational Methods in Structural Dynamics and Earthquake Engineering*. 15-18 June 2025, Rhodes Island, Greece, 2025.

[53] G. R. Darbre and J. Proulx. "Safety of large dams and reservoirs under seismic excitation". In: *Soil Dynamics and Earthquake Engineering* 22.9–12 (2002), pp. 1085–1092. DOI: 10.1016/S0267-7261(02)00121-8.

[54] Binita Dash et al. "A review of computational methods for vibroacoustic analysis of advanced material structures". In: *Archives of Computational Methods in Engineering* 31.4 (2024), p. 10204.

[55] J. P. Den Hartog. *Mechanical Vibrations*. McGraw-Hill, 1956.

[56] W. Desmet. "A wave based prediction technique for structural–acoustic problems at medium frequencies". In: *Journal of Sound and Vibration* 262.4 (2002), pp. 849–875. DOI: 10.1006/jsvi.2002.5102.

[57] P. A. Deymier. *Acoustic metamaterials and phononic crystals*. Springer, 2013. DOI: 10.1007/978-3-642-31232-8.

[58] F. T. Dodge. *The New "Dynamic Behavior of Liquids in Moving Containers"*. San Antonio, Texas: Southwest Research Institute, 2000.

[59] Jean Donea et al. “Arbitrary Lagrangian–Eulerian Methods”. In: *Encyclopedia of Computational Mechanics*. Ed. by Erwin Stein, René de Borst, and Thomas J. R. Hughes. Wiley, 2004.

[60] James F. Doyle. *Nonlinear Structural Dynamics: Using FE Methods*. Cambridge University Press, 2014. ISBN: 9781107045705.

[61] James F. Doyle. *Wave Propagation in Structures: Spectral Analysis Using Fast Discrete Fourier Transforms*. 2nd ed. New York: Springer, 1997.

[62] J. K. Dukowicz. “A finite-difference method for modeling sloshing”. In: *Journal of Computational Physics* 49.2 (1983), pp. 147–165.

[63] N. Engheta and R. W. Ziolkowski, eds. *Metamaterials: Physics and Engineering Explorations*. Wiley-IEEE Press, 2006. DOI: 10.1002/0471784192.

[64] B. Erkus and E. A. Johnson. “Nonlinear viscoelastic base isolation bearings under earthquake loading”. In: *Earthquake Engineering & Structural Dynamics* 33.7 (2004), pp. 687–706.

[65] G. C. Everstine. “A symmetric potential formulation for fluid–structure interaction”. In: *Journal of Sound and Vibration* 79.1 (1981), pp. 157–160. DOI: 10.1016/0022-460X(81)90481-0.

[66] G. C. Everstine. “Finite element formulations of structural–acoustics problems”. In: *Computers & Structures* 65.3 (1997), pp. 307–321. DOI: 10.1016/S0045-7949(96)00356-8.

[67] F. Fahy and P. Gardonio. *Sound and structural vibration: Radiation, transmission and response*. 3rd ed. Academic Press, 2007. DOI: 10.1016/B978-012373633-8.50001-9.

[68] Odd Magnus Faltinsen and Alexander N. Timokha. *Sloshing*. Cambridge University Press, 2009.

[69] N. Fang et al. “Ultrasonic metamaterials with negative modulus”. In: *Nature Materials* 5.6 (2006), pp. 452–456. DOI: 10.1038/nmat1644.

[70] Xibing Fang et al. “A dynamic analysis method of liquid-filled containers considering the fluid–structure interaction”. In: *Applied Sciences* 14.7 (2024), p. 2688. DOI: 10.3390/app14072688.

[71] C. Farhat, M. Lesoinne, and P. Le Tallec. “Load and motion transfer algorithms for fluid–structure interaction problems”. In: *Computational Methods in Applied Mechanics and Engineering* 190.24–25 (2001), pp. 2889–2904. DOI: 10.1016/S0045-7825(00)00391-2.

[72] Charbel Farhat, Matthieu Lesoinne, and Patrick Le Tallec. “Load and motion transfer algorithms for fluid/structure interaction problems”. In: *Computers & Structures* 83.2–3 (2006), pp. 219–231.

[73] FEMA. *FEMA 451 – NEHRP recommended provisions: Design examples*. Washington, D.C.: Federal Emergency Management Agency, 2003.

[74] J. Feng, Z. Zheng, and Q. Li. “Wave propagation and band gap phenomenon in periodic systems”. In: *Journal of Applied Mechanics* 80.3 (2013), p. 031005.

[75] H. Frahm. “Device for damping vibrations of bodies”. US989958A. 1911.

[76] Y. Fujino and L. Sun. “Hybrid system of active mass driver and tuned liquid damper”. In: *Earthquake Engineering and Structural Dynamics* 22.8 (1993), pp. 723–736.

[77] Y. Fujino, L. Sun, and B. Pacheco. “Tuned liquid dampers for reducing wind response of structures”. In: *Journal of Engineering Mechanics* 118.9 (1992), pp. 2017–2030. DOI: 10.1061/(ASCE)0733-9399(1992)118:9(2017).

[78] D. Givoli. *Non-Reflecting Boundary Conditions*. Springer, 2001. DOI: 10.1007/978-1-4613-0119-0.

[79] Philip M. Gresho and Ronald L. Sani. *Incompressible Flow and the Finite Element Method*. Wiley, 1998.

[80] J. N. Grima and K. E. Evans. “Auxetic behavior from rotating squares”. In: *Journal of Materials Science Letters* 19.17 (2000), pp. 1563–1565. DOI: 10.1023/A:1006781224002.

[81] Y. Guo and G. Hu. “Band gap formation and tunable low-frequency vibration attenuation in periodic fluid–solid systems”. In: *Journal of Sound and Vibration* 364 (2016), pp. 148–160. DOI: 10.1016/j.jsv.2015.12.032.

[82] A. K. Gupta and J. R. Hutchinson. “Nonlinear fluid–structure interaction in partially filled cylindrical tanks”. In: *Journal of Applied Mechanics* 52.2 (1985), pp. 293–298. DOI: 10.1115/1.3169027.

[83] I. Harari and T. J. R. Hughes. “Cost-effective absorbing boundary conditions for the Helmholtz equation”. In: *Computer Methods in Applied Mechanics and Engineering* 87.1 (1991), pp. 59–96. DOI: 10.1016/0045-7825(91)90092-4.

[84] M. A. Haroun and G. W. Housner. “Seismic design of liquid storage tanks”. In: *Journal of the Technical Councils of ASCE* 107.1 (1981), pp. 191–207.

[85] M. Higashino and S. Okamoto. *Response Control and Seismic Isolation of Buildings*. Taylor & Francis, 2006.

[86] C. W. Hirt, A. A. Amsden, and J. L. Cook. “An Arbitrary Lagrangian–Eulerian Computing Method for All Flow Speeds”. In: *Journal of Computational Physics* 14.3 (1974), pp. 227–253. DOI: 10.1016/0021-9991(74)90051-5.

[87] Jade E. Holliman et al. “Review of foundational concepts and emerging directions in metamaterial research: Design, phenomena, and applications”. In: *Materials Advances* 3.23 (2022), pp. 8390–8406. DOI: 10.1039/D2MA00497F.

[88] G. W. Housner et al. “Structural control: Past, present, and future”. In: *Journal of Engineering Mechanics* 123.9 (1997), pp. 897–971.

[89] G. W. Housner. “The dynamic behavior of water tanks”. In: *Bulletin of the Seismological Society of America* 53.2 (1963), pp. 381–387.

[90] H. H. Huang and C. T. Sun. “Wave attenuation mechanism in an acoustic metamaterial with negative effective mass density”. In: *New Journal of Physics* 11.1 (2009), p. 013003. DOI: 10.1088/1367-2630/11/1/013003.

[91] T. J. R. Hughes. *The Finite Element Method: Linear Static and Dynamic Finite Element Analysis*. Dover Publications, 2000.

[92] T. J. R. Hughes, W. K. Liu, and T. K. Zimmermann. “Lagrangian–Eulerian finite element formulation”. In: *Computer Methods in Applied Mechanics and Engineering* 29.3 (1981), pp. 329–349.

[93] K. H. Hunt and F. R. E. Crossley. “Coefficient of restitution interpreted as damping in vibroimpact”. In: *Journal of Applied Mechanics* 42.2 (1975), pp. 440–445. DOI: 10.1115/1.3423596.

[94] M. I. Hussein, M. J. Leamy, and M. Ruzzene. “Dynamics of phononic materials and structures: Historical origins, recent progress, and future outlook”. In: *Applied Mechanics Reviews* 66.4 (2014), p. 040802. DOI: 10.1115/1.4026911.

[95] J. S. Hwang, C. H. Yang, and K. Y. Lee. “Seismic performance of buildings with TLCDs”. In: *Engineering Structures* 26.8 (2004), pp. 1131–1141.

[96] R. A. Ibrahim. “Liquid sloshing dynamics: Theory and applications”. In: *Applied Mechanics Reviews* 57.4 (2005), pp. 315–386. DOI: 10.1115/1.1704623.

[97] Raouf A. Ibrahim. *Liquid sloshing dynamics*. Cambridge University Press, 2023.

[98] Raouf A. Ibrahim. *Liquid Sloshing Dynamics: Theory and Applications*. Cambridge: Cambridge University Press, 2005.

[99] F. Ihlenburg. *Finite Element Analysis of Acoustic Scattering*. Springer, 1998. DOI: 10.1007/978-1-4612-1764-6.

[100] F. Ihlenburg and I. Babuška. “Finite element solution of the Helmholtz equation with high wave number: Part II, the hp-version of FEM”. In: *Computer Methods in Applied Mechanics and Engineering* 137.3–4 (1997), pp. 373–409. DOI: 10.1016/S0045-7825(96)01089-0.

[101] Y. Ikeda and K. Iwamoto. “Bidirectional tuned liquid dampers”. In: *Structural Engineering/Earthquake Engineering* 13.2 (1996), pp. 123–134.

[102] J. D. Joannopoulos et al. *Photonic Crystals: Molding the Flow of Light*. 2nd ed. Princeton University Press, 2008.

[103] C. D. Johnson and A. Ezquerra. “Finite element analysis of fluid–structure interaction in cylindrical shells”. In: *Journal of Sound and Vibration* 72.1 (1980), pp. 1–17. DOI: 10.1016/0022-460X(80)90620-1.

[104] Joonkyo Jung et al. “Broadband metamaterials and metasurfaces: A review from the perspectives of materials and devices”. In: *Nanophotonics* 9.10 (2020), pp. 2677–2703. DOI: 10.1515/nanoph-2020-0111.

[105] W. S. Jung, S. H. Lee, and J. H. Kim. “Active vibration isolation using piezoelectric actuators in precision engineering”. In: *Precision Engineering* 27.2 (2003), pp. 170–179. DOI: 10.1016/S0141-6359(02)00122-9.

[106] M. Kadic et al. “On the practicability of pentamode mechanical metamaterials”. In: *Applied Physics Letters* 100.19 (2012), p. 191901. DOI: 10.1063/1.4709436.

[107] A. Kareem. “Response of tall buildings to wind: State of the art”. In: *Journal of Wind Engineering and Industrial Aerodynamics* 36 (1990), pp. 833–844. DOI: 10.1016/0167-6105(90)90325-P.

[108] A. Kareem and K. Gurley. “Damping in tall buildings: Overview and state-of-the-art”. In: *Journal of Structural Engineering* 122.9 (1996), pp. 897–906. DOI: 10.1061/(ASCE)0733-9445(1996)122:9(897).

[109] A. Kareem and S. Kline. "Performance of liquid column dampers under random loading". In: *Journal of Structural Engineering* 121.11 (1995), pp. 1614–1624. DOI: 10.1061/(ASCE)0733-9445(1995)121:11(1614).

[110] A. Kareem and S. Kline. "Performance of multiple tuned liquid column dampers under random loading". In: *Journal of Structural Engineering* 121.2 (1995), pp. 348–361.

[111] J. M. Kelly. *Earthquake-Resistant Design with Rubber*. Springer, 1997.

[112] N. Kessissoglou and S. Marburg, eds. *Computational Methods for Optimisation in Structural Acoustics and Vibration*. Springer, 2008. DOI: 10.1007/978-3-540-77448-7_15.

[113] R. Khare, S. K. Chakrabarti, and K. T. Ma. "Dynamic response of offshore structures to wave-induced tank sloshing". In: *Applied Ocean Research* 21.2 (1999), pp. 73–83. DOI: 10.1016/S0141-1187(99)00007-6.

[114] Y. Kim and H. S. Lee. "Nonlinear modeling of sloshing dampers using CFD". In: *Journal of Sound and Vibration* 304.1–2 (2007), pp. 241–260.

[115] S. Kumaraswamy and R. Sundaravadivelu. "Dynamic behavior of elevated tanks under seismic loads". In: *Journal of Sound and Vibration* 191.1 (1996), pp. 29–38. DOI: 10.1006/jsvi.1996.0117.

[116] M. S. Kushwaha, Y. Halevi, and R. Fleury. "Acoustic band gaps in periodic elastic composites". In: *Physical Review Letters* 71.13 (1993), pp. 2022–2025.

[117] K. C. S. Kwok and B. Samali. "Performance of tuned mass dampers under wind and earthquake loads". In: *Engineering Structures* 17.9 (1995), pp. 655–667.

[118] S. H. Kwon and J. Kim. "Seismic performance of tuned liquid column dampers in bridge structures". In: *Engineering Structures* 23.12 (2001), pp. 1599–1610. DOI: 10.1016/S0141-0296(01)00028-4.

[119] R. Lakes. "Foam structures with a negative Poisson's ratio". In: *Science* 235.4792 (1987), pp. 1038–1040. DOI: 10.1126/science.235.4792.1038.

[120] S. Lakshmi and M. Gayathri Devi. "A review on tuned liquid column dampers (TLCDs) and tuned liquid column dampers with embossments (ETLCDs)". In: *International Research Journal of Engineering and Technology* 7.3 (2020), pp. 3693–3698.

[121] C. H. Lamarque and P. O. Mattei. "Nonlinear vibration isolation using vibro-impact systems". In: *Nonlinear Dynamics* 11.1 (1996), pp. 1–19.

[122] R. S. Langley. "Analysis of power flow in beams and frameworks using the direct-dynamic stiffness method". In: *Journal of Sound and Vibration* 136.3 (1990), pp. 439–452.

[123] R. S. Langley and K. H. Heron. "Elastic wave propagation in periodic structures using finite elements". In: *Journal of Sound and Vibration* 140.2 (1990), pp. 243–260. DOI: 10.1016/0022-460X(90)90566-K.

[124] U. Lee. *Spectral Element Method in Structural Dynamics*. Singapore: Wiley, 2009.

[125] Huan Li, Yancheng Li, and Jianchun Li. "Negative stiffness devices for vibration isolation applications: A review". In: *Advances in Structural Engineering* 23.8 (2020), pp. 1739–1755. DOI: 10.1177/1369433219900311.

[126] J. Li and C. T. Chan. "Double-negative acoustic metamaterial". In: *Physical Review E* 70.5 (2004), p. 055602. DOI: 10.1103/PhysRevE.70.055602.

[127] Y. Li and X. Liu. "Application of tuned liquid dampers to offshore platforms". In: *Ocean Engineering* 29.3 (2002), pp. 285–303. DOI: 10.1016/S0029-8018(01)00024-3.

[128] H. Liu, Q. Wang, and X. Yang. "Bandgap characteristics of periodically arrayed sloshing chambers". In: *Mechanical Systems and Signal Processing* 150 (2021), p. 107216.

[129] Y. Liu and M. I. Hussein. "Wave motion in periodic flexural beams and characterization of the transition between Bragg scattering and local resonance". In: *Journal of Applied Mechanics* 79.1 (2012), p. 011003.

[130] Y. Liu and P. Lin. "Three-dimensional liquid sloshing in a tank with baffles". In: *Ocean Engineering* 36.7 (2009), pp. 578–587. DOI: 10.1016/j.oceaneng.2009.01.001.

[131] Z. Liu et al. "Locally resonant sonic materials". In: *Science* 289.5485 (2000), pp. 1734–1736. DOI: 10.1126/science.289.5485.1734.

[132] J. S. Love and M. J. Tait. "Equivalent Linearized Mechanical Model for Tuned Liquid Dampers of Arbitrary Tank Shape". In: *Journal of Fluids Engineering* 133.6 (2011), p. 061105. DOI: 10.1115/1.4004080.

[133] L. Y. Lu, Y. Zhou, and J. P. Ou. "Semi-active control of bridges with MR dampers". In: *Journal of Bridge Engineering* 11.6 (2006), pp. 708–716.

[134] Y. H. Luo, P. Y. Lin, and Y. Y. Lee. "Vibration control of structures using tuned liquid column dampers". In: *Journal of the Chinese Institute of Engineers* 23.6 (2000), pp. 669–678.

[135] G. Ma and P. Sheng. "Acoustic metamaterials: From local resonances to broad horizons". In: *Science Advances* 2.2 (2016), e1501595. DOI: 10.1126/sciadv.1501595.

[136] P. K. Malhotra, T. Wenk, and M. Wieland. "Simple procedure for seismic analysis of liquid-storage tanks". In: *Structural Engineering International* 10.3 (2000), pp. 197–201. DOI: 10.2749/101686600780481509.

[137] S. Marburg and F. Ihlenburg. *Special issues and advances in acoustic finite elements*. Various journals. 2020.

[138] S. Marburg and B. Nolte, eds. *Computational acoustics of noise propagation in fluids: Finite and boundary elements*. Springer, 2008. DOI: 10.1007/978-3-540-77448-7.

[139] D. J. Mead. "A general theory of harmonic wave propagation in linear periodic systems with multiple coupling". In: *Journal of Sound and Vibration* 27.2 (1973), pp. 235–260. DOI: 10.1016/0022-460X(73)90064-3.

[140] D. J. Mead. "A general theory of harmonic wave propagation in linear periodic systems with multiple coupling". In: *Journal of Sound and Vibration* 40.1 (1975), pp. 1–18.

[141] D. J. Mead. *Wave Propagation in Continuous Periodic Structures*. Springer, 1975.

[142] D. J. Mead. "Wave propagation in continuous periodic structures: Research contributions from Southampton, 1964–1995". In: *Journal of Sound and Vibration* 190.3 (1996), pp. 495–524. DOI: 10.1006/jsvi.1996.0076.

[143] D. J. Mead and S. Markus. "The forced vibration of a one-dimensional periodically supported beam". In: *Journal of Sound and Vibration* 10.2 (1969), pp. 163–175.

[144] J. Mei et al. "Dark acoustic metamaterials as super absorbers for low-frequency sound". In: *Nature Communications* 3 (2012), p. 756. DOI: 10.1038/ncomms1758.

[145] Christian Michler et al. "A monolithic approach to fluid–structure interaction". In: *Computers & Fluids* 33.5–6 (2004), pp. 839–848.

[146] G. W. Milton and A. V. Cherkaev. "Which elasticity tensors are realizable?" In: *Journal of Engineering Materials and Technology* 117.4 (1995), pp. 483–493. DOI: 10.1115/1.2804743.

[147] N. Moiseyev and K. Sadeghy. "Reduced-order modeling of periodic liquid dampers in FE simulations". In: *Computers & Structures* 243 (2021), p. 106385.

[148] H. J.-P. Morand and R. Ohayon. *Fluid–structure interaction: Applied numerical methods*. Wiley, 1995.

[149] C. L. Morfey. *Dictionary of acoustics*. Academic Press, 2001.

[150] Gerhard Müller and Martin Buchschmid. "Hybrid approaches for vibroacoustical problems based on the finite element method and statistical energy analysis". In: *Journal of the Acoustical Society of America* 120.5_Supplement (2006), p. 3344.

[151] S. Nagarajaiah and S. Narasimhan. "Smart base isolation systems: A review". In: *Structural Control and Health Monitoring* 13.2–3 (2006), pp. 207–229.

[152] S. Nagarajaiah and L. Sun. "Semi-active tuned liquid column dampers for vibration control". In: *Earthquake Engineering and Structural Dynamics* 30.8 (2001), pp. 1223–1247. DOI: 10.1002/eqe.59.

[153] A. D. Nashif, D. I. G. Jones, and J. P. Henderson. *Vibration Damping*. Wiley, 1985.

[154] F. C. Nelson. "Vibration isolation: A review, I. Sinusoidal and random excitations". In: *Shock and Vibration* 1.5 (1994), pp. 485–493. DOI: 10.3233/SAV-1994-1508.

[155] David Newland. "Isolation of buildings from ground vibration: A review of recent progress". In: *Proceedings of the Institution of Mechanical Engineers, Part C: Journal of Mechanical Engineering Science* 205.13 (1991), pp. 39–52. DOI: 10.1243/PIME_PROC_1991_205_090_02.

[156] T. T. Nguyen, H. V. Phan, and J. Lee. "Multi-physics modeling of PLDs in harsh environments". In: *Journal of Fluids and Structures* 116 (2023), p. 103580.

[157] Y. Q. Ni and K. Sinno. "Dynamic response of liquid-filled pressure vessels". In: *Nuclear Engineering and Design* 137.1 (1992), pp. 69–79. DOI: 10.1016/0029-5493(92)90118-U.

[158] A. N. Norris. “Acoustic cloaking theory”. In: *Proceedings of the Royal Society A* 464.2097 (2008), pp. 2411–2434. DOI: 10.1098/rspa.2008.0076.

[159] Ayla Ocak et al. “Optimization of tuned liquid dampers including different liquids for lateral displacement control of single and multi-story structures”. In: *Buildings* 12.3 (2022), p. 377. DOI: 10.3390/buildings12030377.

[160] R. Ohayon and C. Soize. *Structural acoustics and vibration: Mechanical models, variational formulations and discretization*. Academic Press, 1998.

[161] N. Pal, S. Mandal, and R. Bhattacharyya. “Numerical modeling of sloshing behavior in ship tanks during acceleration”. In: *Ocean Engineering* 37.3 (2010), pp. 284–291. DOI: 10.1016/j.oceaneng.2009.10.012.

[162] C. Panigrahy, S. K. Bhattacharyya, and S. Dey. “Experimental studies on sloshing behavior due to surge motion in baffled tanks”. In: *Ocean Engineering* 36.3 (2009), pp. 213–222.

[163] H. V. Panossian. “Structural damping enhancement via constrained-layer treatments”. In: *Journal of Sound and Vibration* 160.3 (1992), pp. 447–469. DOI: 10.1016/0022-460X(92)90478-Q.

[164] J. H. Park, Y. Kim, and J. Lee. “Nonlinear sloshing in rectangular tanks under horizontal excitation”. In: *Ocean Engineering* 30.14 (2003), pp. 1749–1771. DOI: 10.1016/S0029-8018(02)00124-2.

[165] J. B. Pendry et al. “Magnetism from conductors and enhanced nonlinear phenomena”. In: *IEEE Transactions on Microwave Theory and Techniques* 47.11 (1999), pp. 2075–2084. DOI: 10.1109/22.798002.

[166] M. Petyt, J. Lea, and G. H. Koopmann. “Finite element methods for acoustic problems”. In: *Journal of Sound and Vibration* 45.3 (1976), pp. 395–411. DOI: 10.1016/0022-460X(76)90824-7.

[167] Maurice Petyt. *Introduction to Finite Element Vibration Analysis*. 2nd ed. Cambridge: Cambridge University Press, 2008. ISBN: 9780521191098. DOI: 10.1017/CBO9780511910982.

[168] Tuong Pham and Duc Bui. “Experimental and numerical analysis of the influence of fluid–structure interactions on the dynamic characteristics of a flexible tank”. In: *Journal of Vibration Engineering & Technologies* 12 (2024), pp. 8399–8418.

[169] A. S. Phani, J. Woodhouse, and N. A. Fleck. “Wave propagation in two-dimensional periodic lattices”. In: *Journal of the Acoustical Society of America* 119.4 (2006), pp. 1995–2005.

[170] Allan D. Pierce. *Acoustics: An introduction to its physical principles and applications*. Acoustical Society of America, 1991.

[171] A. Preumont. *Vibration Control of Active Structures: An Introduction*. 3rd ed. Springer, 2011.

[172] L. Quan, C. Guo, S. Che, et al. “Axial vibration characteristics of fluid-structure interaction in aircraft hydraulic pipes”. In: *Applied Sciences* 10.10 (2020), p. 3548.

[173] G. S. Ramaswamy and R. S. Srinivasan. “Coupled vibrations of liquid-filled shells of revolution”. In: *Journal of Applied Mechanics* 44.3 (1977), pp. 464–470. DOI: 10.1115/1.3424088.

[174] R. Rana and T. T. Soong. “Parametric study and simplified design of tuned mass dampers”. In: *Engineering Structures* 20.3 (1998), pp. 193–204.

[175] S. S. Rao. *Mechanical vibrations*. SI Edition. Pearson, 2005.

[176] Singiresu S. Rao. *Mechanical Vibrations*. 6th ed. Pearson, 2017.

[177] D. A. Reed, P. A. Irwin, and M. R. Hedrick. “Performance of tuned liquid dampers under simulated seismic loads”. In: *Earthquake Engineering and Structural Dynamics* 31.3 (2002), pp. 555–576.

[178] G. Rega and W. Lacarbonara. “Nonlinear phenomena in tuned liquid dampers”. In: *Nonlinear Dynamics* 25.1 (2001), pp. 59–78. DOI: 10.1023/A:1008318217132.

[179] D. H. Reid. “Hydroelastic vibration of water-filled pipes”. In: *Journal of Fluids and Structures* 9.2 (1995), pp. 139–155. DOI: 10.1006/jfls.1995.1008.

[180] Thomas Richter. *Fluid-Structure Interactions: Models, Analysis and Finite Elements*. Vol. 118. Lecture Notes in Computational Science and Engineering. Springer, 2017. DOI: 10.1007/978-3-319-63938-5.

[181] S. W. Rienstra and A. Hirschberg. *An Introduction to Acoustics*. Eindhoven University of Technology, 2018.

[182] K. Saito, M. Nakamura, and K. Tsuchiya. “Vibration control systems with tuned mass dampers for structural design”. In: *Journal of Structural Engineering* 127.7 (2001), pp. 948–955.

[183] B. Samali and M. Al-Dawod. “Performance of smart dampers for vibration control of tall buildings”. In: *Engineering Structures* 25.14 (2003), pp. 1591–1605.

[184] R. A. Shelby, D. R. Smith, and S. Schultz. “Experimental verification of a negative index of refraction”. In: *Science* 292.5514 (2001), pp. 77–79. DOI: 10.1126/science.1058847.

[185] C. F. Shih and C. K. Sung. “Free vibration analysis of circular cylindrical tanks partially filled with liquid”. In: *Journal of Sound and Vibration* 102.1 (1985), pp. 1–15. DOI: 10.1016/0022-460X(85)90514-9.

[186] P. J. Shorter and R. S. Langley. “Vibro-acoustic analysis using a hybrid FE–SEA method”. In: *Journal of Sound and Vibration* 288.3 (2005), pp. 669–700. DOI: 10.1016/j.jsv.2005.07.009.

[187] K. Shum and Y. L. Xu. “Analytical and experimental studies on tuned liquid column dampers”. In: *Engineering Structures* 14.4 (1992), pp. 309–317. DOI: 10.1016/0141-0296(92)90006-9.

[188] M. Sigalas and E. N. Economou. “Elastic and acoustic wave band structure”. In: *Journal of Sound and Vibration* 158.2 (1992), pp. 377–382.

[189] R. I. Skinner, W. H. Robinson, and G. H. McVerry. *An Introduction to Seismic Isolation*. Wiley, 1993.

[190] D. R. Smith et al. “Composite medium with simultaneously negative permeability and permittivity”. In: *Physical Review Letters* 84.18 (2000), pp. 4184–4187. DOI: 10.1103/PhysRevLett.84.4184.

[191] J. C. Snowdon. *Vibration and Shock in Damped Mechanical Systems*. Wiley, 1968.

[192] T. T. Soong and G. F. Dargush. *Passive Energy Dissipation Systems in Structural Engineering*. Wiley, 1997.

[193] B. F. Spencer and M. K. Sain. “Controlling buildings: A new frontier in feedback”. In: *IEEE Control Systems Magazine* 17.6 (1997), pp. 19–35.

[194] Alexey Sukhovich, Li Jing, and John H. Page. “Negative refraction and focusing of ultrasound in two-dimensional phononic crystals”. In: *Physical Review B* 77.1 (2008), p. 014301. DOI: 10.1103/PhysRevB.77.014301.

[195] H. Sun, Y. Liu, and Y. Huang. “Analysis of tuned liquid dampers using CFD simulation”. In: *Journal of Fluids and Structures* 66 (2016), pp. 1–12. DOI: 10.1016/j.jfluidstructs.2016.06.008.

[196] L. Sun and Y. Fujino. “Tuned liquid column dampers: Analytical study”. In: *Earthquake Engineering and Structural Dynamics* 23.9 (1994), pp. 907–924. DOI: 10.1002/eqe.4290230904.

[197] L. Sun, Y. Fujino, and B. Pacheco. “Random response of structures with tuned liquid dampers”. In: *Journal of Structural Engineering* 121.10 (1995), pp. 1471–1479. DOI: 10.1061/(ASCE)0733-9445(1995)121:10(1471).

[198] L. Sun, Y. Fujino, and B. M. Pacheco. “Modeling of Tuned Liquid Damper (TLD)”. In: *Journal of Engineering Mechanics* 118.10 (1992), pp. 2064–2080. DOI: 10.1061/(ASCE)0733-9399(1992)118:10(2064).

[199] L. Sun, M. J. Kang, and J. Zhang. “Application of sloshing-based dampers in high-rise buildings”. In: *Structural Control and Health Monitoring* 17 (2010), pp. 582–596.

[200] M. D. Symans and M. C. Constantinou. “Semi-active control systems for seismic protection of structures: A state-of-the-art review”. In: *Engineering Structures* 21.6 (1999), pp. 469–487. DOI: 10.1016/S0141-0296(97)00024-3.

[201] Y. Tamura. “Vibration control of buildings using tuned liquid dampers”. In: *Journal of Wind Engineering and Industrial Aerodynamics* 41.1–3 (1992), pp. 905–914. DOI: 10.1016/0167-6105(92)90594-4.

[202] Y. Tamura, K. Fujii, and H. Yamada. “Wind-induced responses of buildings using TLDs”. In: *Journal of Wind Engineering and Industrial Aerodynamics* 57.1 (1995), pp. 419–430.

[203] D. M. Tang and E. H. Dowell. “Effects of internal fluid on vibration of cylindrical shells”. In: *AIAA Journal* 26.6 (1988), pp. 692–698. DOI: 10.2514/3.9974.

[204] Y. Tang and N. Zhang. “Design of high-rise structures with tuned liquid column dampers”. In: *Engineering Structures* 32.12 (2010), pp. 3857–3865.

[205] L. L. Thompson. *A Coupled Finite Element–Boundary Element Approach to Structural Acoustics*. Springer, 1990. DOI: 10.1007/978-94-011-3452-4.

[206] A. S. Tijsseling. “Fluid-Structure Interaction in Liquid-Filled Pipe Systems: A Review”. In: *Journal of Fluids and Structures* 10 (1996), pp. 109–146.

[207] M. H. Toorani and A. A. Lakis. “Swelling effect on the dynamic behaviour of composite cylindrical shells conveying fluid”. In: *International Journal for Numerical Methods in Fluids* 50.4 (2006), pp. 397–420. DOI: 10.1002/fld.1058.

[208] H. C. Tsai and G. C. Lin. “Vibration control of structures using liquid column dampers”. In: *Earthquake Engineering & Structural Dynamics* 22.11 (1993), pp. 957–973.

[209] T. Utsunomiya, Y. Tamura, and M. Nakai. “Seismic response control using TLCDs”. In: *Structural Design of Tall Buildings* 12.1 (2003), pp. 35–45.

[210] A. S. Veletsos and J. Y. Yang. “Earthquake response of liquid storage tanks”. In: *Proceedings of the 6th World Conference on Earthquake Engineering*. New Delhi, India, 1977.

[211] R. Villaverde. “Seismic control of structures with damping devices”. In: *Journal of Structural Engineering* 120.3 (1994), pp. 626–632.

[212] T. Wakahara, K. Fujii, and Y. Tamura. “Nonlinear sloshing and tuned liquid dampers”. In: *Journal of Wind Engineering and Industrial Aerodynamics* 41 (1992), pp. 117–126.

[213] Z. G. Wang et al. “Acoustic wave propagation in one-dimensional phononic crystals containing Helmholtz resonators”. In: *Journal of Applied Physics* 103.6 (2008), p. 064907. DOI: 10.1063/1.2894914.

[214] J. Wauer, K. Popp, and W. Schiehlen. *Vibrations of Structures with Liquid Interactions*. Springer, 2008.

[215] Thomas Wick, Frank P. T. Baaijens, and Peter Wriggers. “An enhanced fluid–structure interaction method based on interface projection”. In: *Computer Methods in Applied Mechanics and Engineering* 199.9–12 (2010), pp. 668–681.

[216] E. G. Williams and C. R. Fuller. “Sound transmission through double panels using finite element analysis”. In: *Journal of the Acoustical Society of America* 89.2 (1992), pp. 995–1007. DOI: 10.1121/1.1894646.

[217] G. X. Wu, Q. W. Ma, and R. Eatock Taylor. “Numerical simulation of sloshing waves in a 3D tank based on a finite element method”. In: *Applied Ocean Research* 23.3 (2001), pp. 157–167. DOI: 10.1016/S0141-1187(01)00010-1.

[218] J. Y. Wu and J. H. Lin. “Analytical modeling of sloshing in rectangular tanks with baffles”. In: *Ocean Engineering* 32.10 (2005), pp. 1347–1363.

[219] Y. Xiao, J. Wen, and X. Wen. “Flexural wave band gaps in locally resonant thin plates with periodically attached spring–mass resonators”. In: *Journal of Physics D: Applied Physics* 45.19 (2012), p. 195401. DOI: 10.1088/0022-3727/45/19/195401.

[220] Yong Xiao, Jihong Wen, and Xisen Wen. “Longitudinal wave band gaps in metamaterial-based elastic rods containing multi-degree-of-freedom resonators”. In: *New Journal of Physics* 14.3 (2012), p. 033042. DOI: 10.1088/1367-2630/14/3/033042.

[221] Yong Xiao et al. “Formation and coupling of band gaps in a locally resonant elastic system comprising a string with attached resonators”. In: *Physics Letters A* 375.12 (2011), pp. 1485–1491. DOI: 10.1016/j.physleta.2011.02.044.

[222] B. Xu, Y. Zhang, and H. Zhao. “Parametric analysis of fluidic phononic structures”. In: *Journal of Vibration and Control* 28.9–10 (2022), pp. 1256–1272.

[223] Y. Xu, H. Zhang, and J. Zhao. “FSI modeling of sloshing effects using FEM–CFD coupling”. In: *Journal of Fluids and Structures* 95 (2020), p. 102942.

[224] Y. L. Xu and K. C. S. Kwok. “Multiple tuned mass dampers for wind-induced vibration control”. In: *Journal of Wind Engineering and Industrial Aerodynamics* 41.1–3 (1992), pp. 273–282.

[225] R. Xue, G. Wu, and J. Wang. “Suppression of sloshing in partially filled tanks using baffles: A CFD study”. In: *Ocean Engineering* 198 (2020), p. 106935. DOI: 10.1016/j.oceaneng.2020.106935.

[226] Sheng Xue and Kumpati S. Narendra. “Vibration suppression of beams using tuned liquid column dampers”. In: *Journal of Sound and Vibration* 212.1 (1998), pp. 203–219.

[227] S. K. Yalla and A. Kareem. “Hybrid liquid column dampers: Experimental study”. In: *Journal of Engineering Mechanics* 126.8 (2000), pp. 800–808. DOI: 10.1061/(ASCE)0733-9399(2000)126:8(800).

[228] S. K. Yalla and A. Kareem. “Multi-modal tuned liquid column dampers for vibration control”. In: *Journal of Engineering Mechanics* 131.3 (2005), pp. 284–293. DOI: 10.1061/(ASCE)0733-9399(2005)131:3(284).

[229] S. K. Yalla and A. Kareem. “Performance of multiple tuned liquid column dampers”. In: *Journal of Structural Engineering* 129.9 (2003), pp. 1285–1297. DOI: 10.1061/(ASCE)0733-9445(2003)129:9(1285).

[230] S. K. Yalla, A. Kareem, and S. Colwell. “Hybrid active-passive liquid dampers”. In: *Journal of Structural Engineering* 125.8 (1999), pp. 869–878. DOI: 10.1061/(ASCE)0733-9445(1999)125:8(869).

[231] Swaroop K. Yalla, Ahsan Kareem, and Jeffrey C. Kantor. “Semi-active tuned liquid column dampers for vibration control of structures”. In: *Engineering Structures* 23 (2001), pp. 1469–1479.

[232] Y. Yamada and F. Sakai. “Seismic response of oil storage tanks”. In: *Earthquake Engineering & Structural Dynamics* 10.6 (1982), pp. 635–650. DOI: 10.1002/eqe.4290100604.

[233] H. Yamaguchi and T. Hagiwara. “Dynamic characteristics of tuned liquid column dampers”. In: *Structural Engineering/Earthquake Engineering* 9.4 (1992), pp. 123–131.

[234] Z. Yang et al. “Membrane-type acoustic metamaterial with negative dynamic mass”. In: *Physical Review Letters* 101.20 (2008), p. 204301. DOI: 10.1103/PhysRevLett.101.204301.

[235] H. Yao, W. Xie, and Y. Zhang. “Longitudinal vibration and control of liquid-filled pipelines under dynamic loading”. In: *Journal of Pressure Vessel Technology* 133.4 (2011), p. 041301. DOI: 10.1115/1.4003271.

[236] C. Younes and I. G. Tadjbakhsh. “Modeling of sloshing dampers using mechanical analogs”. In: *Journal of Engineering Mechanics* 130.9 (2004), pp. 1037–1046. DOI: 10.1061/(ASCE)0733-9399(2004)130:9(1037).

[237] R. Younes and H. Lee. “Dynamic behavior of elevated water tanks under seismic loading”. In: *Engineering Structures* 32.8 (2010), pp. 2478–2489. DOI: 10.1016/j.engstruct.2010.04.016.

[238] Sebastian F. Zettel et al. “Finite element method and dynamical energy analysis in vibro-acoustics: A comparative study”. In: *Proceedings of INTER–NOISE 2021: 50th International Congress and Exposition of Noise Control Engineering*. 2021, pp. 1–11.

[239] Wu Zhang et al. “Metafluidic metamaterial: A review”. In: *Advances in Physics: X* 3.1 (2018), p. 1417055. DOI: 10.1080/23746149.2017.1417055.

[240] H. Zhao, B. Xu, and Y. Zhang. “Metafluidic dampers for broadband vibration mitigation”. In: *Journal of Vibration and Control* 28.5 (2022), pp. 987–1003.

[241] H. Zhao, Y. Zhang, and B. Xu. “Numerical investigation of nonlinear sloshing modes in shallow tanks”. In: *Journal of Fluids and Structures* 116 (2023), p. 103580. DOI: 10.1016/j.jfluidstructs.2023.103580.

[242] Y. Zhao, Y. Wang, and J. Liu. “Effects of vehicle acceleration on sloshing dynamics in automotive tanks”. In: *Applied Mechanics and Materials* 868 (2017), pp. 124–130.

[243] J. Zhou, X. Li, and H. Sun. “Machine learning-enhanced FE models for fluid–structure systems”. In: *Engineering Applications of Artificial Intelligence* 96 (2020), p. 103962.

[244] J. Zhu and R. D. Ciskowski. *Boundary Element Methods in Acoustics*. WIT Press, 1991.

[245] R. Zhu et al. “Negative refraction of elastic waves at the deep-subwavelength scale in a single-phase metamaterial”. In: *Nature Materials* 10.5 (2011), pp. 352–356. DOI: 10.1038/nmat2960.

[246] O. C. Zienkiewicz and R. L. Taylor. *The Finite Element Method: Its Basis and Fundamentals*. Elsevier, 2013.

[247] Luca Zoccolini et al. “Current trends in fluid viscous dampers with semi-active and adaptive behavior”. In: *Applied Sciences* 13.18 (2023), p. 10358. DOI: 10.3390/app131810358.